

Identifcation and Attenuation of Multiple Reflections using Wavefront Characteristics

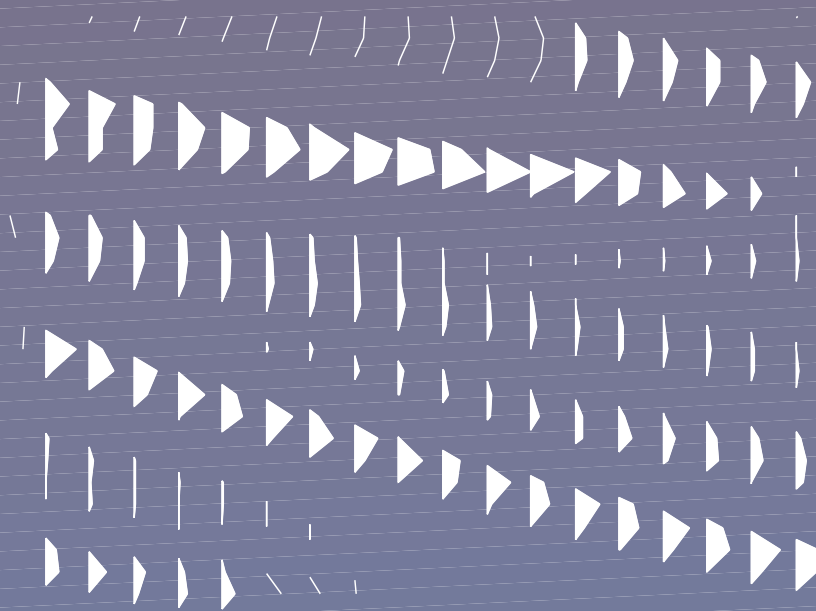


Table of Contents

Dissertation
Jörg Zinke
July 2000

Geophysical Institute
Karlsruhe University
Germany

Identifizierung und Unterdrückung Multipler Reflexionen unter Verwendung der Wellenfrontcharakteristik

Identification and Attenuation of Multiple Reflections Using Wavefront Characteristics

Zur Erlangung des akademischen Grades eines

DOKTORS DER NATURWISSENSCHAFTEN

von der Fakultät für Physik der
Universität Karlsruhe (TH)
genehmigte

DISSERTATION

von

Dipl.-Geophys. Jörg Zaske
aus Esslingen am Neckar

Tag der mündlichen Prüfung:

Referent:

Korreferent:

21. Juli 2000

Prof. Dr. Peter Hubral

Prof. Dr. Friedemann Wenzel

Contents

Zusammenfassung	I
1 Introduction	1
1.1 Primary and multiple reflections	2
1.2 Overview of multiple attenuation methods	5
1.3 Multiple attenuation using kinematic wavefront parameters	10
2 Common-Shot-Point (CSP) Homeomorphic-Imaging (HI) method	15
2.1 Introduction	15
2.2 The method	15
2.3 Remarks	18
2.4 Relation to other stacking methods	18
3 Horizon-based wavefront-parameter estimation	20
3.1 Introduction	20
3.2 Local and global circular wavefront approximation	20
3.3 Optimization strategy	23
3.4 Hyperbolic moveouts	25
3.4.1 Global angle analysis	26
3.4.2 Synthetic example: four layer model	27
3.4.3 Real data example: marine data set	33

3.4.4	Results	35
3.5	Non-hyperbolic moveouts	35
3.5.1	Local angle analysis	36
3.5.2	Synthetic examples	37
3.5.2.1	Hyperbolic case	37
3.5.2.2	Non-hyperbolic case	39
3.5.2.3	Mixed case	42
3.5.3	Results	44
3.6	Summary	46
4	Multiple prediction using wavefront parameters of multiple generators	49
4.1	Introduction	49
4.2	Geometrical considerations	49
4.3	Kinematic prediction of multiples	52
4.3.1	Method and implementation	52
4.3.2	Synthetic example: four layer model	54
4.3.3	Real data example: marine data set	57
4.3.4	Results	61
4.4	Dynamic prediction of multiples	62
4.4.1	Primaries and their true amplitudes	62
4.4.2	Method and Implementation	64
4.4.2.1	1D problem: impulsive plane source	64
4.4.2.2	1D problem: finite source wavelet	66
4.4.2.3	2.5D problem: point source	68
4.4.2.4	Implementation	69
4.4.3	Synthetic example	70
4.4.4	Results	75

4.5	Summary	75
5	Attenuation of predicted multiples using the parabolic Radon transform	77
5.1	Introduction	77
5.2	Multiple attenuation in the parabolic τ - p domain	79
5.2.1	Elliptical multiple rejection filter	79
5.2.1.1	The method	79
5.2.1.2	Synthetic example: flat layer model	83
5.2.2	Data adaptive 2D demultiple filter	85
5.2.2.1	The method	85
5.2.2.2	Synthetic example: flat layer model	86
5.2.2.3	Synthetic example: four layer model	88
5.2.3	Remarks and limitations	89
5.3	Multiple attenuation in the x - t domain	91
5.3.1	The method	91
5.3.2	Real data example: marine data set	94
5.4	Results	101
6	Conclusions	103
	References	107
A	Derivation of the CSP HI moveout formula	113
B	Search of wavefront radius (R_{CSH})	116
B.1	Golden section search	116
B.2	Limits of radius search	118
C	Forward calculation of kinematic wavefront parameters	119

Zusammenfassung

Die vorliegende Arbeit ist mit Ausnahme dieser Zusammenfassung und einigen Passagen in der Danksagung in Englischer Sprache geschrieben. Um auch dem ausschließlich deutschsprachigen Leser einen Überblick über diese Dissertation zu ermöglichen, wird eine deutsche Zusammenfassung vorangestellt. Da die englische Fachterminologie auch unter deutschsprachigen Geophysikern eingesetzt wird, habe ich auf eine Übersetzung verzichtet und entsprechende Worte kursiv geschrieben.

Einleitung

Reflexionsseismische Messungen haben sich bei der Erkundung der obersten Schichten der Erdkruste besonders bewährt und spielen deshalb in der Rohöl und Erdgasexploration eine äußerst wichtige Rolle. Bei einem reflexionsseismischen Experiment werden mittels einer seismischen Quelle, knapp unter der Erdoberfläche, elastische Wellen im Erduntergrund angeregt. Diese Wellen werden an Diskontinuitäten im Untergrund reflektiert, transmittiert und gestreut. Das nach oben zurücklaufende Wellenfeld wird an der Erdoberfläche von Empfängern (Geophonen) als sogenanntes 'Seismogramm' registriert. Ziel der seismischen Abbildungsverfahren ist es, unter Verwendung dieser Information ein möglichst realistisches Abbild des Erduntergrundes zu gewinnen.

Hierbei sind Primärreflexionen ('Primäre'), d.h. Wellen, die auf ihrem Laufweg zwischen Quelle und Empfänger nur einmal an einer Diskontinuität reflektiert wurden, von entscheidender Bedeutung und werden deshalb als Nutzsignal betrachtet. Neben den Primären wird jedoch auch andere seismische Energie registriert, die gewöhnlich als Störsignal betrachtet wird. Einen großen Anteil des Störsignals bilden die multiplen Reflexionen ('Multiple'). Dies sind Wellen, die auf ihrem Laufweg zwischen Quelle und Empfänger mehr als einmal reflektiert und in Multiple der freien Oberfläche und interne Multiple unterschieden werden, wie im folgenden Abschnitt erläutert wird.

Viele seismische Datenverarbeitungsmethoden legen die Annahme zugrunde, daß sich das Seismogramm lediglich aus Primären zusammensetzt. Da dies nicht zutrifft und im Gegenteil die Multiplen zum Teil so stark sind, daß sie die Primären komplett überdecken, müssen diese in einem separaten Datenverarbeitungsschritt eliminiert werden. Eine komplette Eli-

II

minierung ist jedoch gewöhnlich nicht möglich und bereits die Identifikation von Primären und Multiplen ist oft sehr schwierig. Es muß deshalb das Ziel sein, Multiple zu identifizieren und so gut als möglich zu unterdrücken, ohne dabei die Primären in Mitleidenschaft zu ziehen.

Die Multiplenunterdrückung ist seit langem ein wesentlicher Bestandteil der seismischen Datenverarbeitung, doch trotz großer Anstrengungen, ist dieses Problem bis heute nicht zufriedenstellend gelöst. Viele der entwickelten Methoden funktionieren sehr gut, wenn die zugrunde liegenden, vereinfachenden Annahmen erfüllt sind. Oft sind diese Annahmen jedoch unzureichend, um die tatsächlichen Gegebenheiten des Erduntergrunds realistisch genug zu beschreiben, so daß die Multiplenunterdrückung erfolglos ist oder, noch schlimmer, sogar die Primären beeinträchtigt. Desweiteren sind viele Methoden auf einzelne Multiplenarten beschränkt. Insbesondere die Unterdrückung von internen Multiplen stellt ein großes Problem dar. In dieser Arbeit wird eine neue Methode vorgestellt, die sowohl für die Vorhersage als auch für die Unterdrückung von Multiplen der freien Oberfläche und internen Multiplen, verwendet werden kann. Diese Methode erfordert keine explizite Kenntnis über den Untergrund. Lediglich die oberflächennahe Wellenausbreitungsgeschwindigkeit wird als bekannt vorausgesetzt, also im marinen Fall die des Wassers. Alle anderen notwendigen Informationen können direkt von den Meßdaten abgeleitet werden.

Primäre und Multiple Reflexionen

Eine weitverbreitete Technik, die Ausbreitung von elastischen Wellen in einem Medium zu beschreiben, ist die Methode der Strahlenseismik. Diese basiert auf einer Hochfrequenzapproximation der elastodynamischen Wellengleichung für inhomogene Medien, wobei sich die Energie einer seismischen Welle mit einer lokalen Ausbreitungsgeschwindigkeit entlang von Strahlen ausbreitet und die Gesetze analog zur geometrischen Optik gelten. In isotropen Medien sind die seismischen Strahlen definiert als die Normalen einer Wellenfront und zeigen deren Ausbreitungsrichtung an.

In Abbildung 1 wird die marine Datenaquisition unter Verwendung der Strahlenseismik illustriert. Knapp unter der Erdoberfläche befindet sich eine seismische Quelle, die elastische Wellen abstrahlt. Die verschiedenen Strahlen kennzeichnen die Laufwege verschiedener seismischer Wellen zwischen der Quelle und den Empfängern: (1) Direkte Wellen und Oberflächenwellen, (2) Primärreflexionen und (3) Multiple Reflexionen. (1) Direkte Wellen und Oberflächenwellen breiten sich lateral (und nicht nach unten) knapp unter der Erdoberfläche aus. Im Fall der marinen Seismik breitet sich die direkte Welle von der seismischen Quelle zu den Geophonen aus ohne reflektiert zu werden. Im Fall der Landseismik werden verschiedene Oberflächenwellen erzeugt. Direkte Wellen und Oberflächenwellen sind für die vorliegende Arbeit nicht von Bedeutung und werden deshalb nicht berücksichtigt. (2) Primärreflexionen werden erzeugt durch Wellen, die sich nach unten ausbreiten und einmal reflektiert werden, um danach an der Erdoberfläche registriert zu werden. Primäre werden für die Erzeugung eines seismischen Abbildes des Untergrundes verwendet. (3) Multiple Reflexionen sind in dieser Arbeit charakterisiert durch mindestens drei Reflexionen

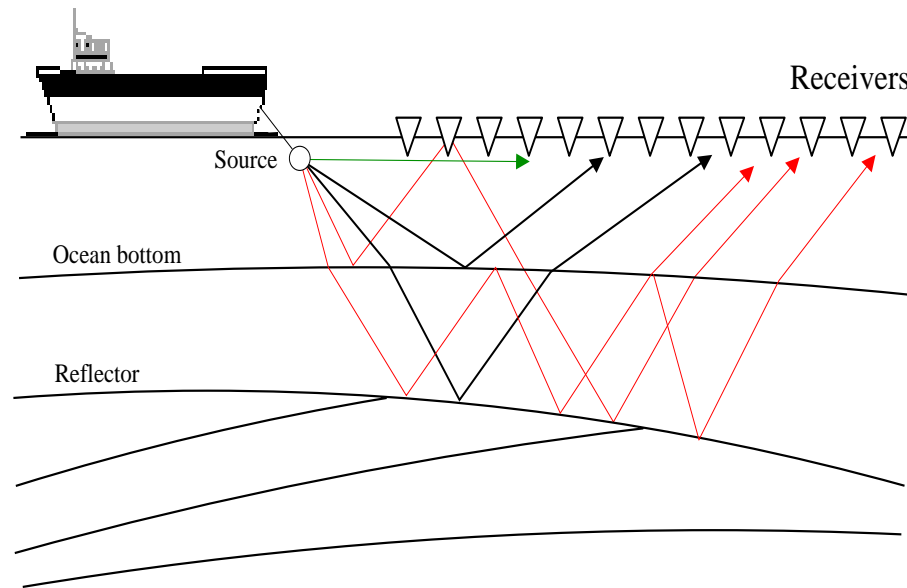


Abbildung 1: Laufwege verschiedener seismischer Wellen zwischen einer seismischen Quelle und den Empfängern in der marinen Datenerfassung. (1) Direkte P-Welle (grün), (2) Primärreflexionen (schwarz) und (3) Multiple Reflexionen (rot). Die multiplen Reflexionen werden unterschieden in Multiple der freien Oberfläche, d.h. Multiple die mindestens einmal an der Oberfläche reflektiert wurden, und die internen Multiplen, die alle Reflexionen unterhalb der Erdoberfläche erfahren. In isotropen Medien stehen die als Strahlen gezeichneten Laufwege senkrecht auf der korrespondierenden Wellenfront.

(aufwärts, abwärts, aufwärts) auf ihrem Strahlweg zwischen Quelle und Empfänger. Multiple werden weiter unterschieden in Multiple der freien Oberfläche und interne Multiple (siehe Abbildung 1). Die Multiplen der freien Oberfläche wurden mindestens einmal an der Oberfläche reflektiert, während die internen Multiplen alle Reflexionen unterhalb der Oberfläche erfahren.

Das bei einem, wie in Abbildung 1 gezeigten, seismischen Experiment mit einer Quelle und mehreren Empfängern in einem Zeitintervall registrierte Wellenfeld wird als *common shotpoint* (CSP) Sektion (*gather*) bezeichnet. Gewöhnlich wird bei der Darstellung der CSP Sektion ($x-t$ Datenraum) die Laufzeit t über dem Quelle-Empfänger Abstand x aufgetragen. Die an der Erdoberfläche gemessene Quelle-Empfänger Distanz wird als *offset* bezeichnet. Befinden sich Quelle und Empfänger an derselben Position, so ist der Quelle-Empfänger Abstand gleich null und man spricht demnach vom *zero-offset*. Eine Spur (*trace*) in einer CSP Sektion gibt das Wellenfeld eines Schusses am Empfänger für ein bestimmtes Zeitfenster wieder. Sämtliche Spuren in einer CSP Sektion zeichnen sich dadurch aus, daß sie denselben Schußpunkt besitzen. Betrachtet man eine einzelne reflektierte Wellenfront, die an den Empfängern registriert wird, so spricht man von einem seismischen Ereignis (*event*), z.B. Primäre oder Multiple. Die unterschiedliche Ankunftszeit eines seismischen Ereignisses an den verschiedenen Empfängerpositionen wird als *moveout* bezeichnet. Die in zahlreichen CSP Sektionen entlang einer seismischen Linie (*seismic line*) ge-

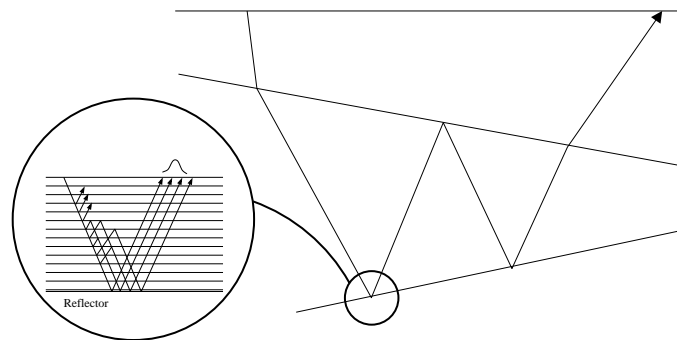


Abbildung 2: Die langperiodischen, störenden Multiplen, werden zwischen Materialdiskontinuitäten hin- und herreflektiert, deren Abstand größer ist als die Wellenlänge des seismischen Signals. Die extrem kurzperiodischen Multiplen, dargestellt im Bildausschnitt, entsprechen kleinskaligen Reverberationen zwischen den dünn geschichteten Strukturen und sind mittels konstruktiver Interferenz für die Entstehung eines signifikanten Reflexionssignals verantwortlich.

messenen Daten werden oft umsortiert in andere Sektionen mit bestimmten geometrischen Vorteilen, z.B. in *common midpoint* (CMP) Sektionen. Die Spuren in einer CMP Sektion sind dadurch ausgezeichnet, daß sie alle denselben Mittelpunkt (*midpoint*) zwischen Quelle und Empfänger besitzen.

Es muß unterschieden werden zwischen sehr kurzperiodischen und langperiodischen Multiplen. Einerseits sollen langperiodische Multiple, d.h. Multiple die zeitlich auflösbar sind und im Vergleich zur Periodendauer des seismischen Signals eine lange Periodendauer haben, möglichst gut unterdrückt werden, andererseits werden die zeitlich nicht auflösbaren sehr kurzperiodischen Multiplen benötigt, da ohne diese nur sehr viel schwächere Reflexionen an der Erdoberfläche registriert werden könnten. Der Unterschied zwischen langperiodischen und kurzperiodischen Multiplen wird in Abbildung 2 erklärt.

Die langperiodischen Multiplen werden zwischen Materialdiskontinuitäten hin- und herreflektiert deren Abstand größer ist als die Wellenlänge des seismischen Signals, während die kurzperiodischen Multiplen kleinskaligen Reverberationen entsprechen, die durch Reflexionen an dünn geschichteten Medien entstehen aus denen im Prinzip jeder für die Erdölexploration interessante, sedimentäre Untergrund aufgebaut ist. Da sich viele der nach oben zurückgestreuten Wellenfelder der kleinskaligen Reverberationen aufgrund konstruktiver Interferenz kohärent aufsummieren, wird genügend Energie nach oben reflektiert, um an der Erdoberfläche als signifikantes Signal (Primäre oder auch langperiodische Multiple) registriert werden zu können [O'Doherty and Anstey, 1971; Shapiro and Hubral, 1999].

Bisher wurden die Laufwege von Wellen mit Hilfe von Strahlen beschrieben, die für isotrope Medien senkrecht auf der korrespondierenden Wellenfront stehen. Im allgemeinen Fall wird die Wellenausbreitung durch die elastodynamische, inhomogene und anisotrope Wellengleichung beschrieben [Aki and Richards, 1980]:

$$(c_{ijkl}u_{k,l})_{,j} + f_i = \rho\ddot{u}_i, \quad i = 1, 2, 3. \quad (1)$$

Hierbei bezeichnen u_k die Komponenten des Verschiebungsvektors, c_{ijkl} die Komponenten des Elastizitätstensor, f die Quellfunktion, ρ die Dichte, $(\)_{,j}$ die räumliche Ableitung in j -Richtung, $u_{k,l}$ die räumliche Ableitung der k -ten Komponente von u in l -Richtung, und \ddot{u}_i die zweite Ableitung der i -ten Komponente des Verschiebungsvektors nach der Zeit.

Eine Welle, die sich von einer seismischen Quelle zu einem Empfänger ausbreitet, wird auf ihrem Weg an Streuzentren gestreut und erzeugt so ein gestreutes Wellenfeld. Wird das Wellenfeld nur einmal gestreut zwischen Quelle und Empfänger, so entspricht dies dem Primäranteil des gesamten Wellenfeldes. Wird das Wellenfeld erneut gestreut von einem Streuzentrum in einer Entfernung von mehr als einer Wellenlänge, so gehört es zum Multiplenanteil.

Die Lösung von Gleichung 1 im Falle einer impulsförmigen seismischen Quellfunktion in Raum und Zeit wird als Green'sche Funktion G bezeichnet. Ist es möglich diese Green'sche Funktion G aufzuspalten in das gestreute primäre Wellenfeld G_P , das gestreute multiple Wellenfeld G_M und das gestreute Wellenfeld G_N , das die unberücksichtigten Effekte beinhaltet (z.B. Instrumentenrauschen, Wind, etc.), so ist das Multiplenproblem gelöst und es gilt:

$$G = G_P + G_M + G_N. \quad (2)$$

Leider kann sowohl die Green'sche Funktion G , als auch ihre Aufspaltung nach Gleichung 2 auf analytischem Wege nur für Probleme mit einfacher Geometrie und in homogenen, isotropen und unbegrenzten Medien erfolgen. Im Allgemeinen muß die Lösung der elastodynamischen Wellengleichung 1 approximiert werden. Eine Möglichkeit hierbei ist die Strahlenseismik [Červený and Ravindra, 1971], die auf einer Hochfrequenzapproximation basiert und sehr häufig in der Reflexionsseismik sowie in der vorliegenden Arbeit verwendet wird.

Bevor ich auf eine neue Methode zur Vorhersage und Unterdrückung von Multiplen eingehen werde, möchte ich kurz einige traditionelle Methoden vorstellen.

Überblick über Verfahren zur Multiplenunterdrückung

Die existierenden Methoden zur Multiplenunterdrückung können grob in zwei Kategorien unterteilt werden: Die erste Kategorie umfaßt Filtermethoden, die darauf basieren, charakteristische physikalische Eigenschaften von Primären und Multiplen auszunutzen, die es ermöglichen diese voneinander zu trennen. Eigenschaften, die dabei von Filtermethoden ausgenutzt werden sind Periodizität und Trennbarkeit. Die zweite Kategorie begründet sich auf der Vorhersage von Multiplen basierend auf einer Vorwärtsmodellierung oder auf

der Inversion des gemessenen Wellenfeldes. Bei der Vorwärtsmodellierung wird ein seismisches Wellenfeld berechnet, dem ein bekanntes Modell zugrunde liegt. Bei der Inversion wird das gemessene Wellenfeld dafür verwendet ein Modell abzuleiten, das die gemessenen Daten möglichst gut erklärt.

Die folgenden Verfahren gehören zur ersten Kategorie: *Moveout* Filter und Stapelmethoden basieren darauf, Primäre und Multiple aufgrund ihrer oft unterschiedlichen Krümmung der Laufzeithyperbeln, also aufgrund von *moveout* Unterschieden, zu separieren. Da sich diese *moveout* Unterschiede oft weit besser in anderen Datenbereichen abzeichnen (bessere Trennbarkeit), werden die Daten zuerst in einen anderen Datenbereichen transformiert, dort die Multiplen gefiltert und danach wieder in den ursprünglichen Bereich zurücktransformiert. In Tabelle 1.1 sind die bekanntesten Filtermethoden aufgelistet, auf die an dieser Stelle nicht näher eingegangen werden kann.

Die Stapelverfahren werden dazu verwendet eine simulierte *zero-offset* Sektion zu erzeugen, d.h. eine hypothetische Sektion wie sie gemessen würde, wenn sich in allen CSP Sektionen entlang der seismischen Linie Schuß und Empfänger an derselben Stelle befänden. Um eine derartige *zero-offset* Sektion zu erzeugen, werden seismische Daten entlang hyperbolischer Laufzeitkurven in den CMP Sektionen aufsummiert und das Ergebnis in den *zero-offset* plaziert. In den CMP Sektionen haben die Laufzeitkurven von Primären und Multiplen Reflexionen als Funktion des *offset* oft einen näherungsweise hyperbolischen Verlauf. Die Krümmung dieser Laufzeithyperbeln wird durch die sogenannte Stapelgeschwindigkeit bestimmt, die ihrerseits aus einer Geschwindigkeitsanalyse gewonnen werden kann. Die Stapelgeschwindigkeit kann dann im nächsten Schritt dazu verwendet werden ein Geschwindigkeitsmodell (*macro-velocity-model*) abzuleiten [e.g. Dix, 1955], wobei jedem Tiefenpunkt eines Modells eine Geschwindigkeit zugeordnet wird. Stimmen die Stapelgeschwindigkeiten genügend gut mit der Realität überein, so werden Primärreflexionen kohärent entlang der Hyperbeln aufsummiert, sofern diese tatsächlich hyperbolisch sind. Hierbei wird das Signal/Störverhältnis von Primären erhöht. Im Gegensatz dazu sind Multiple, die oft eine geringere Stapelgeschwindigkeit und somit einen anderen *moveout* aufweisen als Primäre, in der gestapelten *zero-offset* Sektion unterdrückt. Die *moveout* Filter und Stapelmethoden sind nur dann erfolgreich, wenn sich der *moveout* von Primären und Multiplen ausreichend voneinander unterscheidet und die Primären einen näherungsweise hyperbolischen *moveout* besitzen. In vielen Fällen lassen sich jedoch die Primären aufgrund ihres *moveouts* nicht von den Multiplen unterscheiden. Gründe sind nichthyperbolische *moveouts* und zu geringe *moveout* Unterschiede, was speziell im Falle von internen Multiplen zu einem Versagen dieser Methode führen kann.

Eine sehr bekannte Methode, die auf der Annahme basiert, daß sich der Multiplenanteil im gemessenen Wellenfeld, im Gegensatz zum Primäranteil streng periodisch verhält, ist die Methode der *predictive deconvolution* [Robinson and Treitel, 1980; Peacock and Treitel, 1969]. Hierbei wird ein optimales Filter erzeugt, das die Multiplen vorhersagt und anschließend subtrahiert. Die Annahme, daß Primäre nichtperiodisch sind, impliziert eine zufällig verteilte Anordnung der Reflektoren im Untergrund, eine Situation, die sicherlich oft nicht gegeben ist. Auch die Annahme der Periodizität der Multiplen ist oft nur für kleine

offsets und für Multiple von oberflächennahen Reflektoren erfüllt. Speziell interne Multiple von tiefer gelegenen Reflektoren verhalten sich nicht periodisch innerhalb des Registrierzeitraumes und können somit nicht mit dieser Methode unterdrückt werden. Auch die Annahme, daß sich das Quellsignal zeitinvariant verhält, d.h. seine Eigenschaften während der Propagation durch das Medium nicht verändert, kann schnell verletzt sein.

Bei der zweiten Kategorie von Methoden zur Multiplenunterdrückung wird das gemessene Wellenfeld auf der Grundlage der Wellentheorie nach unten propagiert, das multiple Wellenfeld wird vorhergesagt und anschließend subtrahiert. Dieses Verfahren wird ausschließlich für die Unterdrückung von Multiplen der Wasserschicht verwendet: Das gemessene Wellenfeld wird nach unten und oben durch die Wasserschicht propagiert, so daß aus Primären Multiple erster Ordnung werden, aus Multiplen erster Ordnung Multiple zweiter Ordnung werden, etc. Somit werden alle Multiplen der ersten Schicht vorhergesagt. Die anschließende adaptive Subtraktion der vorhergesagten Multiplen unterdrückt alle Multiplen der ersten Schicht. Die für die adaptive Subtraktion verantwortlichen Koeffizienten sind abhängig von der Reflektivität des Ozeanbodens und dem Quellsignal. Nachteile dieser Methode sind, daß lediglich Multiple der freien Oberfläche der ersten Schicht unterdrückt werden können und die Reflektivität des Ozeanbodens bekannt sein muß.

Multiplenunterdrückung unter Verwendung der Wellenfrontcharakteristik von Primären

Die im letzten Abschnitt vorgestellten Multiplenunterdrückungsmethoden funktionieren gut, wenn die zugrundeliegenden Annahmen (z.B. physikal. Modell, *moveout* Unterschiede, Kenntnis der seismischen Quellfunktion, etc.) erfüllt sind. Falls diese Annahmen stark verletzt sind, werden diese Methoden versagen. Besonders die Unterdrückung der internen Multiplen ohne Kenntnis des Geschwindigkeitsmodells stellt ein großes Problem dar, da sich diese oft kaum von Primären unterscheiden.

In dieser Dissertation wird eine neue Methode vorgeschlagen, die sowohl die Vorhersage und Unterdrückung von Multiplen der freien Oberfläche als auch von internen Multiplen beinhaltet. Abgesehen von der oberflächennahen Geschwindigkeit, d.h. im marinen Fall der Wassergeschwindigkeit, wird keine weitere Kenntnis über den Untergrund benötigt. Alle benötigten Parameter können direkt von den Meßdaten abgeleitet werden. Diese Methode nutzt die kinematischen Wellenfrontparameter von identifizierten Primärreflexionen, insbesondere die Laufzeit und den Auftauchwinkel an allen Quelle-Empfänger Positionen in der CSP Sektion, um Multiple vorherzusagen.

Die Idee Multiple unter Verwendung von Primären vorherzusagen ist nicht neu, doch konnten bisher lediglich Multiple der freien Oberfläche ohne explizite Kenntnis des Geschwindigkeitsmodells vorhergesagt werden. Um eine interne Multiple voraussagen zu können, mußte das gemessene Wellenfeld bis zu derjenigen Schichtgrenze, welche die interne Multiple erzeugt, nach unten propagiert werden, was wiederum die Kenntnis des Geschwindig-

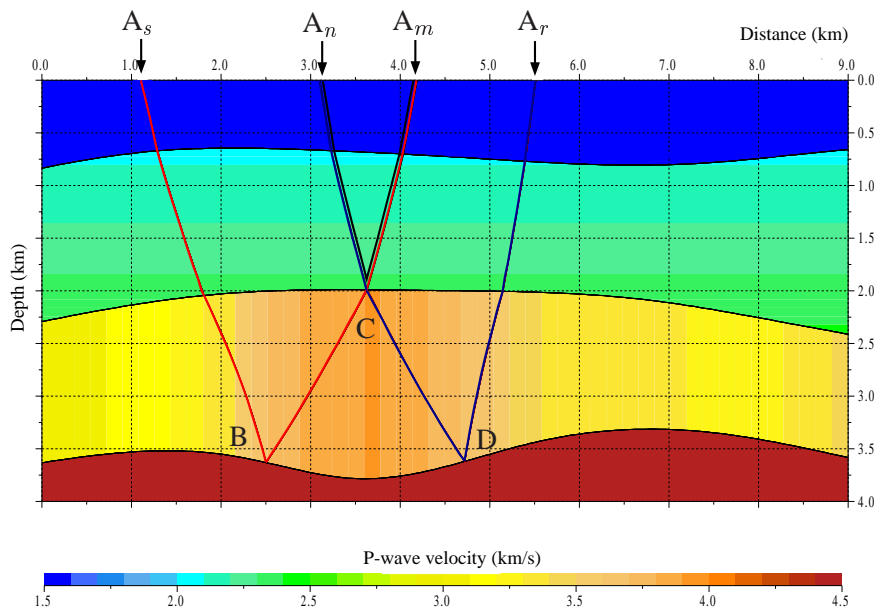


Abbildung 3: Laufweg einer internen Multiplen A_sBCDA_r , berechnet unter Verwendung der ray tracing Methode [see Červený and Ravindra, 1971], und die Zerlegung in Laufwege primärer Reflexionen, die in unterschiedlichen Farben dargestellt sind, siehe Text.

keitsmodells für diesen Tiefenbereich erforderte [z.B. Dragoset and Jericevic, 1998].

Keydar et al. [1998] zeigte eine Möglichkeit auf, um ohne explizite Kenntnis des Geschwindigkeitsmodells mit Hilfe der Laufzeiten von Primären die Laufzeiten von Multiplen der freien Oberfläche und auch von internen Multiplen vorherzusagen. Die entscheidende Idee ist hierbei, daß der Laufweg einer jeden Multiplen, so kompliziert er auch sein mag, dargestellt werden kann als eine Kombination von Laufwegen von Primärreflexionen.

Dies wird anhand Abbildung 3 erklärt. Der Laufweg der internen Multiplen A_sBCDA_r von der seismischen Quelle A_s zum Geophon A_r kann ausgedrückt werden als Summe der Laufwege der beiden Primären A_sBA_m (rot) und A_nDA_r (blau), minus dem Laufweg der dritten Primären A_nCA_m (schwarz). Daher kann auch die Laufzeit der Multiplen vorhergesagt werden. Um die Laufzeit einer spezifizierten Multiplen für ein bestimmtes Quelle-Empfänger Paar A_s und A_r vorhersagen zu können, müssen sämtliche Quelle-Empfänger Paare der involvierten multiplen-generierenden Primären bekannt sein. Im Fall der internen Multiplen in Abbildung 3 mit der Quelle bei A_s und dem Empfänger bei A_r ist dieses Problem gelöst, wenn die beiden Oberflächenpunkte A_m und A_n identifiziert sind.

Die Positionen von A_m und A_n können identifiziert werden aufgrund einfacher geometrischer Überlegungen: Anhand Abbildung 3 ist ersichtlich, daß die Auftauchwinkel der Primären A_sBA_m (rot) und der Primären A_nCA_m (schwarz) am Oberflächenpunkt A_m identisch sind. Außerdem sind die Auftauchwinkel der Primären A_rDA_n (blau) und der Primären A_mCA_n (schwarz) identisch am Oberflächenpunkt A_n . Werden die Auftauchwinkel der involvierten primären Wellenfronten an allen Quelle-Empfänger Positionen an

der Erdoberfläche miteinander verglichen, können die beiden Oberflächenpunkte A_n und A_m gefunden werden und die Laufzeit der Multiplen von der Quelle A_s zum Empfänger A_r kann berechnet werden. Der wichtigste zu identifizierende Parameter ist demnach der Auftauchwinkel. Wie im nächsten Kapitel beschrieben wird, kann dieser direkt anhand der gemessenen CSP Sektionen bestimmt werden, ohne daß hierfür ein Geschwindigkeitsmodell erforderlich wäre. Lediglich die oberflächennahe Wellenausbreitungsgeschwindigkeit wird als bekannt vorausgesetzt.

Nachdem die Multiplen vorhergesagt sind und somit identifiziert werden können, sollten diese so gut als möglich unterdrückt werden, ohne dabei die Primären zu beeinträchtigen. Hierfür bietet es sich an, die Meßdaten in einen anderen Datenraum zu transformieren, in denen Primäre und Multiple besser voneinander trennbar sind als in der ursprünglichen CSP Sektion ($x-t$ Bereich). Landa et al. [1999c] und Zaska et al. [1999] verwenden die kinematisch vorhergesagten Multiplen, um ein Multiplenmodell zu konstruieren und führen die Multiplenunterdrückung im parabolischen $\tau-p$ Datenraum durch, da hier eine sehr gute Trennung von Primären und Multiplen (aufgrund von *moveout* Unterschieden) erzielt werden kann. Die Unterdrückung von Multiplen umfaßt somit drei Arbeitsschritte:

- Bestimmung der Auftauchwinkel der identifizierten 'Primären',
- Vorhersage und Identifizierung der Multiplen,
- Unterdrückung der Identifizierten Multiplen.

Hierbei ist es nicht unbedingt erforderlich im ersten Arbeitsschritt tatsächlich Primäre zu identifizieren, sondern es könnten prinzipiell auch Multiple verwendet werden, um andere Multiple vorherzusagen (siehe Abbildung 4.1). Im Rahmen dieser Dissertation wurden für alle drei erwähnten Arbeitsschritte verschiedene Methoden mit besonderen Vor- und Nachteilen entwickelt und anhand von synthetischen und realen Daten getestet. Diese Verfahren werden im Folgenden kurz zusammengefaßt.

Bestimmung kinematischer Wellenfrontparameter (Kapitel 2 und 3)

Ein wesentlicher Schritt ist die Bestimmung der Auftauchwinkel für jedes Quelle-Empfänger Paar in jeder gemessenen CSP Sektion. Hierfür verwende ich die *CSP Homeomorphic Imaging (HI)* Methode [Gelchinsky, 1989; Keydar et al., 1996]. Die CSP HI Methode basiert auf einer lokalen sphärischen Approximation der an einem beliebig gewählten Empfänger in der CSP Sektion gemessenen reflektierten Wellenfront und der daraus abgeleiteten lokalen *moveout* Formel, die in der vorliegenden Arbeit als 'CSP HI *moveout* Formel' bezeichnet wird. Wählt man ein beliebiges Quelle-Empfänger Paar in einer CSP Sektion und bezeichnet den Strahl, der beide verbindet, als Zentralstrahl, so läßt sich mit Hilfe der CSP HI *moveout* Formel die Laufzeit eines beliebigen Strahls in der Umgebung des Zentralstrahls mittels zweier Parameter beschreiben: Diese sind der Auftauchwinkel

des Zentralstrahls und der Krümmungsradius der reflektierten Wellenfront, wobei sich alle Größen auf den Zentralstrahl beziehen. Desweiteren hängt die CSP HI *moveout* Formel lediglich von der oberflächennahen Wellenausbreitungsgeschwindigkeit ab, die lokal als konstant und bekannt vorausgesetzt wird. Die CSP HI *moveout* Formel ist also unabhängig von einem Geschwindigkeitsmodell des Erduntergrundes. Keydar et al. [1996] wählt als Zentralstrahl den *zero-offset* Strahl, der senkrecht auf einen zu betrachtenden Reflektor trifft, um eine simulierte *zero-offset* Sektion anhand von CSP Daten zu gewinnen. Da ich in der vorliegenden Arbeit von dieser Formel Gebrauch mache, gebe ich in Kapitel 2 eine Zusammenfassung der CSP HI Methode.

In Kapitel 3 werden dann verschiedene Verfahren zur Bestimmung der Auftauchwinkel von einzelnen identifizierten Primären an allen Quelle-Empfänger Positionen in allen CSP Sektionen entwickelt und getestet. Diese Methoden basieren auf der CSP HI *moveout* Formel. Während sich die erste Methode in Unterkapitel 3.4 für Laufzeitkurven mit hyperbolischem *moveout* eignet, ist die zweite Methode in Unterkapitel 3.5 auch anwendbar für komplizierte, nichthyperbolische *moveout* Kurven.

Hyperbolische moveouts (Kapitel 3.4): Eine simulierte *zero-offset* Sektion stellt oft schon ein gutes Abbild des Erduntergrundes im Zeitbereich dar. Hier kann räumlich und zeitlich korrelierte seismische Energie, die z.B. von Primärreflexionen eines bestimmten Reflektors (geolog. Horizont) im Untergrund erzeugt wurde, identifiziert und deren Laufzeiten entlang der seismischen Linie (*horizon-based*) registriert ('gepickt') werden. Die *horizon-based* gepickten *zero-offset* Laufzeiten von z.B. Primärreflexionen werden dann verwendet, um die kinematischen Wellenfrontparameter, d.h. den Auftauchwinkel und den Krümmungsradius, an der *zero-offset* Position entlang der gesamten seismischen Linie zu bestimmen. Hierzu wurde ein benutzerfreundliches, interaktiv oder vollautomatisch anwendbares Optimierungsverfahren entwickelt, das auf der CSP HI *moveout* Formel und dem *Semblance* Kohärenzmaß basiert [Zaske et al., 1999]. Die interaktive Anwendung ermöglicht es, Probleme bedingt durch lokale *Semblance* Maxima, z.B. im Falle von sich kreuzenden Schichtgrenzen im Erduntergrund (*conflicting dip*) zu beseitigen, indem die optimalen Auftauchwinkel entlang des in der *zero-offset* Sektion identifizierten Horizonts manuell gepickt werden. Kriterien für ein erfolgreiches picken sind wie üblich ein kontinuierlicher Verlauf der Wellenfrontparameter entlang des Horizonts sowie a-priori Informationen, z.B. durch vorhandene Bohrlöcher. Die für die *zero-offset* Position bestimmten Wellenfrontparameter werden im nächsten Schritt dazu verwendet, die Auftauchwinkel an allen Quelle-Empfänger Positionen zu berechnen. Voraussetzung für diese Vorgehensweise ist eine globale sphärische Wellenfront und somit eine hyperbolische Laufzeitkurve zwischen der Quelle und dem am weitesten entfernten Empfänger. Diese Methode wurde globale Winkelanalyse (*global angle analysis*) genannt. In synthetischen Datenbeispielen zeigte sich eine sehr gute Übereinstimmung zwischen den analytisch berechneten und den mit Hilfe der *global angle analysis* bestimmten Wellenfrontparametern. Auch im Falle real gemessener mariner Daten konnten Wellenfrontparameter bestimmt werden, die gut mit den anhand von Bohrlochinformationen gewonnenen Ergebnissen übereinstimmen. Die Vorteile der *global angle analysis* liegen in

der kurzen Berechnungszeit und in der Tatsache, daß lediglich die *zero-offset* Laufzeiten von multiplen-generierenden Reflexionen in einer simulierten *zero-offset* Sektion gepickt werden müssen. Im Falle von nichthyperbolischen *moveouts* in den CSP Sektionen führt diese Methode jedoch zu ungenauen Resultaten, da es nicht ausreichend ist, mit Hilfe eines Wellenfrontparametersatzes, d.h. mit einem Auftauchwinkel und einem Krümmungsradius, der eine globale hyperbolische Laufzeitkurve definiert, den nichthyperbolischen *moveout* an allen Quelle-Empfänger Positionen korrekt zu beschreiben. Deshalb wurde eine zweite neue Methode für nichthyperbolische Laufzeitkurven entwickelt.

Nichthyperbolische moveouts (Kapitel 3.5): Für derartige Situationen wurde eine Methode entwickelt, die auf lokalen *Semblance* Kohärenzmessungen unter der Verwendung einer lokalen Anwendung der CSP HI *moveout* Formel an jeder beliebigen Quelle-Empfänger Lokation basiert. Diese Methode wurde lokale Winkelanalyse (*local angle analysis*) genannt. Die lokale Anwendung der *moveout* Formel ermöglicht es, die kinematischen Wellenfrontparameter, d.h. Auftauchwinkel und Krümmungsradius der reflektierten CSP Wellenfront, auch für nichthyperbolische Laufzeitkurven an allen Quelle-Empfänger Positionen zu bestimmen. Allerdings werden hierfür die Laufzeiten einer multiplen-generierenden Primären an allen Quelle-Empfänger Positionen in allen CSP Sektionen benötigt. Für relativ einfache Situationen reicht es aus, die *zero-offset* Laufzeit von multiplen-generierenden Reflexionen in einer simulierten *zero-offset* Sektion zu picken und automatisch dem *moveout* in der CSP Sektion zu folgen. In komplizierten Situationen müssen allerdings die Laufzeiten in den CSP Sektionen direkt gepickt werden. Die *local angle analysis* Methode wurde an verschiedenen synthetischen Datensätzen getestet. Der Vergleich mit den analytisch berechneten Ergebnissen zeigte, daß es mit dieser Methode möglich ist, die Auftauchwinkel auch für nichthyperbolische Laufzeitkurven korrekt an jeder Quelle-Empfänger Position zu bestimmen. Dies ermöglicht es prinzipiell auch nichthyperbolische Laufzeitkurven von Primären (oder sogar von Multiplen) für die Vorhersage multipler Reflexionen zu verwenden.

Vorhersage multipler Reflexionen (Kapitel 4)

In Kapitel 4 werden die kinematischen Wellenfrontparameter von identifizierten multiplen-generierenden Primären für die Vorhersage von Multiplen verwendet. In beiden Verfahren werden die Quelle-Empfänger Paare der multiplen-generierenden Primärstrahlen anhand von sogenannten 'Multiplen Bedingungen' selektiert und anschließend für die Vorhersage verwendet. Die 'Multiplen Bedingungen' eines gewählten Multiplentyps, z.B. einer Multiplen der freien Oberfläche 1. Ordnung, resultieren aus einfachen geometrischen Überlegungen und beinhalten bestimmte Anforderungen an die Auftauchwinkel der involvierten Primärstrahlen. Im ersten Verfahren in Unterkapitel 4.3 wird die Kinematik von Multiplen vorhergesagt. Dieses Verfahren definiert die Laufzeiten von Multiplen und gibt keine Information über die deren Amplituden. In vielen Situationen wäre es allerdings hilfreich für die Identifizierung und Unterdrückung einer Multiplen, wenn Amplitudeninformation vorhanden wäre. Aus diesem Grund habe ich in Unterkapitel 4.4

die kinematische Vorhersagemethode direkt weiterentwickelt zu einer dynamischen Vorhersagemethode. Diese Methode ist nach wie vor gültig für Multiple der freien Oberfläche als auch für interne Multiple, erfordert jedoch zusätzlich Annahmen und Informationen.

Kinematische Vorhersage von Multiplen (Kapitel 4.3): In der kinematischen Version werden die Laufzeiten der selektierten multiplen-generierenden Primärerereignisse benutzt, um die Laufzeit der Multiplen an jeder Quelle-Empfänger Position vorherzusagen. Dies beinhaltet einfaches Addieren und Subtrahieren von Laufzeiten. Die kinematische Vorhersage von Multiplen erfordert außer der oberflächennahen Geschwindigkeit keine weitere explizite Kenntnis. Es muß lediglich eine Identifizierung der multiplen-generierenden Primären, die prinzipiell auch Multiple sein können, erfolgen. Diese Methode wurde sowohl an synthetischen Daten als auch an realen marinen Daten getestet. Die vorhergesagten Multiplenlaufzeiten im Fall des synthetischen Datensatzes stimmen sehr gut mit den vorwärtsmodellierten Daten überein, sowohl in der CSP Sektion als auch in der *zero-offset* Sektion. Auch im Fall der marinen Daten folgen die vorhergesagten Laufzeitkurven korrelierter seismischer Energie, die tatsächlich Multiplen entsprechen könnte, was bei realen Daten nicht garantiert werden kann. Amplitudeninformation wäre hilfreich für die Identifizierung.

Dynamische Vorhersage von Multiplen (Kapitel 4.4): In der dynamischen Version zur Vorhersage von Multiplen werden nicht nur die Laufzeiten der selektierten multiplen-generierenden Primären benutzt, sondern das gesamte in einem Zeitfenster gemessene Primärsignal. Da genau bekannt ist welche Quelle-Empfänger Paare der Primären Wellenfronten eine Multiple an einer bestimmten Quelle-Empfänger Position vorhersagt, ist es im Gegensatz zu anderen Verfahren möglich, diese selektierten multiplen-generierenden Primärsignale mittels einfacher 1D Konvolutionen und Korrelationen für die Vorhersage der Multiplen zu verwenden. Da die 1D Operationen den Effekt der sphärischen Divergenz (*geometrical spreading*) in 2D oder 3D Medien nicht implizit berücksichtigen, muß dieser explizit in einem separaten Schritt berücksichtigt werden. Außerdem sind Korrekturen bezüglich des seismischen Quellsignals erforderlich, die mittels einer deterministischen Dekonvolution [Robinson and Treitel, 1980] durchgeführt werden können. Hierfür ist allerdings die Kenntnis des Quellsignals nötig. Vor allem die Korrekturen des *geometrical spreadings* mit Hilfe der Primären, erfordern Approximationen und einschränkende Annahmen an das zugrundeliegende Modell. So ist diese Methode strenggenommen nur gültig für 3D horizontal geschichtete Medien mit einer punktförmigen seismischen Quelle. Als Anwendungsbeispiel wurde ein derartiger synthetischer Datensatz, der mittels *ray tracing* [Červený and Ravindra, 1971] berechnet wurde, verwendet. Das Ziel war es, eine Multiple der freien Oberfläche sowie eine interne Multiple vorherzusagen. Die Ergebnisse sind vielversprechend. Zwischen den vorhergesagten und modellierten Multiplen wurden nur kleine Unterschiede beobachtet, die hauptsächlich auf die Signaldekonvolution zurückzuführen sind.

Unterdrückung multipler Reflexionen mittels der parabolischen Radon (τ - p) Transformation (Kapitel 5)

Das Ergebnis der kinematischen Multiplenvorhersage sind die Laufzeiten der Multiplen in allen CSP Sektionen. An diesen vorausgesagten Multiplenlaufzeiten können, neben den Multiplen, prinzipiell auch Primäre im Wellenfeld enthalten sein. Die als Nutzsignal betrachteten Primären sollten aber bei der Multiplenunterdrückung nicht beeinträchtigt werden. Ziel war es somit, ein Verfahren zu entwickeln, das die kinematisch vorhergesagten Multiplen so gut als möglich unterdrückt, ohne daß dabei das restliche Wellenfeld, d.h. alles außer den vorhergesagten Multiplen, in Mitleidenschaft gezogen wird. Dies ist speziell in den Situationen, in denen Primäre und vorhergesagte Multiple stark miteinander interferieren, eine Herausforderung. Eine Möglichkeit ist es, die Primären und Multiplen mittels der Transformation in einen anderen Datenraum so gut als möglich voneinander zu trennen und dort die Multiplenunterdrückung vorzunehmen. Hierfür bietet sich die parabolische τ - p Transformation an, da diese interferierende Primäre und Multiple optimal zu trennen vermag [Zhou and Greenhalgh, 1994]. In Kapitel 5 werden drei Verfahren zur Unterdrückung der kinematisch vorhergesagten Multiplen vorgestellt. Diese Verfahren nutzen alle die Eigenschaft der parabolischen τ - p Transformation, Primäre und Multiple optimal voneinander trennen zu können. Ausgangspunkt bei der Multiplenunterdrückung mit Hilfe dieser Verfahren sind die in CMP Sektionen angeordneten Meßdaten (*offset*-Zeit Datenbereich (x - t)), was entscheidende Vorteile beinhalten kann.

Landa et al. [1999c] und Zaska et al. [1999] erstellen anhand der vorhergesagten Multiplenlaufzeiten ein Multiplenmodell im x - t Datenraum und führen die eigentliche Multiplenunterdrückung mittels einer Filterung automatisch im parabolischen τ - p Datenraum durch. Die Erstellung des Filters ist hierbei von entscheidender Bedeutung und kann auf unterschiedliche Art und Weise erfolgen. In Unterkapitel 5.2 werden zwei verschiedene Möglichkeiten aufgezeigt.

Eine weitere Möglichkeit (Unterkapitel 5.3) ist es, die parabolische τ - p Transformation lediglich zur Multiplenmodellierung zu verwenden und die eigentliche Multiplenunterdrückung im x - t Bereich (CMP Sektion) durchzuführen. Diese Vorgehensweise kann entscheidende Vorteile gegenüber den in Unterkapitel 5.2 vorgestellten Verfahren beinhalten, da hier das restliche Wellenfeld, d.h. alles außer den vorhergesagten Multiplen, keiner parabolischen Radon Transformation ausgesetzt ist.

Bei ausreichenden *moveout* Unterschieden zwischen Primären und Multiplen funktionieren die in diesem Kapitel vorgestellten Verfahren sehr gut. Sind jedoch die *moveout* Unterschiede im x - t Bereich zwischen Primären und Multiplen zu klein, um eine Trennung im parabolischen τ - p Datenraum zu gewährleisten, so versagen diese Methoden.

Multiplenunterdrückung im τ - p Datenraum (Kapitel 5.2): Die parabolische τ - p Transformation transformiert parabolische Laufzeitkurven optimal in den parabolischen τ - p Datenraum, d.h. idealerweise ergeben Parabeln im x - t Bereich Punkte im τ - p Bereich. Da die Primären und Multiplen im x - t Bereich aber einen eher hyperbolischen Charakter haben,

werden diese vor einer parabolischen τ - p Transformation in Parabeln überführt. Dies geschieht mittels dem sogenannten t^2 -*stretching* [Yilmaz, 1989], d.h. einem Quadrieren der Zeitachse im x - t Bereich. Das Ergebnis sind die Daten im x - t^2 Bereich. Die Daten im x - t^2 Bereich werden dann in den parabolischen τ - p Datenraum transformiert. Dort sind Primäre und Multiple oft besser voneinander getrennt als im ursprünglichen x - t Bereich. Im nächsten Schritt wird anhand der kinematischen Multiplenvorhersage automatisch ein Filter entworfen, das im Idealfall lediglich die Multiplen unterdrückt. Hierfür werden zwei Methoden vorgestellt. Die gefilterten Daten werden zurücktransformiert in den x - t^2 Bereich, ein inverses t^2 -*stretching* wird durchgeführt, und die gefilterten Daten im ursprünglichen x - t Bereich (CMP Sektion) werden erhalten.

Diese Methoden wurden anhand von synthetischen Daten erfolgreich getestet. Die vorhergesagten Multiplen konnten unterdrückt werden, ohne dabei die Primären in Mitleidenschaft zu ziehen. Ein Nachteil der Multiplenfilterung im parabolischen τ - p Datenraum ist, daß das gesamte Wellenfeld einer zweifachen parabolischen τ - p Transformation ausgesetzt ist und somit durch verschiedene numerische Effekte der parabolischen τ - p Transformation selbst (inklusive des t^2 -*stretchings*), auch Primäre, die überhaupt nicht mit Multiplen interferieren, beeinträchtigt werden kann (siehe Kapitel 5.2.3). Um dies zu vermeiden muß die Filterung im x - t Bereich durchgeführt werden. Hierzu habe ich eine anderes Verfahren entwickelt, das im Folgenden beschrieben wird.

Multiplenunterdrückung im x - t Datenraum (Kapitel 5.3): Bei diesem Verfahren wird die Multiplenunterdrückung im ursprünglichen x - t Bereich durchgeführt. Die parabolische τ - p Transformation wird lediglich für eine Multiplenmodellierung verwendet, d.h. die Daten werden in den parabolischen τ - p Bereich überführt. Dort werden anhand der vorhergesagten Multiplenlaufzeiten automatisch Filter entworfen, die alles bis auf die vorhergesagten Multiplen filtern. Das Ergebnis sind im Idealfall lediglich die vorhergesagten Multiplen im parabolischen τ - p Bereich. Diese werden zurücktransformiert in den x - t Datenraum, so daß nun ein verbessertes x - t Multiplenmodell vorliegt. Dieses Modell wird nun für die Filterung im x - t Datenraum verwendet.

Die Multiplenfilterung hängt stark von Amplituden und Phasenänderungen des Multiplenmodells und der original CMP Sektion ab. Um diese Instabilitäten zu reduzieren wurde eine andere Wellenfeldrepräsentation verwendet. Die original CMP Sektion wurde separiert in Envelope (Einhüllende) und 'normalisiertes Seismogramm' [Gelchinsky et al., 1985]. Das simple Produkt von Envelope und normalisiertem Seismogramm ergibt wieder die ursprüngliche CMP Sektion ohne dabei Information zu verlieren. Während das normalisierte Seismogramm die Phase der ursprünglichen CMP Sektion behält, hat die Envelope eine sehr viel geringere Frequenzcharakteristik. Deshalb bietet es sich an, für die Unterdrückung der Multiplenenergie die Envelope zu verwenden und das Ergebnis mit dem normalisierten Seismogramm zu multiplizieren.

Die Multiplenunterdrückung im x - t Datenraum hat den Vorteil, daß das restliche Wellenfeld, d.h. alles bis auf die vorhergesagten Multiplen, keiner parabolischen τ - p Transformation ausgesetzt ist und somit nicht durch numerische Effekte beeinträchtigt werden kann. Diese Methode wurde anhand eines real gemessenen marinen Datensatzes illustriert.

Abschließende Bemerkungen

In dieser Dissertation wurden verschiedene Verfahren zur Vorhersage, Identifizierung und Unterdrückung von Multiplen der freien Oberfläche als auch von internen Multiplen entwickelt und getestet.

Alle Verfahren wurden erfolgreich auf synthetische (1D & 2D) und zum Teil auf reale (2D) seismische Datensätze angewandt. Es stellte sich heraus, daß die kinematische Vorhersagemethode die wenigsten Annahmen an das zugrundeliegende Modell und an die Meßparameter erfordert und somit das 'robusteste' Vorhersageverfahren ist. Auf der anderen Seite hat die dynamische Vorhersagemethode, die auch die Amplituden der Multiplen vorhersagt, entscheidende Vorteile bei der Identifikation und Unterdrückung der vorhergesagten Multiplen. Das vorgestellte Verfahren zur Vorhersage von Amplituden multipler Reflexionen erfordert Einschränkungen bezüglich des Modells, d.h. horizontale Schichtung und keine Neigung der Schichten quer zur seismischen Linie (*cross line dip*) sowie die Kenntnis der Signalform der seismischen Quelle. Da die kinematischen Wellenfrontparameter der involvierten multiplen-generierenden Primärreflexionen eine entscheidende Rolle spielen, wurden auch für ihre Bestimmung neue Verfahren entwickelt, die auch nichthyperbolische *moveout* Kurven berücksichtigen. Somit ist es möglich, Multiple unter Verwendung von komplizierten Primärreflexionen vorhersagen zu können. Auch für die Unterdrückung der vorhergesagten Multiplen wurden verschiedene Verfahren dargestellt und weiterentwickelt, wobei sich die Methode der Multiplenmodellierung mit der parabolischen τ - p Transformation und der anschließenden Unterdrückung im Seismogramm am besten eignet, wenn garantiert sein soll, daß nichtinterferierende Primäre bei der Multiplenunterdrückung nicht in Mitleidenschaft gezogen werden. Der Hauptvorteil der Multiplenunterdrückung mit Hilfe der parabolischen τ - p Transformation basierend auf einer Multiplenvorhersage unter Verwendung der Wellenfrontcharakteristik, ist die automatische und vom Geschwindigkeitsmodell unabhängige Definition des Filteroperators.

Erweiterung der Methode von 2D auf 3D:

Die in dieser Arbeit vorgestellte 2D Methode zur Vorhersage und Unterdrückung multipler Reflexionen könnte direkt auf eine 3D Methode ausgedehnt werden. In diesem Fall würde die Wellenfrontparametersuche unter Verwendung einer *moveout* Formel mit fünf Wellenfrontparametern erfolgen, zwei Auftauchwinkel und eine Krümmungsmatrix mit drei unabhängigen Parametern. Die Meßapertur quer zur seismischen Linie müßte allerdings groß genug sein, um auch die zur Vorhersage von 3D Multiplen benötigten Primären erfassen zu können. In der marinen Datenaquisition ist diese Situation jedoch nicht gegeben, da hier in der Praxis nur eine kleine Meßapertur quer zur seismischen Linie verwendet wird.

Chapter 1

Introduction

The problem of multiple reflections, included in seismic data processing, is as old as the seismic method itself and still a major problem. Many methods have been developed in order to address this problem. These methods work very well if the underlying simplifying assumptions are fulfilled. Often they are limited to certain multiple types only and fail because the assumptions are too simple to describe the real conditions closely enough. Especially the identification and attenuation of interbed multiples is still a major problem. A method is needed that works for surface-related and interbed multiples without unrealistic assumptions about the subsurface. In this thesis, I propose and discuss such a new method that works equally well for the prediction and attenuation of surface-related multiples, as well as for interbed multiples. This method does not require any explicit subsurface information. Only the near surface velocity is assumed to be known. All information needed is completely data-derived.

One aspect of seismic measurements, performed and interpreted by geophysicists, is to explore new oil and gas reservoirs. These experiments involve the propagation of elastic body waves from a seismic source close to the surface into the unknown subsurface. Whenever these waves encounter strong spatial changes in the earth's elastic properties, the elastic waves are partly reflected, and partly transmitted. Thus, the reflected waves recorded at the earth's surface are carrying information about the structural changes of the earth's physical properties along their travel path. The goal of seismic measurements and the later seismic data-processing is to obtain the best possible structural image (including the physical properties) of the subsurface. There exist different imaging techniques that can be used to solve this problem. These methods are based on the assumption that the seismogram includes primary reflections (waves reflected once) only. However, in reality the seismogram includes also multiple reflections which may become so strong that the desired primary arrivals reflected from deeper target reflectors are completely invisible. Especially in marine data acquisition the water layer often behaves like a wave trap and the waves are repeatedly reflected at the sea surface and sea bottom without significant amplitude loss. In order to correctly identify and locate a target reflector which might indicate for instance an oil reservoir, these interfering multiple reflections must be eliminated or, because this is usually not

realizable, at least attenuated.

1.1 Primary and multiple reflections

In Figure 1.1 the marine data acquisition technique is illustrated using *ray theory*. Ray theory is based on an asymptotic high-frequency approximation of the elastodynamic wave equation and implies that the energy of seismic body waves travels with a local propagation speed along so-called *raypaths* or *rays*. In isotropic media these rays are perpendicular to the associated *wavefronts*. The rays in Figure 1.1 indicate the travel paths of different seismic waves. Three main types of seismic events are detected at the recording surface: (1) direct waves and surface waves, (2) primary events, and (3) multiple events. (1) Direct waves and surface waves correspond to waves that travel laterally (not downward) just below the surface. In the marine case the direct P-wave propagates from the source to the receivers without any reflection. In land acquisition different surface waves are traveling just below the surface (ground roll). For this thesis direct waves and surface waves are not of particular interest. (2) Primary events are caused by waves that propagate downward and upward in the subsurface and are reflected only once. These events are usually seen as the seismic signal and are used for subsurface imaging. (3) Multiple events considered in this work are caused by waves that propagate downward and upward in the subsurface and have been reflected at least three times (up, down, up). Multiples are usually seen as unwanted seismic noise masking primaries. In this work any seismic energy other than primary reflections is considered as noise. The multiple reflections can be divided in surface related multiples and interbed multiples, see Figure 1.1. The surface related multiples are reflected at least once from the free surface. The interbed multiples are those events which have all downward reflections below the surface. The order of a multiple defines the number of downward reflections along its travel path from the source to a receiver, e.g. a first-order multiple is reflected downward once, a second-order multiple is reflected downward twice, etc.

In many seismic processing methods it is assumed that the seismic wavefield includes only primary reflections. Because in most situations the multiples cannot be neglected, they should be removed in a separate processing step. Due to the fact that the subsurface model is usually unknown and that the measured primaries and multiples may strongly interfere with each other it is often very difficult to separate or even to identify a certain multiple or primary event. Thus, the goal must be the identification and maximum multiple attenuation with minimum damage to the primary wavefield.

There also exist ideas to use multiples for subsurface imaging [Helbig and Brouwer, 1993]. Due to the fact that multiples propagate through a certain part of the subsurface many times, they reveal important information about the geology in this region. Nevertheless, I follow the dominant viewpoint which considers primaries as signal and multiples as noise.

However, it should be distinguished between long-period and short-period multiples. On

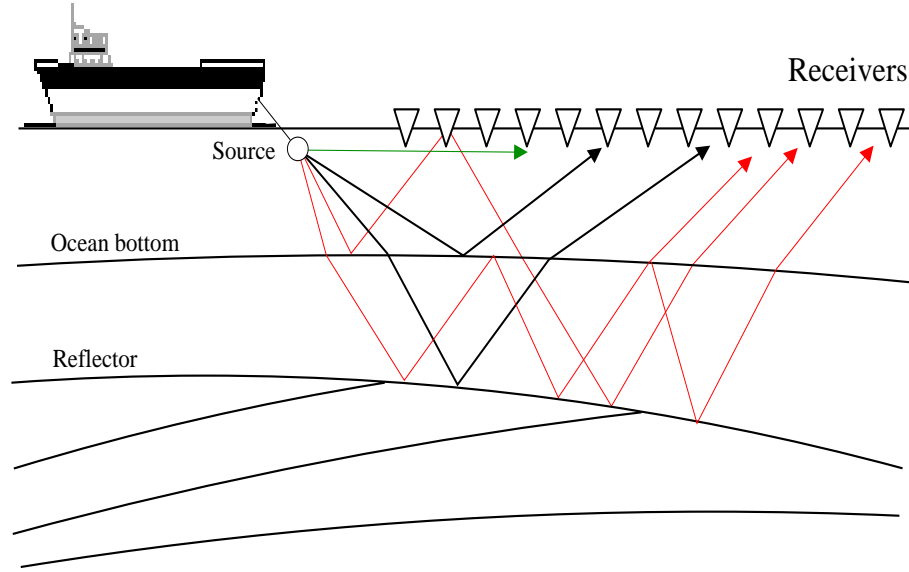


Figure 1.1: *Travel paths of different seismic events in marine data acquisition: (1) travel paths of direct P-wave (green), (2) primary reflections (black), and (3) multiple reflections (red). For isotropic media the raypaths are trajectories perpendicular to the corresponding wavefronts.*

the one hand, we try to attenuate the unwanted long-periodic multiples that are resolvable in time and have a long wavelength compared to the wavelength of a seismic wave. On the other hand, we need the unresolvable very short-periodic multiples because without them there would be a much weaker signal arriving at the recording surface. The very short-periodic interbed multiples created in the fine-layered structures of the subsurface reinforce the energy from weak subsurface reflectors that would otherwise be attenuated [O'Doherty and Anstey, 1971; Shapiro and Hubral, 1999]. The reason is that the upward reflections of many of the small-scale reverberations sum up coherently, and therefore enough seismic energy is reflected back to the recording surface, see Figure 1.2.

So far the multiple problem was explained using ray-paths which are perpendicular to the corresponding wavefront of the propagating wave. This technique is based on ray-theory and is often used in seismics. It implies that techniques based on geometrical optics can be used to separate the desired primaries from the undesired multiples. However, it is also possible to formulate the problem in a more general way using wave theory. The elastodynamic wave equation defines the propagation of seismic waves in perfectly elastic, inhomogeneous, and anisotropic media. It can be written as [Aki and Richards, 1980]

$$(c_{ijkl}u_{k,l})_{,j} + f_i = \rho\ddot{u}_i, \quad i = 1, 2, 3, \quad (1.1)$$

where u_k are the components of the displacement vector, c_{ijkl} are the components of the elasticity tensor, f the source function, ρ the density, $(\)_{,j}$ the spatial derivative in j -

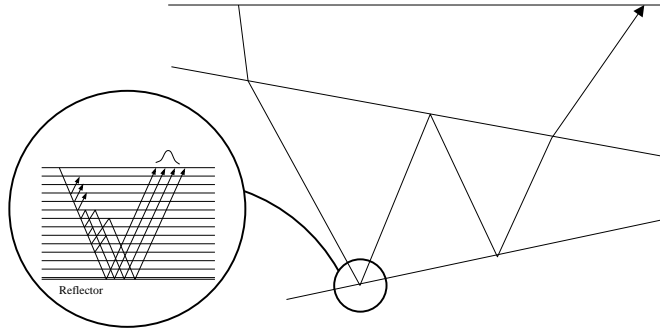


Figure 1.2: *Ray-path of a first-order interbed multiple connecting source and receiver. This multiple has a long period compared to the wavelength of the seismic wave and is considered as undesired noise. The zoomed section shows the extremely short-periodic (not resolvable in time) interbed multiples reflected within the fine-layered subsurface structure. The distance between the fine-layers is smaller than the wavelength of the signal.*

direction, $u_{k,l}$ the spatial derivative of component k in l -direction, and \ddot{u}_i is the second time derivative of the i -th component of the displacement vector. In case of an impulsive source in space and time, the solution of Equation (1.1) is called the Green's function G . So far, the Green's function can only be found analytically for simple problems with homogeneous, isotropic and unbounded media. In general the solution of Equation (1.1) has to be approximated, e.g. by a high frequency asymptotic method like ray theory [Červený and Ravindra, 1971]. The ray method can be applied to compute rays, traveltimes, and wavefronts as well as amplitudes in an effective way.

Assume that a wave propagates through an arbitrary inhomogeneous subsurface. This wave will be scattered at inhomogeneities producing a scattered wavefield. The primary part of this wavefield consists of the wavefield which is scattered only once (including the short-path multiples scattered multiply between the fine-layered structure) between source and receiver. If the wavefield is scattered again at a scatterer located at a distance larger than the wavelength of the seismic signal from the previous scattering point it belongs to the multiple part of the wavefield. If the primary and multiple wavefield could be separated the multiple problem would be solved. This equals to the problem of separating the Green's function G which solves Equation (1.1) into the Green's function for the primary wavefield G_P , the Green's function for the multiple wavefield G_M and the Green's function G_R of a part of the wavefield which includes other effects, like e.g. instrument noise, wind, etc. This can be written as

$$G = G_P + G_M + G_R. \quad (1.2)$$

Such a separation in an analytical way is only possible for simple subsurface models. These Green's functions could be split into further parts, e.g. the Green's function of the multiple wavefield G_M could be split into the surface multiple wavefield and the interbed multiple wavefield.

Each reflection of a seismic wave at a reflector reduces its amplitude. However, this does not necessarily mean that a multiple has a lower amplitude than a primary which arrives at approximately the same time. The amplitude reduction strongly depends on the reflection coefficients of the involved interfaces. For strong reflectors, like the free surface this amplitude reduction is almost zero. This is the reason why in most situations the major part of multiple energy is caused by the free surface, which has a reflection coefficient of $r_0 \approx -1$. This leads to a total reflection of an upcoming wave and to higher amplitudes of the surface related multiples compared to interbed multiples. In the marine situation often also the ocean bottom has a high reflection coefficient, which may lead to the problem that the water layer acts as a wave trap and the whole seismogram is covered by multiple events. However, such first-layer multiples are usually easy to remove because, compared to the primaries at the same zero-offset arrival time, they have a different moveout curve. Besides the surface multiples also interbed multiples may cause major problems in seismic imaging and interpretation. Their moveout is often very similar to the primary moveout so that it is difficult to identify and to separate them from each other. Especially when looking at a certain target region it might be very important to identify and to attenuate the multiple without damaging a weak primary coming for instance from an oil reservoir.

Before I propose a new method for the identification and attenuation of multiples, I give an overview about the traditional multiple attenuation methods.

1.2 Overview of multiple attenuation methods

The existing multiple attenuation techniques can be roughly divided into two broad categories: First, filtering methods that try to exploit a feature or property that differentiates a primary from a multiple and, second methods that first predict and then subtract multiples from seismic data. The latter methods are usually based on the prediction from either modeling or inversion of the recorded seismic wavefield. In modeling a seismic wavefield is calculated based on the known model. In inversion the recorded data are used to derive a subsurface model that is consistent with the data. Features being exploited by the filtering techniques can be divided in periodicity and separability, see Table 1.1. In many cases methods have aspects which are associated with both categories. All of these methods rely on certain individual assumptions, like e.g. the subsurface geometry, the acquisition parameters, etc. If these assumptions are strongly violated the considered method fails. An overview of multiple attenuation methods is given by Weglein [1999]. The most common methods are summarized in the following.

Differential moveout filtering and stacking techniques

These methods exploit the moveout differences between primaries and multiples due to their different apparent velocities. In many cases the differential moveout between primary

and multiple events is only small in a common-mid-point (CMP) gather. In order to get a better separation the data are transformed to another data domain, e.g. using a 2D Fourier transform or a τ - p transform (also called Radon transform). In the next step a filter is applied to the data in the new domain which mutes the multiples. After the inverse transform of the 'primary' data the demultiplied CMP gather is obtained. However, even if primaries and multiples can be separated in another data space there is still the problem of identification. Usually the model-dependent assumption is made that for a given zero-offset time the primary has a higher apparent velocity than a multiple.

A very common method is called velocity-analysis. The data in a CMP gather are repeatedly normal-moveout (NMO) corrected and summed (stacked) using a range of constant stacking velocity values. The result is one stacked trace for each stacking velocity. All the stacked traces calculated this way are displayed on a plane of stacking velocity versus two-way zero-offset traveltime (v - t), which is called the velocity spectrum [Yilmaz, 1987]. If the NMO-correction of an actual event was done using the correct stacking velocity, the subsequent stacking leads to a high amplitude in the velocity spectrum. On the other hand, the amplitude is low if the travel time curve, as a function of the zero-offset travel time and the stacking velocity, does not follow a seismic event. In case of interfering multiple and primary events at the same zero-offset arrival time different local amplitude maxima are obtained in the velocity spectrum. Based on a priori information an experienced interpreter can distinguish primaries from multiples. He may pick all the primary stacking velocities at the corresponding zero-offset times. These stacking velocities can be used to obtain a so called *macro-velocity-model* [e.g. Dix, 1955], which defines a velocity at each depth point in the model. The NMO-correction with the correctly picked stacking velocities, followed by common-midpoint stacking leads to a simulated zero-offset section where the amount of multiple energy is drastically reduced [Schneider et al., 1965].

If the NMO-correction is done using a stacking velocity function lying between primary and multiple velocities, the primaries are over-corrected while the multiples are under-corrected. Transforming the resulting data into the f - k domain maps the primaries and multiples into different half spaces so that the multiples can be muted. The inverse 2D Fourier transform followed by the inverse NMO-correction leads to the pre-stack data with eliminated multiples [Yilmaz, 1987].

Another velocity filtering technique uses the parabolic τ - p transform (also called: generalized Radon transform) which stacks the data along parabolic trajectories after the hyperbolic events have been transformed to parabolic events. This can be done by applying a rough NMO-correction which allows a parabolic description of the residual moveout [Hampson, 1986] or by a t^2 -stretching [Yilmaz, 1989]. In the parabolic τ - p domain the primaries and multiples are better separated than in the f - k , linear τ - p or v - t domain. This technique is also used in this work to attenuate the predicted multiples and is explained in more detail in chapter 5.

If the moveout difference between a surface multiple (or interbed multiple) and an interfering primary is big enough, the multiple can be suppressed. In many cases primaries cannot be distinguished from multiples in the v - t , f - k , or τ - p domain. Reasons might be

Filter domain	Algorithm	Feature
t	Predictive deconvolution	Periodicity
$\tau - p$	Radon transform + predictive deconvolution	Periodicity
$t - x$	Stacking	Separability
$f - k$	2D FT + reject filter	Separability
$\tau - p$	Radon transform + reject filter	Separability
$f - k$	3D FT + reject filter	Separability

Table 1.1: *Different multiple filters (modified from Weglein [1999]). The filter domain, type of algorithm, and feature being exploited is specified.*

complex moveout curves which deviate from simple hyperbolic curves or simply too small moveout differences between primaries and multiples. Especially for interbed multiples the moveout differences to primaries are often very small, so that moveout based filtering methods are likely to fail in such situations. In case of velocity inversions the stacking velocity of an interbed multiple at the same zero-offset arrival time as a primary might be even higher than for a primary. This may lead to incorrect macro-velocity models and instead of attenuating multiples they might be even amplified.

Periodicity based filtering methods

This group of methods is based on the assumption that the multiples are periodic in time while the primaries are not. This implies that the reflectors are distributed randomly in the subsurface. A very successful approach based on this assumption is called predictive deconvolution using Wiener filters [Robinson and Treitel, 1980]. It uses information of the earlier part of the seismic trace to design a filter operator which predicts and subtracts the multiples from the later part of the seismic trace. An advantage of this method is that it is computationally very fast and needs minimum user interaction. A drawback is that it assumes the reflectivity sequence to be a random series of spikes while the multiples are periodic and that the seismic trace is stationary. However, a reflectivity series is never perfectly uncorrelated, and especially at far offsets the multiples are no longer periodic anymore. To overcome the periodicity problem at far offsets, predictive deconvolution can be applied in the τ - p domain [e.g. Carrion, 1986] or in the radial trace space [Taner, 1980]. The multiples are periodic in the τ - p domain for all slowness values presuming a horizontally layered subsurface model. Predictive deconvolution works best for surface related multiples from shallow reflectors and near offset-data. For interbed multiples from deeper interfaces, which are usually not periodic in time, this method fails.

Wavefield extrapolation methods

This method extrapolates the wavefield into the subsurface and subtracts it afterwards from the data [Berryhill and Kim, 1986; Wiggins, 1988]. With this method only the water layer multiples are eliminated. This is achieved by extrapolating the measured wavefield down and up through the water layer so that primaries are becoming first-order multiples, first-order multiples become second-order multiples, etc. The adaptive subtraction of the down and upward continued data from the original data removes all first-layer multiples. A drawback of this method is that it is restricted to first-layer multiples. Furthermore the matching coefficients in the adaptive filter process have an implicit dependence on the water bottom reflectivity and the wavelet.

Feedback and inverse scattering methods

The feedback and inverse scattering methods can be used to remove surface multiples as well as interbed multiples. These methods are based on the multiple prediction within two different inversion schemes. While the feedback method is an interface-related approach, the inverse scattering method is a scattering-theory approach assuming a point scatterer model.

Surface related multiples:

In the case of surface multiple attenuation both methods are very similar and model the free surface as the generator of free-surface multiples. However, the source modeling is different in each method. One drawback is the required knowledge of the source signature which is usually found by energy minimization using the output of the multiple attenuation itself [e.g. Weglein et al., 1997]. In fact the estimation of the source signature by energy minimization includes also instrument response, algorithmic and numerical factors and other effects. This may lead to inaccuracies in multiple attenuation. Another drawback of these methods are the required near offset traces, which are very difficult to obtain in the field. The missing near offset traces can often be reasonably estimated using trace extrapolation methods. However, the current extrapolation methods fail in shallow water environment.

Interbed multiples:

In case of interbed multiples the two methods differ dramatically. The feedback method models primaries and multiples using the actual medium and interfaces that are the sources of those events. The inverse scattering method models primaries and internal multiples in terms of a reference medium (propagation in water) and scattering at every point where the properties differ from the reference model [Weglein, 1999]. These differences lead to different required a priori and a posteriori information to predict interbed multiples. The feedback model needs additionally to the source signature and near offset traces also

a macro-model description of the subsurface from the surface to a particular interbed generating interface for the downward continuation of the wavefield. The point scatterer method does not require any additional a priori knowledge of the subsurface in order to predict interbed multiples. However, as for the surface multiple attenuation, the source signature and the near offset traces have to be known.

Multiple attenuation using the neural network technique

A very recent approach is to suppress multiples by making use of the neural network technique [Calderòn-Macias et al., 1997; Essenreiter, 1999]. Essenreiter [1999] used back-propagation neural networks and self-organizing maps for the identification and attenuation of multiples. In his back-propagation neural network scheme well log data are used to train networks to attenuate multiples. The neural net generalizes from the empirically learned rules and tries to remove multiple energy on the remaining part of the data set. In case that no a priori information in form of well logs is available, self-organizing map algorithms can be used to classify and separate primaries from multiples. A number of attributes computed from the seismic data (e.g. wavefront-parameters, instantaneous attributes, wavelet attributes, velocity spectrum) are used to train the network. An advantage of this method compared to conventional filter techniques is that data information of different parameter domains is used at the same time to classify multiples and primaries. If the differences of the calculated primary attributes and multiple attributes are negligible this method fails, too. This might be especially a problem in case of interbed multiples where the differences to primaries are rather small. However, the probability to successfully suppress multiples is much higher than if only one parameter is used to classify multiples and primaries.

1.3 Multiple attenuation using kinematic wavefront parameters

The multiple attenuation methods introduced in the last section work very well if the underlying assumptions (e.g. physical model, moveout difference between multiples and primaries, etc.) are sufficiently close to reality. If these assumptions are not fulfilled the methods are likely to fail. Especially the attenuation of interbed multiples without information about the macro-velocity-model is a major problem because they often behave very similar to primaries.

In this dissertation I propose a method which uses identified multiple-generating reflections (e.g. primaries) for the prediction and attenuation of surface-related multiples and interbed multiples. Apart from the near surface velocity this method does not need any explicit subsurface information. All information needed can be obtained directly from the measured seismic data set. The idea to predict multiples using primaries is not new. However, so far only surface multiples could be predicted without information about the macro-velocity-model [e.g. Dragoset and Jericevic, 1998]. Keydar et al. [1998] introduced the idea to kinematically predict surface as well as interbed multiples using primary traveltimes without explicit information about the subsurface model. The key-point in this procedure is the simple but powerful idea that any multiple, no matter how complicate its ray-path is, can be represented as a combination of primaries. This is explained in Figure 1.3. The ray-path of the interbed multiple A_sBCDA_r from source point A_s to receiver point A_r can be also expressed as the sum of the primary ray-paths A_sBA_m (red) and the primary ray-path A_nDA_r (blue) minus the primary ray-path A_nCA_m (black). In the same manner the traveltimes of the primaries corresponding to these ray-segments can be used to predict the arrival time of the multiple. This requires that in order to predict a specified multiple event for a given source-receiver pair A_s and A_r , we need to identify the source-receiver pair of each multiple generating primary. For the interbed multiple in Figure 1.3 this problem is solved if the two intermediate points A_m and A_n are identified.

These points can be found using simple geometrical considerations: From Figure 1.3 it is evident that the emergence angles of the primary A_sBA_m (red) and the primary A_nCA_m (black) at the intermediate point A_m are identical. Further, the emergence angle of the primary A_rDA_n (blue) and the primary A_mCA_n (black) are identical at the other intermediate point A_n . By comparing the emergence angles of the involved primary wavefronts arriving at the surface, the intermediate points can be found, and the multiple arrival time can be predicted using the primary traveltimes. The essential parameter in this procedure is the emergence angle of the identified primary wavefronts which can be estimated directly from the measured data as will be explained below.

After the multiples have been predicted, they should be attenuated as good as possible without affecting primary information. This can be done in an other data space where multiples and primaries are better separated than in the original common-shot-point (CSP) gather. Landa et al. [1999c] and Zaske et al. [1999] used the kinematically predicted multiples in

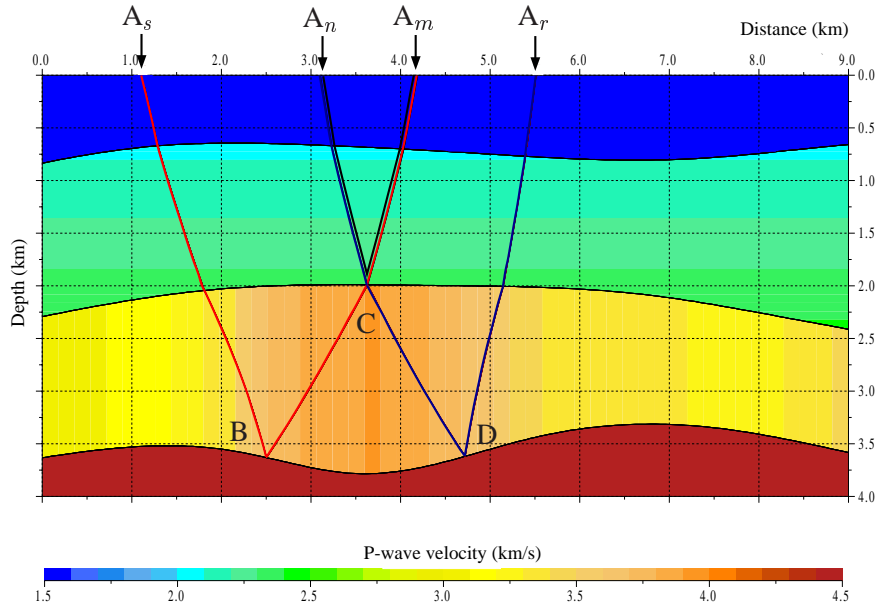


Figure 1.3: Raypath of an interbed multiple A_sBCDA_r , calculated by ray tracing, and its decomposition into the primary raypaths A_sBA_m (red), A_nDA_r (blue), and A_mCA_n (black).

order to construct a multiple model and performed the multiple attenuation in the parabolic τ - p domain.

According to the already explained strategy of the proposed multiple prediction and attenuation method the topics of the three main chapters of this thesis are:

- Estimation of the emergence angles of identified 'primaries',
- Prediction and identification of multiples,
- Attenuation of identified multiples.

In general it is not required that the identified events are really primaries. In fact also the wavefront-parameters of multiples could be used to predict other multiples. A crucial step in this procedure is the estimation of the emergence angle at each source-receiver position in all common-shot-point (CSP) gathers. Several algorithms have been suggested for the derivation of the emergence angle of a given reflected wavefront at a certain receiver position [e.g. Shultz and Claerbout, 1978]. They usually involve numerical differentiation procedures, which are known to be highly sensitive to uncertainties in the traveltimes, or slant-stack procedures, which assume a locally linear travel time approximation.

In this work, I use the CSP Homeomorphic-Imaging (HI) method for the estimation of the emergence angles [Gelchinsky, 1989; Keydar et al., 1996]. This method is based on a local hyperbolic moveout formula (called CSP HI moveout formula), which is parameterized

by the emergence-angle and the radius of wavefront curvature of a reflected wavefront in a CSP gather. The CSP HI method uses the prestack data in the CSP gather in order to calculate a simulated zero-offset section. Similarly to the stacking velocity in the velocity-analysis in the CMP gather it implies to determine the emergence angle together with the radius of wavefront curvature. This method does not require any subsurface information, only the near surface velocity is assumed to be known. Because I make use of the CSP HI moveout formula I will give a review in chapter 2.

In chapter 3 I propose two different horizon-based methods for the estimation of kinematic wavefront-parameters, which are based on the CSP HI moveout formula. The first in section 3.4 is an interactive and user-friendly procedure for the estimation of kinematic wavefront-parameters corresponding to the normal rays of a multiple-generating event, identified in a simulated zero-offset section [Zaske et al., 1999]. Assuming a *global* spherical reflected wavefront the zero-offset parameters can be used in order to calculate the emergence angles and traveltimes at all source-receiver positions. I call this method *global angle analysis*. This approach is valid as long as the moveout of a multiple generating event is of hyperbolic character. If the moveout is non-hyperbolic the estimated wavefront-parameters are inaccurate and also the multiple prediction procedure is getting inexact or might even fail.

For this reason I introduce in section 3.5 another new horizon-based wavefront-parameter estimation procedure for non-hyperbolic moveout curves. This approach uses a *local* spherical wavefront approximation and the corresponding *local* CSP HI moveout correction at each trace separately. The emergence angles and radii of wavefront curvature of an event are locally estimated at arbitrary source-receiver locations in the CSP gather. I call this method *local angle analysis*.

In chapter 4 I use the estimated kinematic wavefront-parameters to predict multiples. First, in section 4.3, the multiples are predicted kinematically. Here, only the arrival time of a predicted multiple is defined and no information about its impact on the observed wavefield, i.e. its amplitude, is given. In many situations it would be helpful for the identification and attenuation of a multiple if amplitude information were available. This is the reason why I extend in section 4.4 the kinematic prediction method straightforwardly to a dynamic prediction method, which is still valid for surface and interbed multiples.

In chapter 5, I present different methods based on the parabolic τ - p transform for the attenuation of the predicted multiples with minimum impact on the residual wavefield, i.e. all except the predicted multiples. These methods can be divided into two categories: The first perform the multiple filtering in the parabolic τ - p domain (section 5.2), the second in the offset-time (x - t) space (section 5.3). The latter method uses the parabolic τ - p transform only for multiple modeling and has the advantage that the primary wavefield, which does not interfere with the predicted multiples, is not exposed to suffer damages due to the multiple attenuation process.

The techniques for the wavefront-parameter estimation of multiple generating reflections as well as for the prediction and attenuation of multiples are illustrated using representative

synthetic data sets as well as a marine real data set. Finally, in chapter 6 I will conclude.

Chapter 2

Common-Shot-Point (CSP) Homeomorphic-Imaging (HI) method

2.1 Introduction

In this section I will review the CSP HI method. The CSP HI method was introduced by Keydar et al. [1996] and is a zero-offset stacking and imaging algorithm for multifold-covered reflection data. It belongs to the Homeomorphic Imaging methods introduced by Gelchinsky [1989]. A common element of all HI methods is to simulate a zero-offset-section using prestack data without knowing the macro-velocity-model; only the near surface velocity is assumed to be known.

In case of the CSP HI method this can be realized on the basis of the CSP HI moveout parameterization depending on kinematic wavefront attributes, such as the emergence angle and radius of wavefront curvature of a reflected CSP wavefront measured at a specified central point in the CSP gather. If this central point coincides with the source location the corresponding stacking operator can be used to obtain a zero-offset section from CSP data, like it is usually done using the NMO stacking operator in the CMP gather, which depends on the stacking velocity only.

2.2 The method

Assume that the actual subsurface, although unknown, can be described by a 2D laterally inhomogeneous isotropic layered model. In this model it is further assumed that the kinematics of body waves is well described by zero-order ray-theory [Červený, 1985]. We assume that a dense multicoverage CSP seismic experiment has been carried out for a shot-point at A_0 in Figure 2.1. We consider a fixed target reflector S in depth, as well as a fixed surface point A_0 in the CSP gather. A normal incident ray, emitted at shot-point A_0 is re-

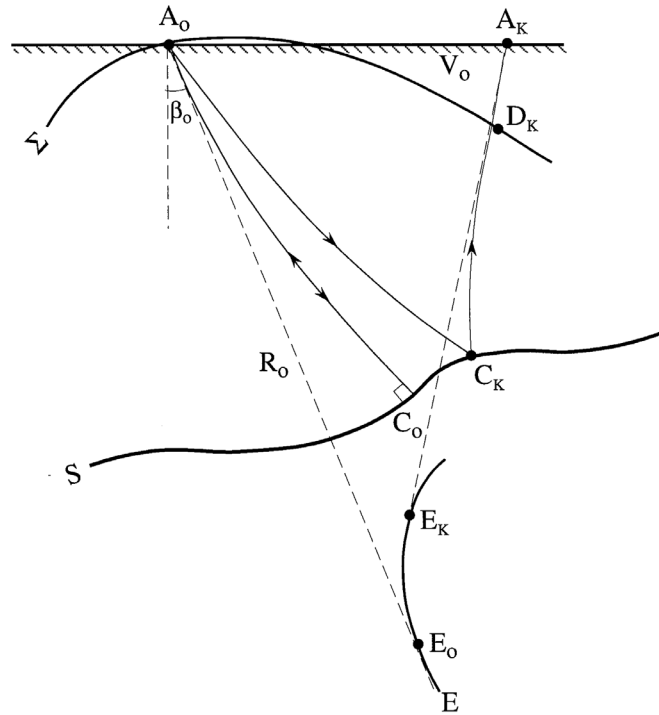


Figure 2.1: Ray diagram illustrating the CSP HI method (from Keydar et al. [1996]). From a source located at A_0 two rays are emitted in a 2D laterally inhomogeneous layered medium. The first is the normal ray $A_0 C_0 A_0$ and the second a ray $A_0 C_k A_k$ emerging at the receiver at A_K . The CSP wavefront Σ emerges at the point A_0 with the angle β_0 and the radius of wavefront curvature R_0 . An effective model consisting of a homogeneous half-space with velocity v_0 replaces the true subsurface model. The wavefront Σ can then be approximated in the vicinity of A_0 by an effective wavefront with the same radius of curvature R_0 and the same emergence angle β_0 . The center of curvature of this wavefront is located at E_0 , the Homeomorphic Image of C_0 . Depending on the source-receiver distance different wavefront approximations can be used.

flected from an interface S at point C_0 and emerges again at A_0 at a time t_0 . Let us further assume that another ray emitted at A_0 is reflected from the interface S at C_k and emerges at A_k at time t_k . The emergence angle of the normal ray at A_0 is labeled β_0 and the local radius of curvature of the CSP wavefront at A_0 is labeled by R_0 .

One of the key ideas of the CSP HI method is to substitute the true laterally inhomogeneous isotropic subsurface model with an effective model. This consists of a homogeneous half space with respect to the source A_0 in the CSP gather. We then assume the true CSP wavefront Σ to be approximated in the vicinity of the central point A_0 by an effective wavefront with the same radius of curvature R_0 and the same emergence angle β_0 . This effective wavefront relates to the propagation in an effective medium with its front caustic or evolute

(locus of the center of wavefront curvature) at E_0 . The envelope of all images constructed for the continuum of all possible central points in the CSP gather represents an effective reflector E that corresponds to S . The element E_0E_k on E is called a *Homeomorphic Image* of the reflector element C_0C_K on S [Gelchinsky, 1989].

The time moveout correction Δt_k for an arbitrary trace k corresponding to a source at A_0 and a receiver at A_k in Figure 2.1 can be described as:

$$\Delta\tau_k = \tau(A_0C_kA_k) - \tau(A_0C_0A_0) = \frac{\overline{D_kA_k}}{v_0} \quad (2.1)$$

where v_0 is the near surface velocity and assumed to be constant in the vicinity of the central point A_0 and, obviously between D_k and A_k ; $A_0C_kA_k$ is the travel path from source A_0 to receiver A_k ; $A_0C_0A_0$ is the travel path corresponding to the zero-offset traveltime; D_kA_k is the difference between the raypath $A_0C_kA_k$ emerging at receiver A_k and the raypath $A_0C_0A_0$ of the normal ray, emerging at A_0 .

By choosing a different order of approximation for the front caustic E , various parameterized relations for the segment D_kA_k can be obtained. The appropriate order of approximation depends on the distance between the source and the furthest receiver. In case of a short distance, the caustic could be placed at infinity, which implies a plane wavefront. In this case time correction can be expressed as follows, see appendix A.

$$\Delta\tau_k = \frac{(A_0A_k) \sin \beta_0}{v_0} = \Delta x_k \frac{\sin \beta_0}{v_0}, \quad (2.2)$$

where Δx_k labels the distance between the central point A_0 and a receiver A_k ; β_0 denotes the emergence angle of the reflected wavefront at the central point location A_0 ; v_0 is the near surface velocity.

For a wide class of models and moderate offsets, the wavefront Σ can be approximated by an arc of a circle with radius $R_0 = 1/K_0$ and center at E_0 . This means that the front caustic E shrinks to a point E_0 . In such a case it can be easily shown by simple geometrical considerations that the angle of emergence β_0 of the normal ray $A_0C_0A_0$ and the radius of wavefront curvature R_0 at point A_0 can be used to compute the local time moveout correction. Assuming a circular wavefront and a locally flat recording plane the following simple relation is obtained, see appendix A:

$$\Delta\tau_k = \frac{\sqrt{R_0^2 + 2R_0\Delta x_k \sin \beta_0 + \Delta x_k^2} - R_0}{v_0}. \quad (2.3)$$

Gelchinsky and Keydar [1993] and Keydar et al. [1996] suggest another wavefront-parameterization if the source-receiver distances are even higher. In this case the caustic element E could be approximated by an arc of a circle with radius ρ_0 , which leads to a

more complicated moveout formula depending on three β_0 , R_0 and ρ_0 . However, this leads to a higher computational effort and is not considered in this work.

In this work I always assume the CSP HI moveout formula corresponding to a circular wavefront approximation in Equation (2.3) which reduces, in case of plane waves ($R_0 = \infty$), to Equation (2.2), compare appendix A. Supposing that the correct CSP HI stacking parameters would be known for each time sample in the target-zone of the zero-offset section to be simulated, the prestack data could be summed up along the stacking trajectories defined by these parameters. The summation result would be placed in the corresponding time sample and a simulated zero-offset section would be obtained.

In reality the subsurface structure is not known and therefore also the stacking parameters are a priori unknown, too. Therefore, the crucial step in the CSP HI method is to find the optimal values of these parameters. This can be done by means of a coherency analysis in the CSP data using the presented moveout correction formula [e.g. Neidell and Taner, 1971]. An optimization strategy for this purpose is presented in section 3.3. Besides using these estimated optimal wavefront-parameters to get a zero-offset stacked section, these parameters form two additional sections called *anglegram* and *radiusgram* [Gelchinsky, 1989; Keydar et al., 1996; Landa et al., 1999b]. These parameter sections provide new physically sound wave attributes which may aid the interpretation, inversion, multiple attenuation, and other purposes. In this dissertation they are used for the prediction of multiple reflections.

2.3 Remarks

The CSP HI moveout parameterization for a given time sample of the image trace at zero-offset time t_0 does not involve the value of t_0 itself. It only involves the incidence angle and curvature measured in the CSP gather. Thus, all samples of a given reflection event on a specified central trace have the same kinematic wavefront-parameters within the duration of the wavelet, and hence the moveout correction is constant for the duration of the wavelet. From this fact it follows that the CSP HI method as well as all HI methods do not cause stretching phenomena, as *NMO stretch*.

While the main purpose of the CSP HI method in this chapter was to get a zero-offset stacked section using CSP data, I will use this method later on in order to determine the kinematic wavefront attributes of multiple-generating reflections, which I need for the prediction of multiples.

2.4 Relation to other stacking methods

Multifocusing (MF) [Berkovitch et al., 1994; Gelchinsky et al., 1999a,b; Landa et al., 1999b; Tygel et al., 1999] is the most general HI stacking method. Like all HI stacking

methods it belongs to the class of macro-model-independent imaging techniques, as the CRS-Stack [Hubral et al., 1998; Müller, 1999, 1998; Mann et al., 1999], and POLYSTACK [de Bazelaire, 1988; de Bazelaire and Viallix, 1994]. MF, CRS-Stack, and POLYSTACK use prestack data in order to simulate a zero-offset section without any velocity information of the subsurface other than the locally constant near surface velocity. This can be realized by a locally spherical representation of wavefronts and the corresponding moveout formulas of a non-zero-offset ray with respect to a fixed zero-offset ray. As I use the CSP HI technique in this work, I will consider especially its relation to other HI methods without any valuation of the mentioned other stacking methods.

The CSP HI method as well as the Common Reflection Element (CRE HI) [Berkovitch and Gelchinsky, 1989], Common Evolute Element (CEE HI) [Keydar et al., 1990], and Common Reflection Point (CRP HI) method are special cases of the Multifocusing method. The main difference between these methods and MF is the types of traces used to image one particular zero-offset sample. In MF and in the CRS stack method, each zero-offset trace is constructed by stacking an arbitrary number of seismic traces which need not to belong to the same CMP gather, but whose sources and receivers are within a certain vicinity of a central point location. This requires a more general moveout correction than the one used in the conventional CMP stacking method. This moveout formula depends on three kinematic wavefront parameters, namely the emergence angle β , and two radii of curvature R_{NIP} and R_N of two fundamental wavefronts [see Hubral, 1983]. Considering the kinematic properties of the normal-incidence-point wave (NIP-wave) and normal wave (N-wave), the NIP wave is a wave that originates at a point source located at the NIP at a specific interface. The N-wave is identical to the wave generated by the exploding reflector scenario.

While MF (and also CRS stack) uses an extensive distribution of traces in the vicinity of a central point (a so-called MF gather), all other methods use data of specific conventional gathers. For this reason the special cases of the MF stack (CRE, CEE, CRP and CSP HI) method can be described in terms of two stacking parameters only, while MF needs the mentioned three parameters. Also the stacking-fold of a MF stack is therefore much higher than for instance in a CMP or CSP gather. According to this fact the two-parametric methods are computationally less expensive than the three-parametric ones.

The currently existing MF moveout formula can be reduced to the CSP HI moveout formula only for the special case that the normal ray is the central ray. However, as shown in appendix A, the CSP HI moveout formula can also be applied locally with respect to any arbitrary central ray in a CSP gather. Because I need to know the emergence angle at each source-receiver position in CSP gathers, I use the CSP HI method in this work.

Chapter 3

Horizon-based wavefront-parameter estimation

3.1 Introduction

I estimate the emergence angles together with the radius of wavefront curvature using the CSP HI moveout formula, which was applied by Keydar et al. [1996] to get a simulated zero-offset section from CSP data, see chapter 2. In this case the correlation analysis is performed for all time samples within the target-zone of a zero-offset image trace. In the proposed multiple prediction method in this work the emergence angles have to be known only for certain, in the simulated zero-offset section identified multiple-generating reflections (e.g. Primaries). This reduces the calculation time dramatically.

I developed two techniques for the horizon-based search of the emergence angle and radius of wavefront curvature of multiple-generating reflections at each source-receiver location in every CSP gather along a seismic line. The difference in the methodology between these methods is that the CSP HI moveout formula is applied with respect to different receiver locations in the CSP gather and that they are either based on a *local* or on a *global* circular wavefront approximation as explained in detail in sections 3.2, 3.4, and 3.5.

In section 3.3 I present the optimization procedure used in the correlation analysis for the search of the two unknown kinematic wavefront-parameters at a specified source-receiver distance and traveltime in the CSP gather. In section 3.6 I will summarize the advantages and drawbacks of the introduced methods.

3.2 Local and global circular wavefront approximation

In Figure 3.1 the CSP moveout formula is applied with respect to different central points in the same CSP gather. In Figure 3.1a the central point coincides with the source location

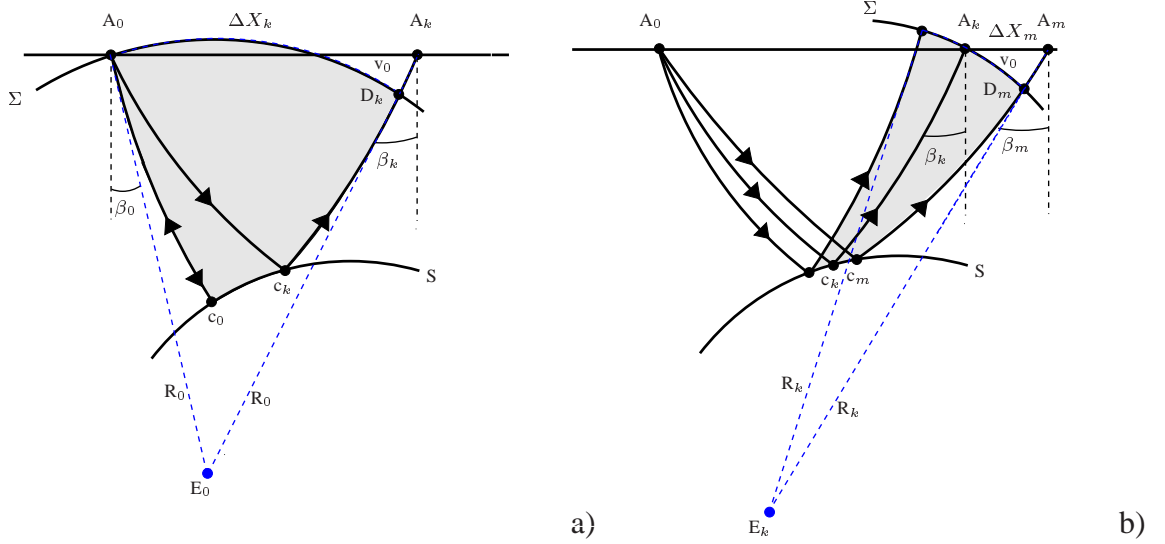


Figure 3.1: Ray diagram illustrating the estimation of the emergence angle and the radius of the wavefront-curvature corresponding to the normal ray and an arbitrary ray in the same CSP gather. a) Two rays are emitted from the source point A_0 . The wavefront emerges at A_0 with an angle β_0 and at A_k with an angle β_k . The radius of this globally spherical wavefront is R_0 . The moveout correction and the offset dependent emergence angle β_k are functions of β_0 and R_0 , the source-receiver distance Δx_k , and the near surface velocity v_0 . b) Same situation as in a) in the local vicinity of an arbitrary central ray. In this case the local moveout correction $\Delta \tau_m$ and the emergence angle β_m are functions of β_k , R_k , source-receiver distance Δx_m , and the near surface velocity v_0 .

and in Figure 3.1b the central point is located at an arbitrary receiver in the CSP gather.

Lets start with Figure 3.1a, which shows a reflected CSP wavefront Σ emerging at the zero-offset location A_0 at an angle β_0 . This wavefront can be approximated in the vicinity of the source A_0 by a fictitious circular wavefront with radius of curvature R_0 and the same emergence angle β_0 . If the circular wavefront approximation holds and the near surface velocity is constant within the source-receiver distance Δx_k it follows from simple geometrical considerations that the moveout correction $\Delta \tau_k$ at a receiver location A_k can be expressed as a function of the emergence angle and the radius of wavefront curvature of the normal ray emerging at point A_0 , see appendix A:

$$\Delta \tau_k = \frac{\sqrt{R_0^2 + 2R_0 \Delta x_k \sin \beta_0 + \Delta x_k^2} - R_0}{v_0}, \quad (3.1)$$

where β_0 and R_0 denote the emergence angle and the radius of wavefront curvature of the reflected CSP wavefront at A_0 , v_0 the near surface velocity and Δx_k the offset between the source at A_0 and the receiver at A_k .

In order to determine the unknown wavefront-parameters R_0 and β_0 a semblance maximization procedure, similar to conventional velocity analysis, has been developed. It is applied in the CSP gather along the traveltime curve defined by the zero-offset travel time and the moveout correction in Equation (3.1) and is explained in section 3.3. Once the optimal emergence angle and the radius of wavefront curvature corresponding to the normal ray, β_0 and R_0 , have been estimated for a multiple-generating reflection, it is possible to obtain the angle of emergence β_k and the radius of wavefront curvature R_k at an arbitrary surface point A_k with offset Δx_k using the following expressions, which follow again from the circular wavefront assumption within the furthest considered source-receiver distance, see appendix A:

$$\sin \beta_k = \frac{\Delta x_k + R_0 \sin \beta_0}{\sqrt{R_0^2 + 2R_0 \Delta x_k \sin \beta_0 + \Delta x_k^2}}, \quad (3.2)$$

$$R_k = \sqrt{R_0^2 + 2R_0 \Delta x_k \sin \beta_0 + \Delta x_k^2}. \quad (3.3)$$

I call this way of estimating the emergence angles and radii of wavefront curvature at each source-receiver position *global angle analysis* and *global radii analysis*, respectively, because a *globally* circular wavefront is assumed in order to extrapolate the wavefront-parameters of the normal ray to arbitrary offsets.

Another situation is shown in Figure 3.1b. Now the same moveout correction formula is applied with respect to an arbitrary central ray emerging at receiver position A_k . In this case, only a *locally* circular wavefront is assumed and the local moveout correction $\Delta \tau_m$ at a point A_m can be expressed as follows:

$$\Delta \tau_m = \frac{\sqrt{R_k^2 + 2R_k \Delta x_m \sin \beta_k + \Delta x_m^2} - R_k}{v_0}. \quad (3.4)$$

Using the local stacking operator defined by Equation (3.4) the emergence angles β_k can be estimated together with the radii R_k directly at the receiver position A_k , provided that the traveltime t_k of the multiple-generating event is known at this receiver location. I call this method *local angle analysis*.

As long as the circular wavefront assumption holds, the wavefront-parameters corresponding to this arbitrary central ray emerging at surface point A_k can be used to calculate the emergence angles and radii of wavefront curvature of the reflected CSP wavefront at a surface point A_m in the local vicinity of the central point A_k using Equations (3.5) and 3.6.

$$\sin \beta_m = \frac{\Delta x_m + R_k \sin \beta_k}{\sqrt{R_k^2 + 2R_k \Delta x_m \sin \beta_k + \Delta x_m^2}}, \quad (3.5)$$

$$R_m = \sqrt{R_k^2 + 2R_k \Delta x_m \sin \beta_k + \Delta x_m^2}. \quad (3.6)$$

Depending on a local or global circular wavefront approximation different implementations are suggested, which are presented in section 3.4 and section 3.5. They can be summarized as follows:

Method I: Global angle analysis for hyperbolic moveouts:

1. Estimate β_0, R_0 at the zero-offset location of a specified event.
2. Use β_0, R_0 in order to calculate the emergence angles β_k at arbitrary source-receiver distances assuming a globally circular wavefront between the source at A_0 and the considered receiver at A_k in the CSP gather.

Method II: Local angle analysis for non-hyperbolic moveouts:

1. Estimate β_k, R_k of a specified event at each receiver location A_k separately assuming a locally circular wavefront only.

3.3 Optimization strategy

In the previous sections I presented a time correction formula which can be applied with respect to an arbitrary receiver location A_k used as a central point in a CSP gather. This formula depends on the two wavefront-parameters β_k and R_k of an arbitrary central ray emerging at this central point A_k . Since the subsurface structure is generally not known the correct wavefront-parameters β_k and R_k are also unknown a priori. In order to determine β_k and R_k at an arbitrary receiver A_k at a given time t_k , the following simple strategy could be applied:

Try all possible combinations of β_k and R_k . Each parameter set defines a stacking trajectory $t_k + \Delta\tau_m(\beta_k, R_k)$ in the CSP gather. Perform a coherency analysis for these curves in the CSP gather. The maximum coherency gives the optimal parameter set. It is optimal in the sense that its associated travelttime curve fits an event in the prestack data in the best way.

This approach has several drawbacks: First of all, the possible parameter space is continuous and has a range from $-\infty$ to $+\infty$ for the searched radius, and a range between -90 and $+90$ degrees for the searched emergence angle. Especially in case of the radius this scanning procedure is very time consuming and computationally expensive even if the search range is limited, and at the end one cannot be sure that the optimal stacking parameters are found. If the grid is too sparse one might miss the optimal parameter set. If it is too fine the computational effort is enormous.

The problem to solve is a typical problem of optimization. It is necessary to find the two unknown parameters that maximize the objective function. This is done by evaluation of a coherency measure (e.g. semblance) in the prestack CSP gather along the travelttime curve

defined by the stacking operator. Global optimization is, in general, a non-trivial task and the convergence depends on the complexity of the objective function, e.g. the objective function can show a smooth or non-smooth behavior and it can be uni-modal or multi-modal¹. The probability to find the global maximum is the higher the less local maxima exist and the smoother the coherence functional is. A priori information might help to reduce the global optimization problem to a local optimization problem. In this case the search can be limited to a certain range of the unknown imaging parameters and the estimated local maximum would be identical to the global one.

In order to find the optimal stacking parameters, namely the emergence angle β_k and radius of wavefront curvature R_k of an event at a certain receiver position A_k (see Figure 3.1b) and time t_k in a CSP gather, I suggest the following optimization strategy:

1. Specify the central point at receiver position A_k in a CSP gather. For $k = 0$ the central point may coincide with the source location A_0 . Specify a time sample corresponding to a seismic event at the trace measured at receiver A_k . Specify the aperture Δx_{max} , defined by the number of traces used in the correlation analysis.
2. Specify an a priori range of the searched emergence angle and an angle-increment $\Delta\beta_k$ used for the angle scan.

$$\beta_k^{min} \leq \beta_k \leq \beta_k^{max} \quad (3.7)$$

3. For a given emergence angle $\hat{\beta}_k$, starting from β_k^{min} defined in step 2, the search of the optimal radius value \hat{R}_k is limited by \hat{R}_k^{min} and \hat{R}_k^{max} using the following equation which is derived in appendix B.2.

$$\hat{R}_k^{min}, \hat{R}_k^{max} = \pm \frac{\cos^2 \hat{\beta}_k \Delta x_{max}^2}{2v_0 \Delta t \epsilon}, \quad (3.8)$$

$$\hat{R}_k^{min} \leq \hat{R}_k \leq \hat{R}_k^{max}, \quad (3.9)$$

where Δx_{max} is the used aperture, $\hat{\beta}_k$ the currently specified emergence angle, Δt is the time sampling rate, and ϵ an adjustment parameter.

4. For a given emergence angle $\hat{\beta}_k$ the optimal radius of wavefront curvature \hat{R}_k is found by applying a non-linear 1D local optimization method, namely the golden section search, see section B.1. This implies to find the maximum coherence value for traces stacked along the trajectories defined by the local time correction in Equation (3.4) within the predefined aperture Δx_{max} in step 1. The search of the radii is limited by \hat{R}_k^{min} and \hat{R}_k^{max} , defined in step 3. The highest coherence value \hat{S}_k and the corresponding parameter duplet $\hat{\beta}_k$ and \hat{R}_k are stored.

¹uni-modal functions are functions with one extremum only.

5. Update angle $\hat{\beta}_k$ by a given increment $\Delta\beta_k$ within the given range in step 2 and repeat step 3 to step 5 until β_k^{max} is reached.
6. The maximum coherence value S_k of all stored coherence values \hat{S}_k in step 4 defines the searched optimal wavefront-parameters β_k and R_k at the time t_k at the receiver location A_k .

The scanning of the emergence angles within a predefined range using a reasonable discretization instead of a local optimization method increases the probability to distinguish between local and global maxima in a multi-modal but smooth coherency functional. A drawback is that even in case that we are close to the desired absolute maximum, the accuracy of the searched parameters might be still limited by the discretization of the emergence angles. However, the accuracy could be increased in a second step by performing a local optimization in the vicinity of the initial estimation results. In this case the local search procedure would lead to the global maximum. However, there are also cases where even the global maximum does not belong to the desired event. Such more complicated situations are considered in section 3.5.

In the following I present different implementations for the horizon-based estimation of kinematic wavefront-parameters at each source-receiver location. The choice of the method depends on the complexity of the data set. As the coherency measure I use the semblance criterion. This is defined by the ratio of the output to the input energy of an M-channel signal f within a time gate of length N [Neidell and Taner, 1971]:

$$S = \frac{\sum_{j=1}^N \left\{ \sum_{i=1}^M f_{i,j(i)} \right\}^2}{M \sum_{j=1}^N \left\{ \sum_{i=1}^M f_{i,j(i)}^2 \right\}}. \quad (3.10)$$

Other coherency criteria can be considered [see Gelchinsky, 1989].

3.4 Hyperbolic moveouts

In case of traveltime curves of hyperbolic character it is reasonable to use the global angle analysis method which is explained in detail in this section.

The method involves in the first step the search of the wavefront-parameters corresponding to the normal ray of a multiple-generating primary reflection and in the second step the calculation of the emergence angles at each offset using the normal ray parameters. In this case the crucial part is to estimate the wavefront parameters corresponding to the normal ray at the zero-offset location of an identified event in all CSP gathers along a seismic line. I suggest a method which can be applied in an automatic or interactive way in case of the horizon-based wavefront-parameter estimation [Zaske et al., 1999].

3.4.1 Global angle analysis

After a multiple-generating primary has been identified in a zero-offset stacked section and its zero-offset traveltimes have been picked along the seismic line, the wavefront-parameters corresponding to the normal rays are estimated. The fact that the search of the unknown parameters is organized along specified horizons allows to perform a convenient, interactive procedure similar to Horizon-Velocity-Analysis (HVA). The difference of this approach is that the search is done, in fact, for two unknown parameters β_0 and R_0 instead of only one parameter v_{stack} in the case of HVA. I estimate the two unknown parameters by maximizing the semblance correlation measure, calculated in the CSP gather along the traveltimes curve defined by the picked zero-offset traveltimes and the moveout formula in Equation (3.1).

The implementation of this parameter estimation procedure is based on the correlation of the signal in the observed seismic traces similar to the optimization strategy explained in section 3.3. For a given emergence angle β_0 of the normal ray at a specified shot-position the optimal radius of wavefront curvature R_0 is found automatically by applying the golden section search, which maximizes the semblance correlation measure. This step is repeated for all possible emergence angles and optimal parameters are chosen corresponding to the semblance maximum. Such an approach leads to correct wavefront-parameters if the search is done for a relatively strong coherent primary reflection.

A basic problem is that automatic procedures optimally stack useful signal as well as noise, especially spatially correlated noise. In addition, the interference between different waves due to conflicting dips, multiples or coherent noise can lead to problems in the correct estimation of the unknown parameters of a specified primary. In such cases, the correlation measure as a function of search parameters might not be uni-modal, thus requiring a global optimization strategy. Nevertheless, even the global maximum might be related to interfering events or noise rather than to the signal. For instance, strong coherent multiple reflections may show higher correlation values than weak primary events. In the interactive velocity analysis such an ambiguity is resolved manually by picking the correct maxima on the basis of a-priori velocity information. Zasko et al. [1999] address such problematic situations in the case of the horizon-based wavefront characteristics estimation and suggest an interactive procedure. This procedure consists of picking the optimal parameter combination between the emergence angle β_0 and the radius of wavefront curvature R_0 of the normal ray, along a specified horizon (identified in the simulated zero-offset section) and is explained in the following.

Using the search procedure described in section 3.3, the semblance as a function of angle and shot-position is defined for all possible angles, when the value of the radius R_0 for each angle is chosen corresponding to the maximum semblance of the non-linear one-parameter golden section search. The results of such a calculation can be displayed in a semblance panel, where the horizontal axis denotes the shot-position and the vertical axis the emergence angle, see Figure 3.4a. In such a semblance panel the optimal emergence angles as a function of shot-position can be picked similar to the stacking velocity v_{stack} in HVA.

As mentioned above an optimal radius R_0 is associated with each picked angle in the semblance plot, see Figure 3.4b. This gives additional information for the interpreter to decide if the 'pick' was reasonable. As usual, the smoothness of parameters as well as a-priori information are leading criteria in this interactive procedure. In cases of interfering events, like e.g. in conflicting dip situations the semblance functional is multi-modal. By picking of reliable parameters along the horizon, based on a priori information, such ambiguity problems can be solved. The parameters in between the picks can be interpolated.

In the next step I extrapolate the wavefront-parameters corresponding to the normal ray β_0 and R_0 to arbitrary offsets using Equation (3.2), which is based on a global circular wavefront approximation within the maximum considered source-receiver distance.

The proposed global angle analysis method for the horizon-based estimation of the time t_k , and emergence angle β_k at each source-receiver distance in the CSP gathers is implemented according to the following flowchart:

1. Input: CSP/CRP gathers and simulated zero-offset section.
2. Identifying and picking of zero-offset traveltimes of a multiple generating event in the zero-offset section.
3. Estimation of emergence angle and radius of wavefront curvature for the normal rays of the identified event in all CSP gathers using the explained horizon-based (interactive or automatic) picking procedure.
4. Calculation of the emergence angles of the wavefronts at each source-receiver distance in all CSP gathers using the corresponding zero-offset parameters.
5. Output: Emergence angle and traveltimes of an event at each source-receiver distance in all CSP gathers along the seismic line.

The following synthetic example illustrates the proposed method.

3.4.2 Synthetic example: four layer model

I use the four-layer model shown in Figure 3.2 which includes dipping interfaces to demonstrate the proposed *global angle analysis* method. According to this model one hundred CSP gathers have been calculated using finite difference (FD) modeling. The receiver-spacing and shot-increment is 20 m. Each CSP gather consists of 50 receivers. The sampling rate is 4 ms. Due to FD modeling artifacts the data include a high level of correlated noise.

The emergence angles are calculated using the global angle analysis method as described in the previous section. In the first step the three multiple-generating primaries are identified

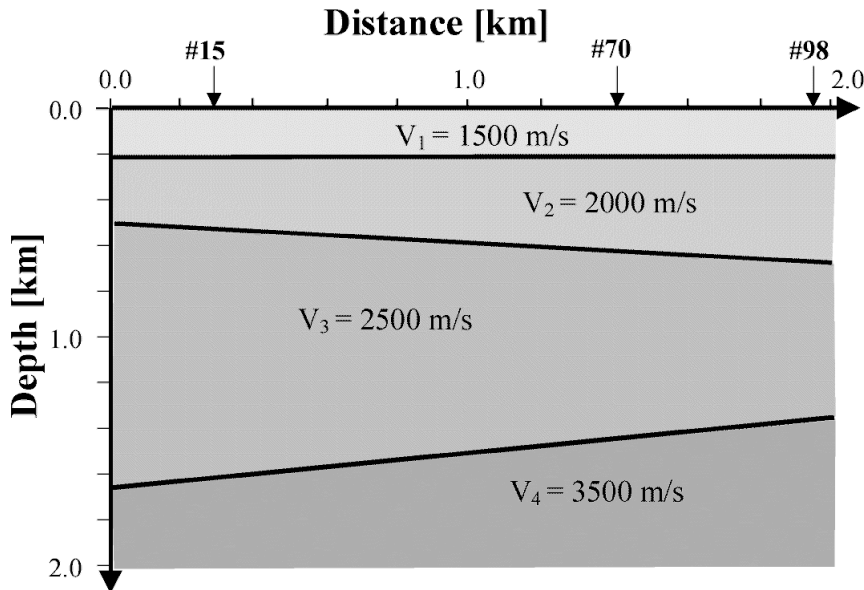


Figure 3.2: A four-layer model with dipping interfaces. According to this model one hundred CSP gathers have been calculated using FD modeling. The receiver spacing and offset increment is 20 m. Each CSP gather consists of 50 traces. The sampling rate is 4 ms. The arrows denote three shot-positions (#15, #70, #98). The zero-offset section and another CSP gather corresponding to the shot-position at the distance 1.0 km is shown in Figure 3.3.

and picked in a zero-offset section as shown in Figure 3.3a. In this case the zero-offset section consists of all modeled zero-offset traces along the seismic line, no zero-offset stacking was done but a strong automatic gain control (AGC) was applied in order to enhance the weaker multiple amplitudes. The picked traveltimes correspond to the traveltimes of the normal rays, emerging at the zero-offset locations along the seismic line. In the second step, I perform the wavefront parameter search in all CSP gathers along the seismic line at the picked zero-offset traveltimes of the normal rays. Figure 3.3b shows one CSP gather as an example, where the moveout curves of the three primaries are defined by the optimal CSP HI stacking operators (best semblance) and are parameterized by the zero-offset wavefront parameters.

The optimal zero-offset wavefront parameters are estimated using the explained horizon-based procedure, which can be applied automatically or interactively along the picked zero-offset traveltimes of the multiple-generating events. This procedure consists of displaying the semblance correlation measure as a function of shot-position and emergence angle of the normal ray, and picking of the optimal emergence angles as a function of shot-position.

The situation is shown in Figure 3.4a: Each semblance value in this panel corresponds to a certain combination of emergence angle and radius of wavefront curvature. This means that each picked emergence angle in this semblance panel has an associated radius of wavefront curvature, which is shown in Figure 3.4b.

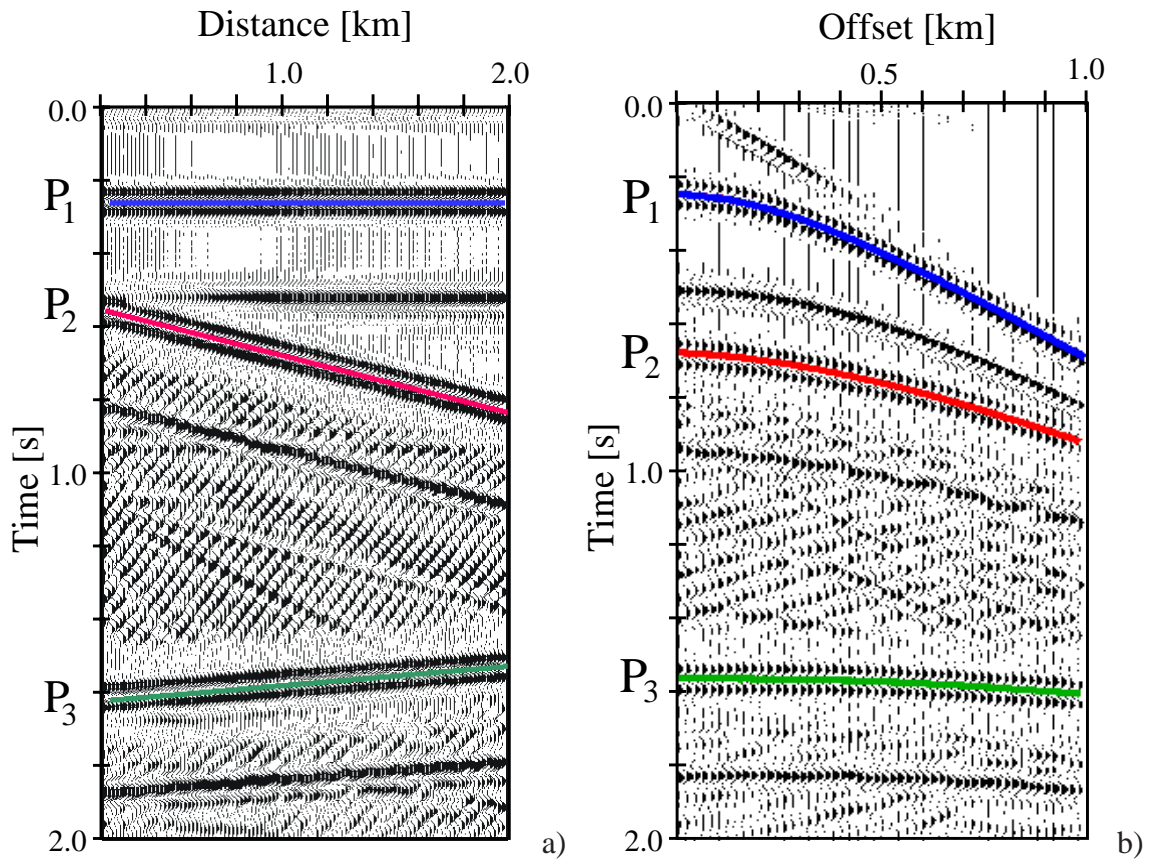


Figure 3.3: a) Zero-offset section of the data set calculated by FD modeling using the model in Figure 3.2. A strong automatic gain control (AGC) was applied in order to enhance weak multiples. The multiple-generating primaries are identified and picked along the seismic line, as shown in different colors. The picked zero-offset traveltimes are used to estimate the kinematic wavefront parameters in the CSP gathers. b) One CSP gather with the shot location at $X_0=1$ km in the model shown in Figure 3.2. The three primary move-out curves correspond to the optimal CSP HI stacking operators (best semblance) and are parameterized by the zero-offset wavefront parameters.

The picking can be done in an automatic or manual manner. The smoothness of the parameters as well as a-priori information are leading criteria for the picking. The advantage of manual picking in a semblance panel like in Figure 3.4a is that it can resolve ambiguity problems in cases, where the absolute maximum for a certain shot-position is not the desired one and belongs e.g. to strong coherent noise or a multiple, which could give a higher semblance maximum than a desired weak non-coherent primary. Also conflicting dip problems could be solved using this method. In the simple case shown in Figure 3.4a automatic picking according to semblance maxima was chosen (black line). The radii corresponding to these picks are shown in Figure 3.4b.

The results of such a horizon-based parameter-estimation for all three multiple-generating reflections, identified in the zero-offset section are shown together with the analytic values in Figure 3.6. The differences are mainly due to the discretization interval of the scanned

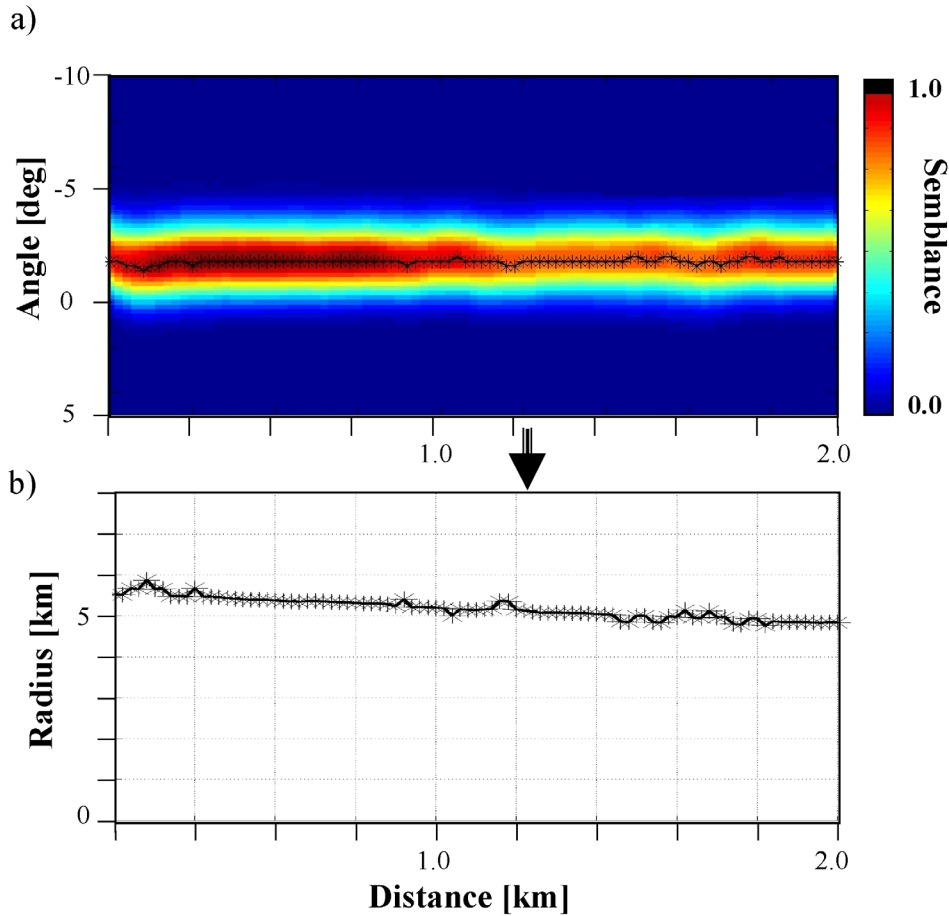


Figure 3.4: Illustration of the interactive horizon-based parameter-estimation along the picked zero-offset times of the third multiple-generating reflection (P_3) in a semblance panel as function of shot-position and emergence angle β_0 of the normal ray. Each semblance value is calculated automatically and corresponds to a combination between the two parameters, angle β_0 and radius R_0 . Picking based on a priori information can resolve ambiguity problems in case of undesired semblance maxima (see text). Each picked angle in a) belongs to a certain radius, which is shown in b). In this simple case automatic picking according to the maximum semblance value has been chosen in a), which gives the corresponding radii in b). Figure from [Zaske et al., 1999].

angles used for the search and due to step-like (instead of smooth) interfaces used for FD modeling. The step-like discretization of dipping reflectors leads to step-like variations in wavefront-parameters. This effect can be observed in case of the second interface (see P_2 in Figure 3.6).

Using the estimated parameters of the normal ray R_0 and β_0 in Equation (3.2) gives the extrapolated emergence angle of the primary wavefronts from the three interfaces at each source-receiver distance. Figure 3.5 shows as an example the results for one CSP gather

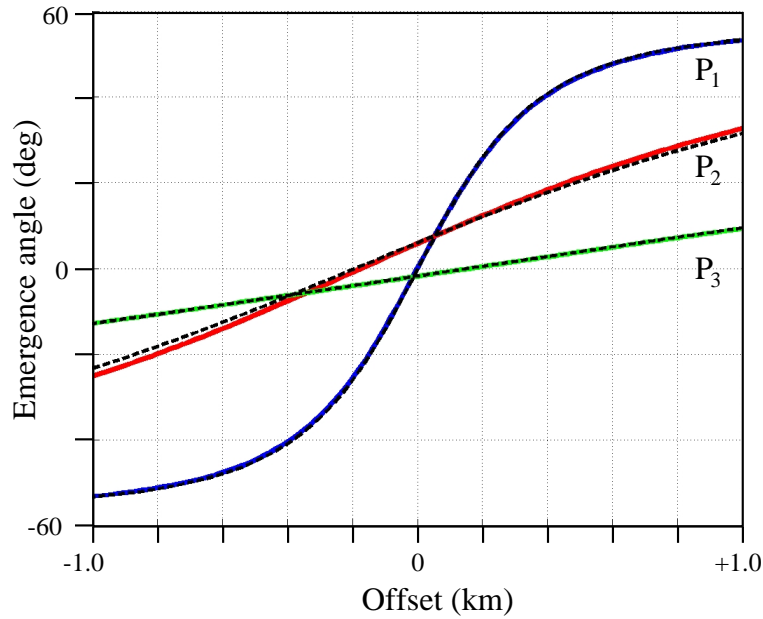


Figure 3.5: Offset-dependent emergence angles of the primary wavefronts in one CSP gather. The angles have been calculated using the estimated parameters R_0 and β_0 of the normal ray for extrapolation in Equation (3.2). The analytic (black) and the estimated (colons) results for the primaries P_1 , P_2 and P_3 essentially coincide.

with especially large differences between the analytic and estimated wavefront-parameters of the normal ray, shown in Figure 3.6. The extrapolated values essentially coincide with the analytic results. Only for the second reflector the differences at far offsets are larger due to the already mentioned larger differences in β_0 and R_0 . The analytic wavefront-parameters have been determined by forward calculation using the known subsurface model, see appendix C.

The estimated emergence angles and the traveltimes of this example at each source-receiver position in all CSP gathers are used later on in the multiple prediction process in section 4.3.2.

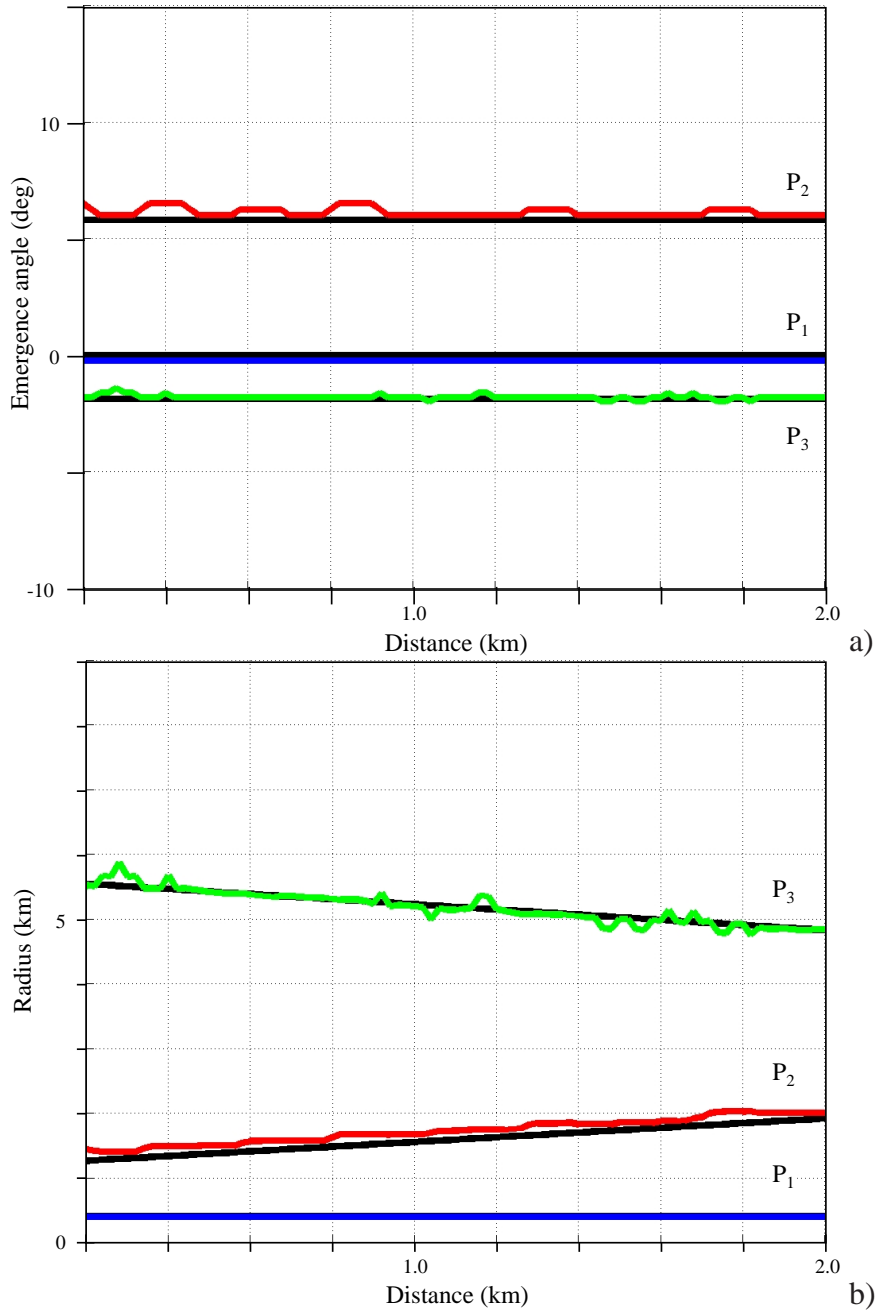


Figure 3.6: Results of the horizon-based parameter-estimation for the multiple-generating primary reflections P_1 , P_2 and P_3 identified in the zero-offset section (see Figure 3.3), together with the analytic results. a) estimated (colored) and analytic (black) emergence angles (β_0), and b) estimated (colored) and analytic (black) radii of wavefront curvature (R_0).

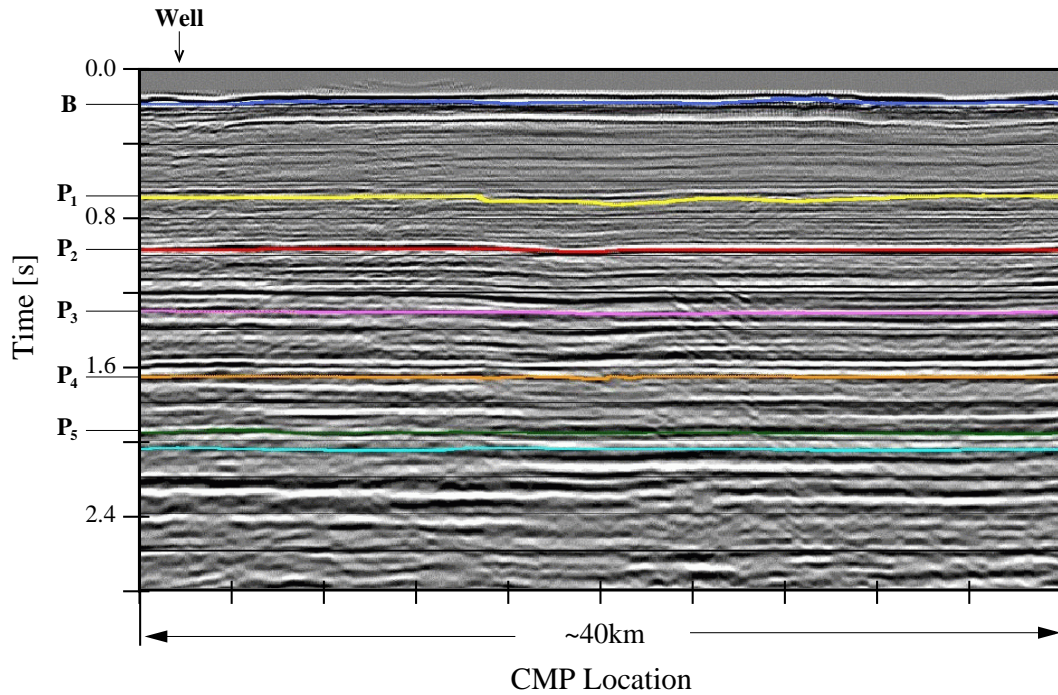


Figure 3.7: a) Stacked section of a marine data set with six identified and picked horizons. The estimation of wavefront-parameters was done for these multiple-generating reflections. The light blue horizon indicates a target region of special interest.

3.4.3 Real data example: marine data set

In this section the *global angle analysis* is applied to a marine real data set which consists of about 1000 CSP gathers. A stacked zero-offset section of this data set is shown in Figure 3.7. Six multiple generating reflections (possibly primaries) have been identified and picked by an interpreter. They are shown in different colors and labeled as B, P₁, P₂, P₃, P₄, and P₅. Also shown in light blue is a potential target-zone, which is of particular interest.

In the first step the wavefront-parameters associated with the normal rays emerging at the zero-offset location are estimated using the picked zero-offset traveltimes of the six multiple generators. Figure 3.8a shows the estimated radii of wavefront curvature at the zero-offset location along the seismic line. The corresponding angles of emergence for the normal rays are approximately zero for all multiple-generators and are not shown. The stars in Figure 3.8 denote radii of wavefront curvature estimations calculated from vertical seismic profiling (VSP) data [Sheriff, 1991] obtained in a borehole. The maximum differences between the horizon-based estimation and the results based on the VSP measurements are about 10%. This supports the rightness of the horizon-based estimation results.

In the next step the zero-offset wavefront-parameters have been used in Equation (3.2) to calculate the emergence angles at each source-receiver position in all CSP gathers. The results are shown for one CSP gather in Figure 3.8b.

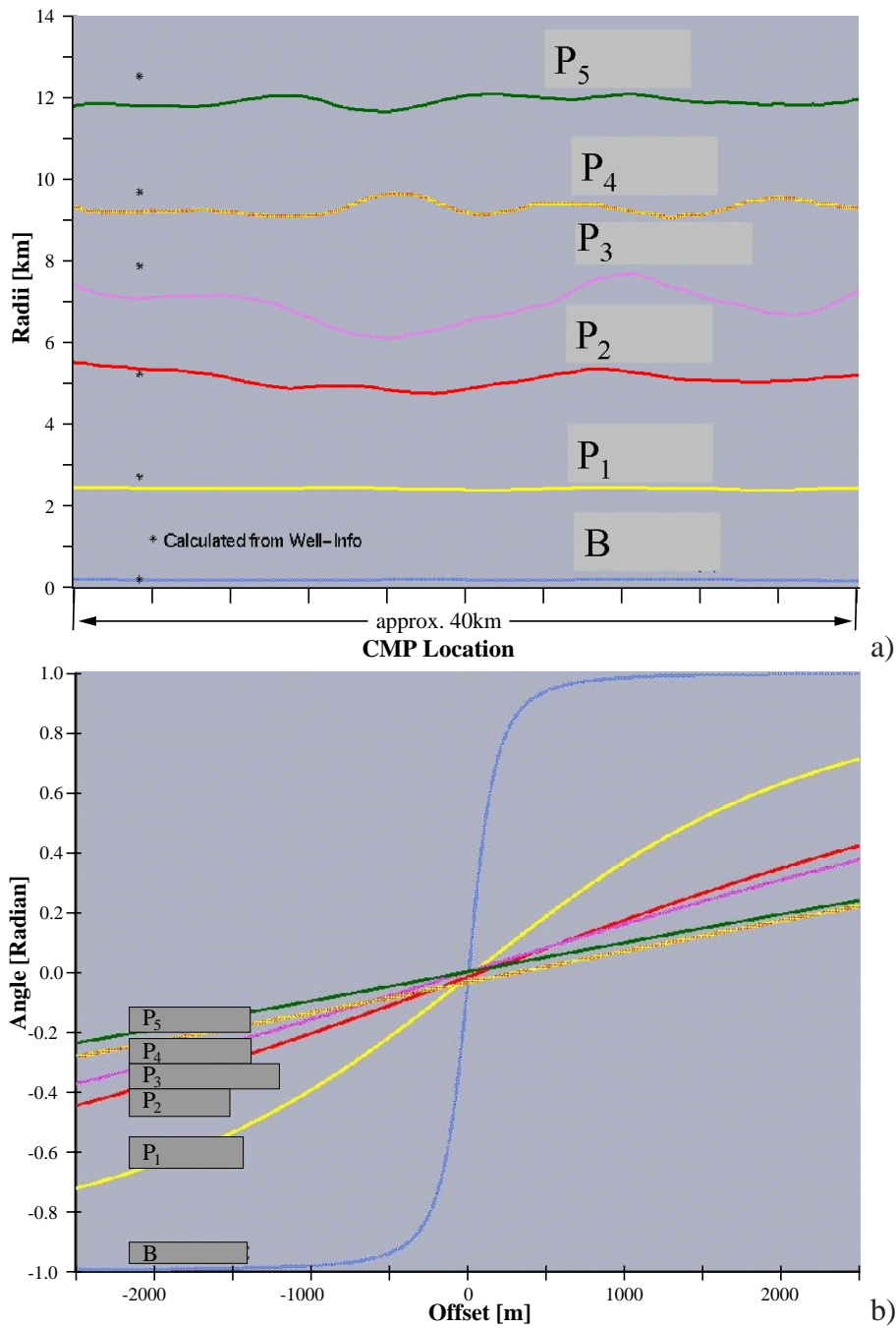


Figure 3.8: a) Estimated radii of wavefront curvature of the six identified multiple generators at the zero-offset locations along the seismic line. The stars denote radii calculated from well information. b) Emergence angles for one CSP gather. Calculated using the zero-offset wavefront-parameters.

The estimated emergence angles at each source-receiver position in all CSP gathers are used later on in the multiple prediction process in section 4.3.3.

3.4.4 Results

I presented a new method for the horizon-based wavefront-parameter estimation. This method can be used in order to estimate the emergence angle and radius of wavefront curvature of the normal ray at the zero-offset location or in any common-offset section, provided that the traveltime of an identified event in this common-offset section is known along the seismic line. In this work I use the proposed procedure only for the zero-offset wavefront-parameter estimation using the zero-offset traveltimes, picked in a stacked section.

Compared to its automatic version the interactive application of this method has several advantages in case of more complicated wavefields. It improves the ability to distinguish between local and global semblance maxima and allows to solve for instance dip problems of interfering events.

In order to get the emergence angles at each source-receiver position the estimated wavefront-parameters at the zero-offset location can be extrapolated using a global circular wavefront approximation between the source point and the furthest considered receiver position. This method is called *global angle analysis* and implies that only events with approximately hyperbolic moveout curves can be correctly described. In case of strongly non-hyperbolic moveouts this procedure gives inaccurate results.

3.5 Non-hyperbolic moveouts

In case of strongly non-hyperbolic traveltime curves, which correspond to non-spherical reflected CSP wavefronts, the global angle analysis cannot be applied. The reason is that the moveout of such an event cannot be correctly parameterized at all offsets by only a single set of wavefront-parameters, like e.g. the zero-offset wavefront-parameters t_0 , β_0 , and R_0 . I propose a method which uses moveout measurements obtained by local coherency operators. Local stacks provide more detailed information on the moveouts in the data than imaging operators which measure the coherency of the data for all offsets.

Sword [1987] presented a method for estimating velocity from data transformed with locally slant stack. Biondi [1992] used beam stacks instead of local slant stacks, which are local hyperbolic or parabolic stacking operators. The curved stacking trajectories of beam stacks, depending on v_{stack} , better approximate the hyperbolic moveouts in the data than straight trajectories of local slant stacks. This improves the resolution of the estimated parameters. In this section, I present a parameter estimation technique which uses the local application of the hyperbolic CSP HI moveout formula in the vicinity of each receiver (Figure 3.1) in order to optimally approximate the local moveout of a seismic event.

3.5.1 Local angle analysis

In order to estimate the emergence angle directly at each source-receiver distance, I choose each receiver location separately as a central point and apply the CSP HI traveltime correction formula in its local vicinity. This situation is shown in Figure 3.1b. Using this approach the emergence angle along any kind of smooth traveltime curve can be estimated provided that the traveltimes are given. Even changes in the sign of the emergence angle and wavefront curvature can be estimated along the traveltime curve in the CSP gather and be used for the later multiple prediction. In order to perform a local wavefront-parameter estimation, using the already introduced moveout correction formula in Equation (3.4) at each source-receiver pair the traveltime of a specified event along its moveout has to be known. One way to solve this problem would be to pick the traveltimes along the events moveout starting from the zero-offset traveltime using a standard automated picking routine or even by manual picking.

I suggest another procedure, which needs only the zero-offset traveltime of an identified multiple-generating event (picked in a stacked section) to be known. Starting from zero-offset the traveltime along the moveout is predicted trace by trace using the traveltime and the estimated wavefront-parameters of the previous traces. I can also predict the 'expected' emergence angles and radii of wavefront curvature for the next traces as long as the local circular wavefront approximation holds. The mean values between many predicted wavefront-parameters for a certain receiver point are used as a first guess in the search procedure. This might be helpful to stabilize the procedure, e.g. if there exist interfering events or the signal to noise ratio is too low at a specified receiver position, the predicted parameters at this receiver can be used instead. A flow chart of the implementation of the *local angle analysis* method shows the processing sequence for one CSP/CRP gather.

1. Input: CSP/CRP gather and zero-offset traveltime t_0 of an identified event. Define aperture, i.e. number of traces, used for the local estimation.
2. Estimation of emergence angle β_0 and radius of wavefront curvature R_0 for the normal ray $k = 0$ using the zero-offset traveltime t_0 , defined in step 1.
3. Predict traveltime t_k^p , emergence angle β_k^p , and radius of wavefront curvature R_k^p at a trace $k = k + 1$ in the local vicinity of the previously considered trace using the estimated parameters in step 2 or step 5 in Equations (3.4), (3.5), and (3.6).
4. Estimate emergence angle $\hat{\beta}_k$ and radius of wavefront curvature \hat{R}_k for the next trace k at the predicted traveltime t_k^p from step 3. Use β_k^p , R_k^p of step 3 as initial guess and apply the optimization procedure described in section 3.3.
5. Compare results of step 4, i.e. $\hat{\beta}_k$ and \hat{R}_k with predicted results of step 3, i.e. β_k^p and R_k^p :

Accept \implies Take results of step 4 ($\beta_k = \hat{\beta}_k, R_k = \hat{R}_k$).

Deny \implies Take predicted results of step 3 ($\beta_k = \beta_k^p, R_k = R_k^p$).

6. Goto step 3 until the furthest trace.
7. Output: Emergence angles and radii of wavefront curvature of an event at all source-receiver distances in the CSP/CRP gather

This method is illustrated in the next sections on different synthetic data examples.

3.5.2 Synthetic examples

In the first example, I apply the local wavefront-parameter estimation technique to hyperbolic traveltimes in order to compare the behavior of the local and the global stacking operator. Next, I use a strongly non-hyperbolic traveltime curve, which reveals the advantages of the *local angle analysis* method. In the third example, I apply the new method to one CSP gather of a more complicated synthetic salt dome data set.

3.5.2.1 Hyperbolic case

In Figure 3.9 a split spread gather with three hyperbolic traveltime curves is shown. I estimate the wavefront-parameters of the different events at each source-receiver point: Starting from zero-offset traveltime, the described local angle analysis is applied. Using the traveltime and the estimated wavefront parameters of the current trace the traveltime and the wavefront-parameters of the next traces are calculated, the parameter search is done at the next trace, the results are compared with the predicted wavefront-parameters for this trace, the more reasonable ones are chosen, and so on, as described above.

The traveltime curve we follow this way is shown in different colors along each of the three events. It is obvious that we follow the true moveout. Also shown is a local stacking operator (light blue) defined by the locally estimated wavefront-parameters corresponding to the central point (arrows) of each event. The larger the zero-offset traveltime of an event, the higher the aperture should be, i.e. the number of traces used for the local parameter estimation, in order to get reliable estimations of the radii.

The estimated emergence angles and radii of wavefront curvature are shown together with the analytic results in Figure 3.10a,b. The excellent agreement for the emergence angles is obvious. The calculation of the emergence angles and radii of wavefront curvature has been done using only 25 traces, 12 on each side of every central trace, i.e. the aperture was 240 m. The estimated radii for layers one and two are in a good agreement with the analytic results, whereas layer three shows some deviations. These deviations are due to the very small aperture. The smaller the aperture the more accurate are the moveout measurements and the more inaccurate are the estimated wavefront-parameters. There is always a tradeoff between accuracy of the measured moveout and the resolution of the estimated parameters, as explained above.

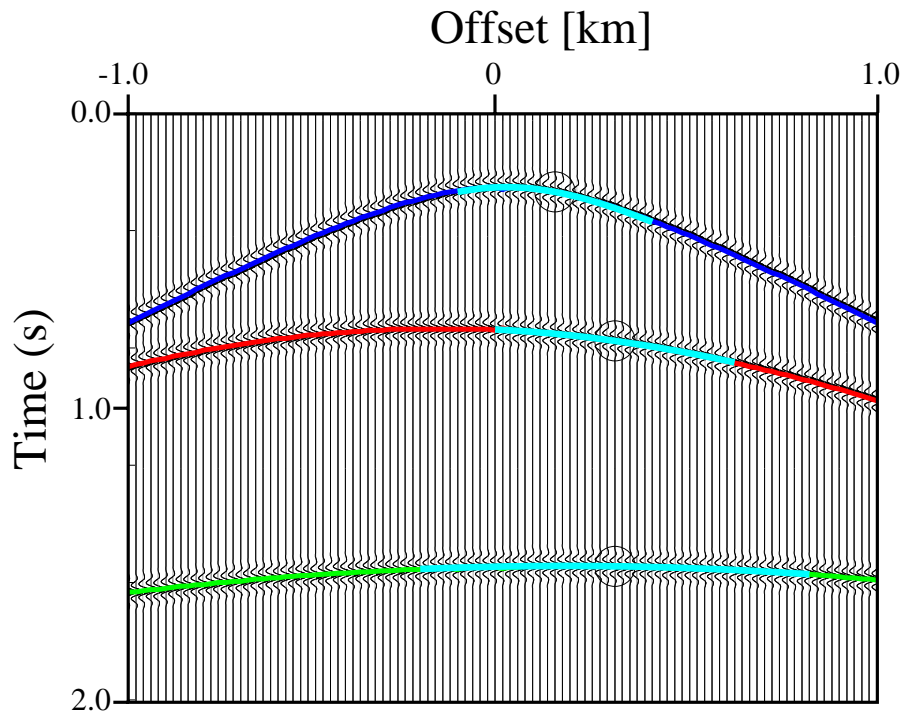


Figure 3.9: *Local parameter estimation in the case of hyperbolic moveouts. The dark blue, red and green lines denote the traveltime curves we follow (starting from zero-offset traveltimes) in a completely automatic manner. The light blue color shows the local moveout parameterizations using the locally estimated wavefront-parameters corresponding to one offset trace (see circles) of each event.*

To demonstrate the effect of an increased aperture the procedure is repeated for all three events using all available traces. In this case in the middle of the split gather 50 traces on each side of the central trace can be used, whereas on the maximum source-receiver distance 100 traces on one side can be taken. The results are shown in Figure 3.10c,d. The estimated radii for layers one and two could be improved at both edges, the radii for the third layer are now almost identical to the analytic results. On the other hand the aperture can only be as large as the circular wavefront approximation holds and the data can be stacked coherently using the local hyperbolic stacking operator.

It has to be pointed out that for the kinematic prediction of multiples only the emergence angles have to be known which can be obtained in such a simple situation already using a much smaller aperture and in the extreme case by applying a local slant-stack operator. However, depending on the signal to noise ratio a greater aperture might be necessary to give correct and stable results even for the emergence angles to be estimated. If the radii show errors this estimation might be still better than using a small aperture or a local slant stack operator. This is due to the greater effective length of the hyperbolic stacking operator compared to the local linear slant stacking operator. The effective length of stacking operator is defined by the maximum aperture which allows coherent stacking [e.g. Biondi, 1992]. In case of a small aperture the hyperbolic stacking operator reduces to a local slant

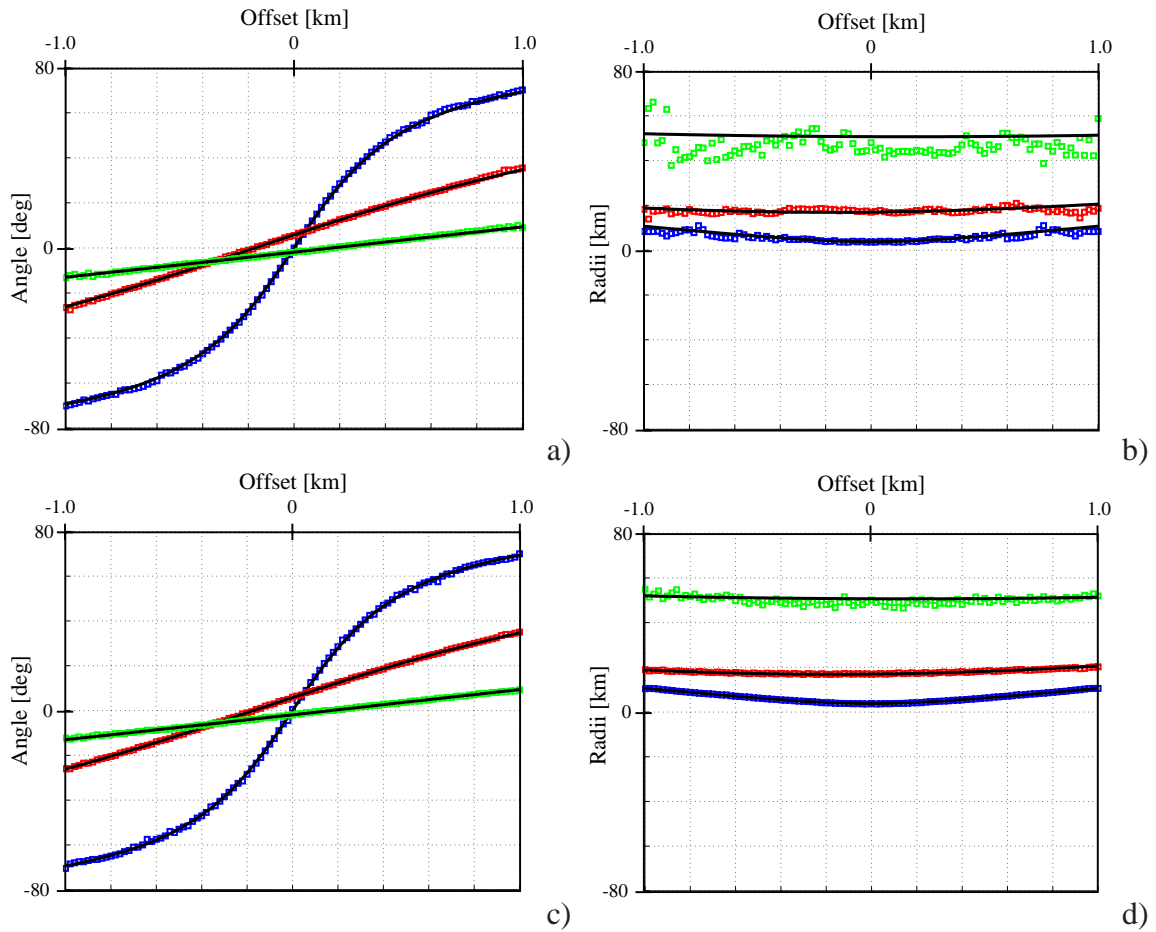


Figure 3.10: Results of the local parameter estimation in the case of hyperbolic moveouts for two extremely chosen apertures: For the results in a) and b) only 12 traces on each side of the central ray have been taken (aperture 240 m). For the results in c) and d) all available traces have been used. The blue, red and green colors denote the parameters corresponding to the three events shown already in Figure 3.9. The black line corresponds to the analytic results. There is almost no difference in the estimated emergence angles, whereas the radii could be improved using a larger aperture.

stack operator, as shown in Figure 3.11.

3.5.2.2 Non-hyperbolic case

According to the model shown in Figure 3.12a a traveltime curve was calculated. The first arrivals form a strongly non-hyperbolic moveout of the reflected CSP wavefront in a split spread gather, see Figure 3.12b. The moveout of such an event cannot be correctly described at all offsets by a single set of wavefront-parameters. A global application of the moveout correction formula in order to find the wavefront-parameters of the normal ray would give inaccurate results. Even if the wavefront-parameters β_0 and R_0 are supposed to

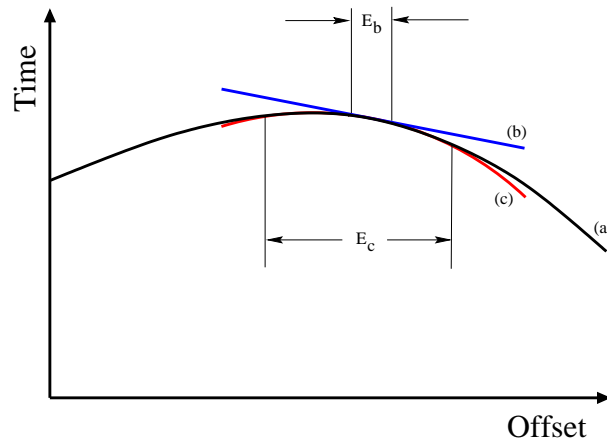


Figure 3.11: Schematic illustration of different local stacking operators. a) Traveltime curve of a seismic event. b) Local slant stack operator. c) Local CSP HI stacking operator. The effective length E_b of the hyperbolic CSP HI stacking operator is much larger than the local slant stack operator due to the fact that it approximates the traveltime curve (black) over a larger offset range.

be estimated correctly using a small aperture in the correlation analysis the extrapolation to arbitrary offsets assuming a globally circular wavefront approximation would be wrong.

The dotted line in Figure 3.12b shows the 'best' global stacking operator (maximum semblance) if all traces are used in the correlation analysis in order to estimate the zero-offset wavefront parameters. It is obvious that this curve only partly fits to the true traveltimes. The blue curve corresponds to the traveltimes predicted trace by trace, using the locally estimated wavefront-parameters, as described above. Also three 'best' local stacking operators (maximum semblance) defined by the locally estimated wavefront-parameters at three different offset traces (see circles) are shown in color. Note that in case of the green traveltime correction curve, which is located around a singular point of the traveltime curve, a negative radius of wavefront curvature was estimated.

The locally estimated emergence angles and radii of wavefront curvature are shown in Figure 3.13 together with the analytic results and the results of the global angle analysis and global radii analysis, obtained using the zero-offset wavefront-parameters for extrapolation to offset. The results of the local parameter estimation almost coincide with the true analytic curves. The only discrepancy exists at the singular points, where the angles and radii do not vary smoothly. This situation is reflected also in singularities of the estimated radii and leads to negative radii of wavefront curvature in these parts.

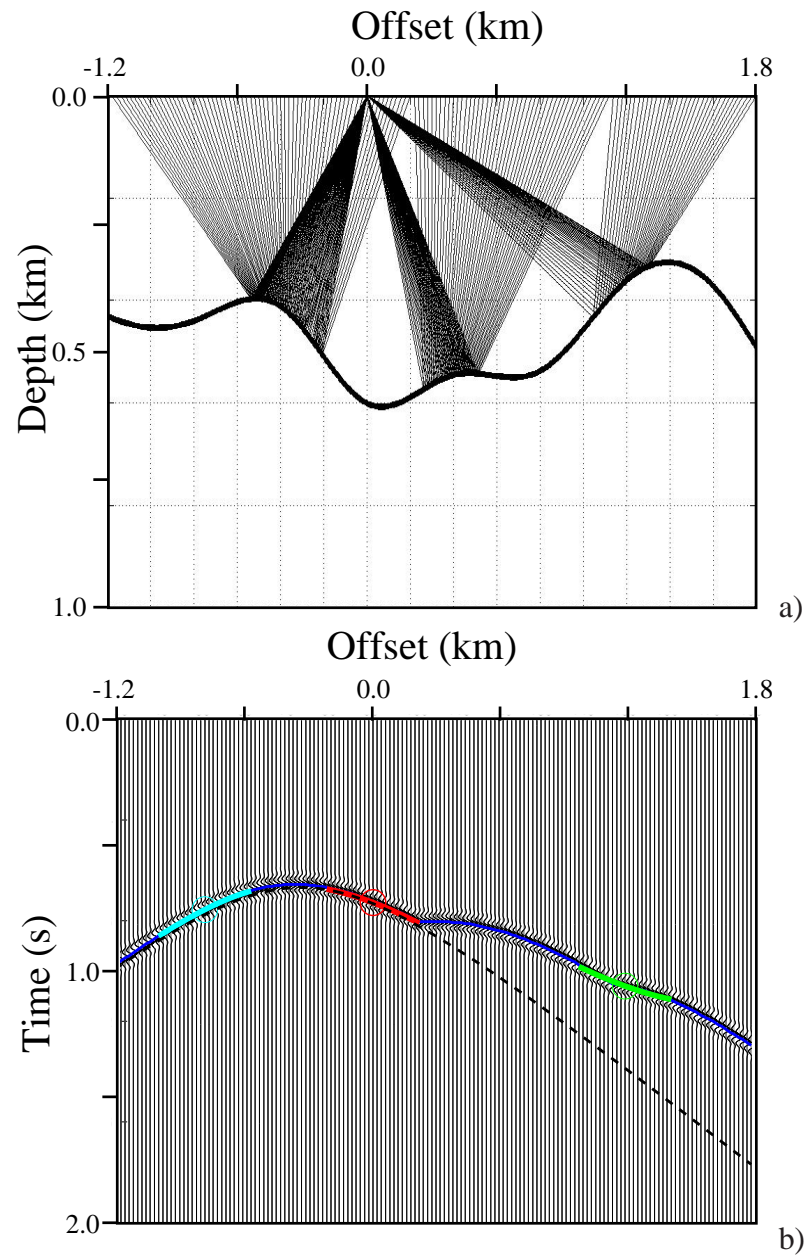


Figure 3.12: a) Model with a strongly undulating reflector used for the calculation of the first arrivals of the non-hyperbolic traveltime curve in b). The green, red and light blue lines correspond to three optimum (maximum semblance) local stacking operators defined by the locally estimated wavefront-parameters at three different receiver positions (see black circles). The dark blue curve corresponds to the traveltimes followed trace by trace, starting from zero-offset using the locally estimated wavefront-parameters. The dotted line represents the optimum (maximum semblance) global stacking operator defined by the globally estimated zero-offset wavefront parameters.

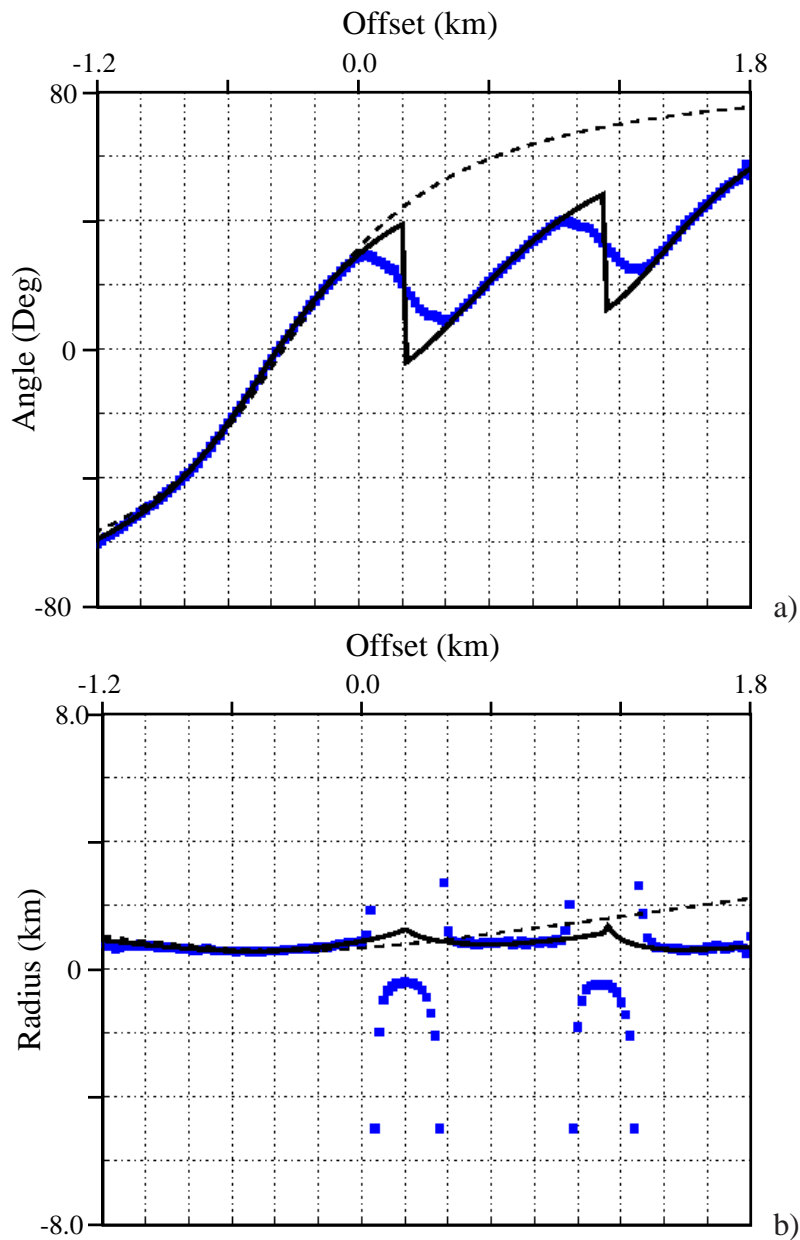


Figure 3.13: Results of the local angle analysis (blue squares) in case of a non-hyperbolic traveltime curve in comparison to the analytic results (black solid line) and the results obtained using the global angle analysis method (black dotted line) a) Emergence angles b) Radii of wavefront curvature.

3.5.2.3 Mixed case

I also compared the global- and local angle analyses method on a CSP gather of a more complicated and realistic salt dome data set. This data set was calculated using full wave equation modeling. Each CSP gather consists of 350 traces, minimum offset is 825 ft, distance between receivers is 75 ft and the sampling rate is 8 ms.

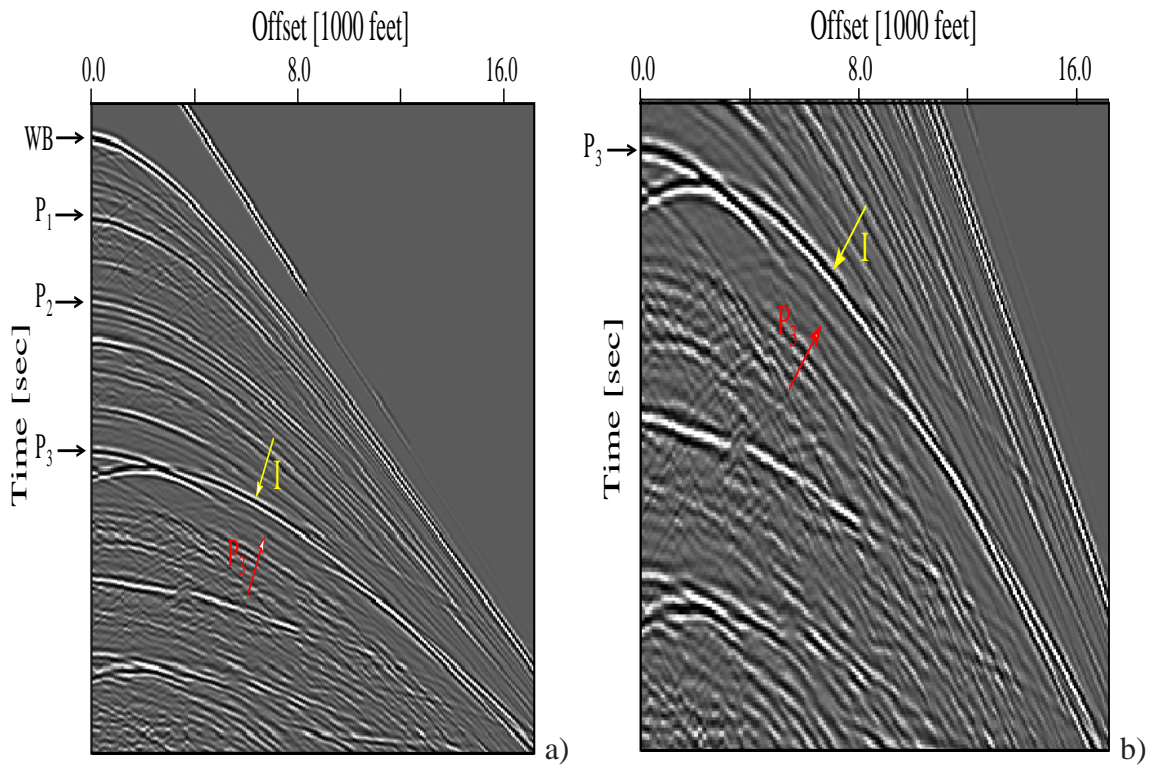


Figure 3.14: a) CSP gather of a salt dome data set with four identified multiple-generators. While WB, P_1 , and P_2 are approximately hyperbolic, P_3 (red) seems to interfere with another event I (yellow), and in this case would be non-hyperbolic. b) Zoomed section showing the two interfering events.

In Figure 3.14 a CSP gather is shown. Four identified multiple-generators WB, P_1 , P_2 and P_3 are labeled. The traveltim curves of the first three events seem to be approximately hyperbolic. For the fourth event P_3 the situation is different and not that easy to decide. One possibility would be that event P_3 interferes with another event (I), compare P_3 and (I) in Figure 3.14a,b.

It is obvious that it would not be possible to describe the wavefront parameters along such a non-hyperbolic event using the global angle analysis. I applied the *local- and global angle analyses* on a section of the CSP data in Figure 3.14a. Like in the previous examples the blue curve in Figure 3.15 denotes the traveltim curve followed automatically using the locally estimated wavefront-parameters in order to predict the traveltimes of the event trace by trace starting from zero-offset traveltim and taking into account a continuous change of the unknown attributes along the moveout. This blue curve follows nicely the different events. The red curve represents the optimal (maximum semblance) global stacking operator using all traces which is defined by the estimated zero-offset wavefront-parameters β_0 and R_0 of event P_3 . As expected for event P_3 this curve differs significantly from the blue one. In the case of WB, P_1 and P_2 the global stacking operators represent the events moveout very well and are not shown additionally.

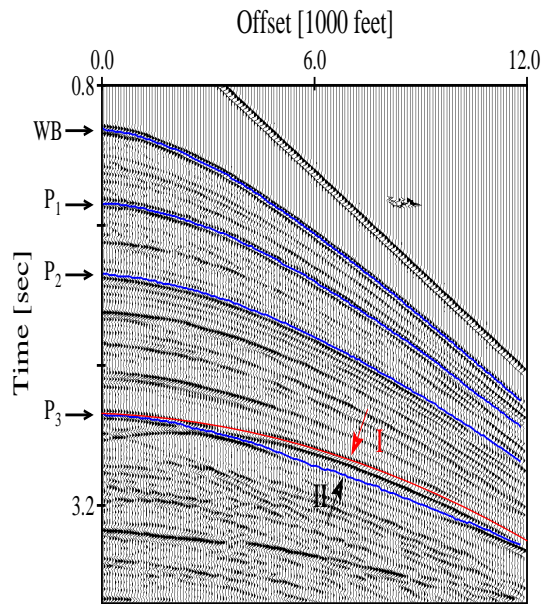


Figure 3.15: Results of the local parameter estimation along the moveout of the four primary events shown already in Figure 3.14. The blue curve belongs to the traveltimes followed trace by trace, starting from zero-offset using the locally estimated wavefront-parameters. The red curve belongs to the 'best' global stacking operator.

The locally and globally estimated emergence angles and radii of wavefront curvature are compared in Figure 3.16 and Figure 3.17. For the first three primaries the moveout seems to be more or less hyperbolic and therefore the local- and global angle analyses yield approximately the same results. Note, there is no smoothing operator applied yet on the local estimation results. In case of the non-hyperbolic event P_3 the results differ as expected. The emergence angles have been calculated using an aperture containing of about 50 traces whereas the radii in Figure 3.17 have been calculated using about 100 traces for the primaries WB, P_1 , and P_2 . For the fourth event P_3 such a large aperture makes no sense because of its non-hyperbolic character. There exists always a tradeoff between the resolution of the estimated parameters and the accuracy of the moveout. I want to emphasize that the radii are only shown for completeness and are not needed in the kinematic prediction procedure. Even if the radii are not correctly estimated the effective length of the hyperbolic CSP HI stacking operator can be much larger than the effective length of a slant stacking operator (see Figure 3.11). This might be especially important for the estimation of the emergence angle in situations where the signal to noise ratio is low.

3.5.3 Results

In case of a non-hyperbolic relation between the traveltime and source-receiver distance two parameters, which define a global CSP stacking operator, are not sufficient to correctly describe the moveout of an event at all source-receiver pairs. In these situations the moveout

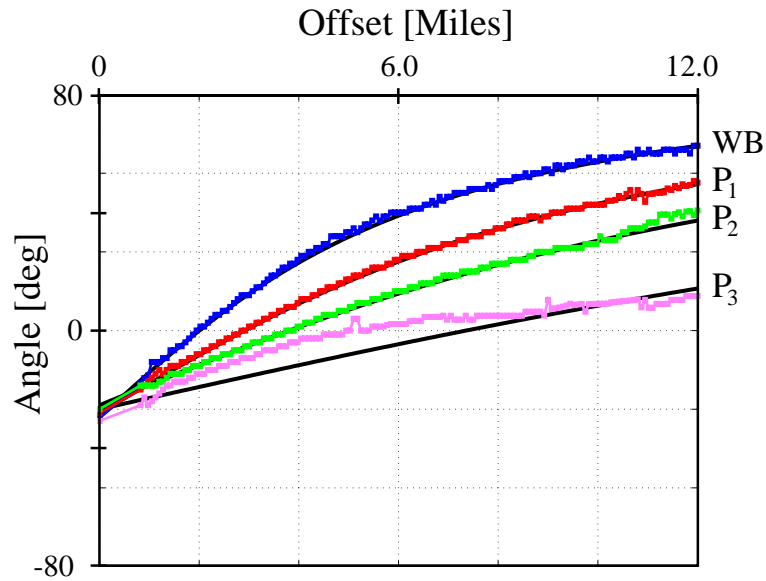


Figure 3.16: Results of the local angle analysis procedure for the four primaries WB (blue), P_1 (red), P_2 (green) and P_3 (pink) shown in comparison to the results obtained using the global angle analysis procedure (black solid lines).

curve has to be decomposed using local stacking operators.

The method presented in this section is called *local angle analysis* and is based on local coherency measurements of a reflection event along hyperbolic stacking trajectories defined by the CSP HI moveout correction. Because it is a local stacking operator it provides information on the wavefront-parameters of non-hyperbolic moveouts in the data.

Nevertheless, if the local hyperbolic CSP HI stacking operator is applied to hyperbolic traveltimes curves, its resolution is not limited by the curvature of the event. Consequently, the resolution of the estimated wavefront parameters and possibly also the signal to noise ratio improves with increasing length of the stacking trajectories. In contrast, the resolution of the linear local slant stack operator decreases with increasing length of the stacking trajectories due to the event's curvature. Therefore the local application of the CSP HI stacking operator is usually superior to the local slant stack operator. In the worst case the CSP HI stacking operator reduces to the local slant stack operator (compare appendix A and Figure 3.11).

Considering non-hyperbolic moveouts, the shorter the stacking trajectory of the CSP HI stacking operator, the more accurate are the moveout measurements. However, this moveout accuracy comes at the expense of the resolution of the estimated wavefront-parameters. In this sense, there is a tradeoff between accuracy and resolution: a small aperture approximates the non-hyperbolic moveout best but the resolution of the estimated parameters is low. A large aperture of the hyperbolic stacking operator is necessary to get a high resolution of the parameters but approximates non-hyperbolic moveouts badly.

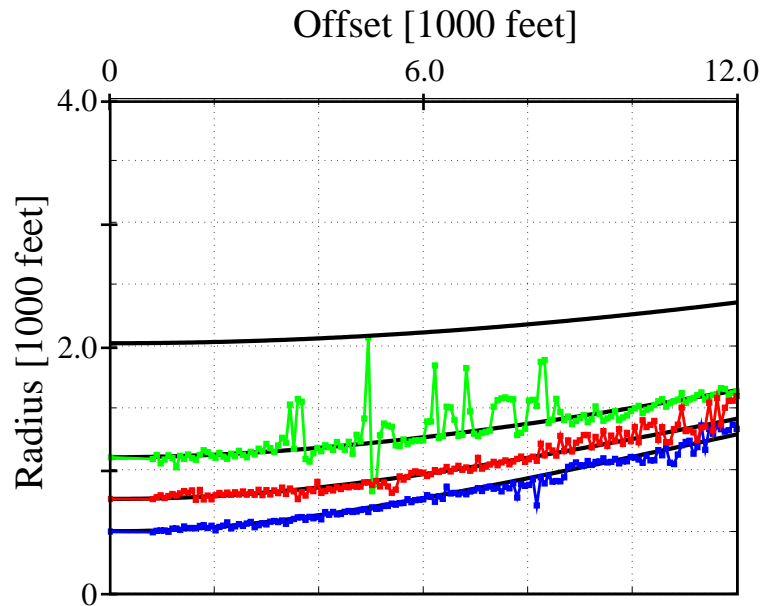


Figure 3.17: Results of the local parameter estimation for the primary events WB (blue), P_1 (red) and P_2 (green) shown in comparison to the results obtained using the global parameter estimation procedure (black solid lines). The used aperture was too small to get stable results for the fourth primary (P_3). Nevertheless the estimated emergence angles are reasonable.

A drawback of the local angle analysis is that the traveltimes of a specified event has to be known at each source-receiver pair along its moveout, in all CSP gathers. I presented a method which follows the events moveout automatically and starts from the zero-offset traveltimes. Problems due to interfering events can be limited taking into account only continuous changes along the events moveout. So far this method works only in the absence of caustics. In complicated situations manual picking in the prestack data might be required which is associated with a much higher effort.

3.6 Summary

In this chapter I presented different horizon-based procedures for the estimation of kinematic wavefront-parameters of a multiple-generating reflection (e.g. a primary), identified in a simulated zero-offset section. The output of these methods is the emergence angle, radius of wavefront curvature and traveltimes of the identified event at all source-receiver pairs in all CSP gathers along the seismic line.

The first technique is called *global angle analysis*. In the first step of this method the wavefront-parameters associated with the normal rays are estimated at all zero-offset locations along the seismic line. This can be done either in a fully automatic or an interactive

manner, depending on the complexity of the data. The interactive application allows manual picking of the optimal wavefront-parameters along the seismic line and resolves problems due to multi-modal correlation functionals, e.g. in conflicting dip situations. The estimated zero-offset wavefront-parameters are used in the next step to calculate the searched emergence angles at finite source-receiver distances in the CSP gathers. This extrapolation is based on a globally circular wavefront approximation within the furthest considered source-receiver distance. Therefore, this approach is only valid if the considered travel-time curve is approximately hyperbolic and can be described sufficiently well by one set of wavefront-parameters, such as the zero-offset parameters t_0 , β_0 and R_0 . When considering only moderate offsets in a CSP gather this assumption is satisfied in many cases.

However, in complex geological situations with strong dips and lateral variations or at far-offsets, the travelttime curve might be strongly non-hyperbolic and one parameter set may not be sufficient to describe the moveout correctly at all source-receiver locations. Consequently some information would be lost. In such situations the complete moveout curve can be decomposed by local moveout measurements.

A local wavefront-parameter estimation technique which uses such local moveout measurements was presented. It is essentially based on a local application of the CSP HI formula and requires only a locally circular wavefront approximation. This method can be used to estimate the emergence angles together with the radii of wavefront curvature locally along non-hyperbolic travelttime curves.

Chapter 4

Multiple prediction using wavefront parameters of multiple generators

4.1 Introduction

After applying one of the presented parameter estimation techniques presented in chapter 3 the emergence angles of identified multiple-generating events are known at each source-receiver position in all CSP gathers. These emergence angles are used in this chapter to predict and identify multiples.

In section 4.2 I explain how surface- as well as interbed multiples can be represented by primaries or more general by *multiple-generators*. In section 4.3 I present an implementation where I predict the arrival time of multiples using the traveltimes of the identified multiple-generators. Two examples, one synthetic and one real data example to illustrate this kinematic prediction procedure. In many cases the multiple amplitude or at least an estimation of it would be very helpful for the multiple identification as well as for the multiple attenuation. This is the reason why I extend in section 4.4 the kinematic prediction method to a dynamic prediction method and illustrate its viability on a synthetic data example. Finally, in section 4.5 I will give some conclusive remarks on the advantages and restrictions of the two multiple prediction methods.

4.2 Geometrical considerations

Surface multiples In order to explain how a multiple event can be represented using primaries or more general subevents, let us start with the surface related multiples shown in Figure 4.1a-e. For instance, the first-order surface multiple A_sBA_r in Figure 4.1a consists of two primary segments shown in different colors: A_sB and BA_r . The same number of primaries can be used to describe the first-order head wave multiple A_sBA_r in Figure 4.1b,

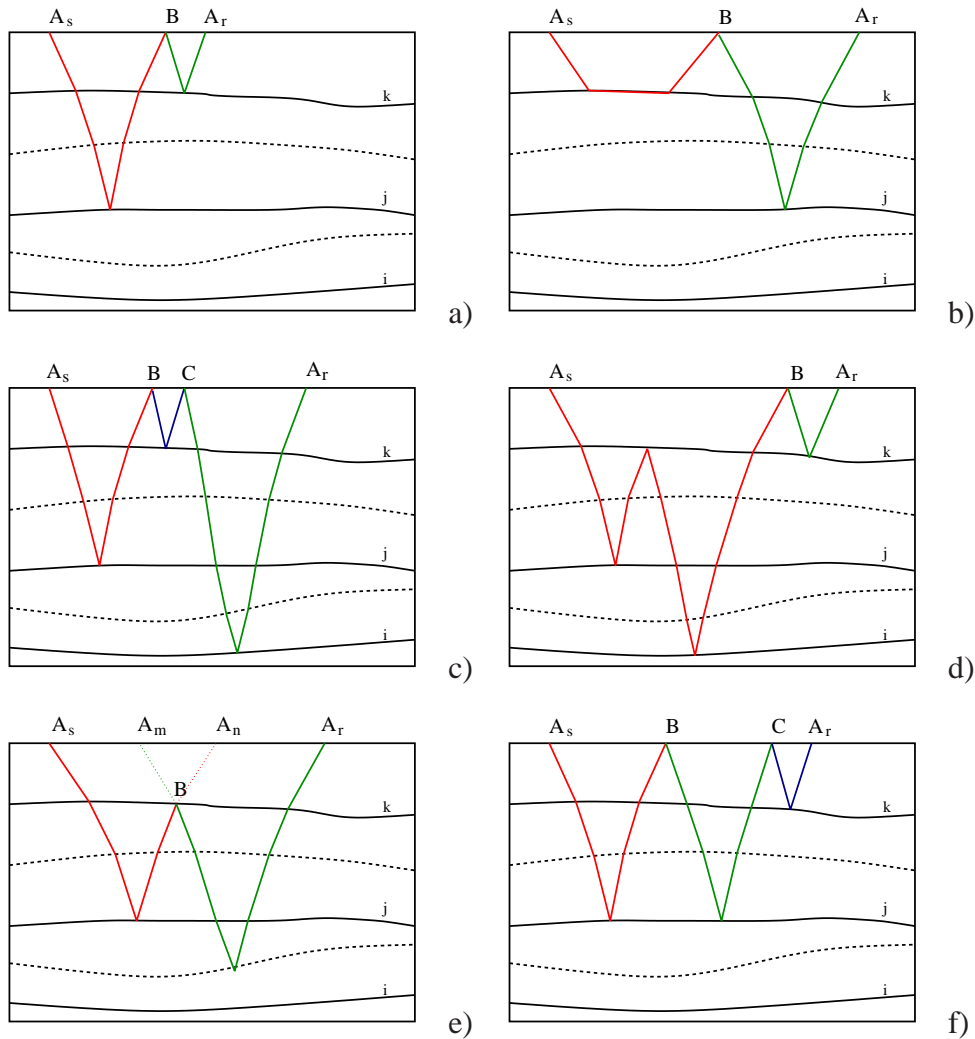


Figure 4.1: Raypaths of different multiple events in a 2D laterally inhomogeneous layered subsurface model: a) first-order surface multiple, b) first-order head wave multiple, c) second-order surface multiple, d) first-order surface multiple that includes a first order interbed multiple, e) purely internal multiple, and f) second-order surface multiple.

although head wave multiples usually have negligible amplitudes. In Figure 4.1c a second-order surface multiple $A_s B C A_r$ includes three primary segments: $A_s B$, BC , and $C A_r$. As another example in Figure 4.1d a first-order surface multiple $A_s B A_r$ includes a primary segment and an internal multiple segment: $A_s B$, and $B A_r$. All of the surface-related multiples mentioned so far can be decomposed into raypath-segments whose both ends are located at the observation surface. Thus, the seismic events corresponding to these raypaths are part of the recorded wavefield. I call these events *multiple-generating reflections* or simply *multiple-generators*.

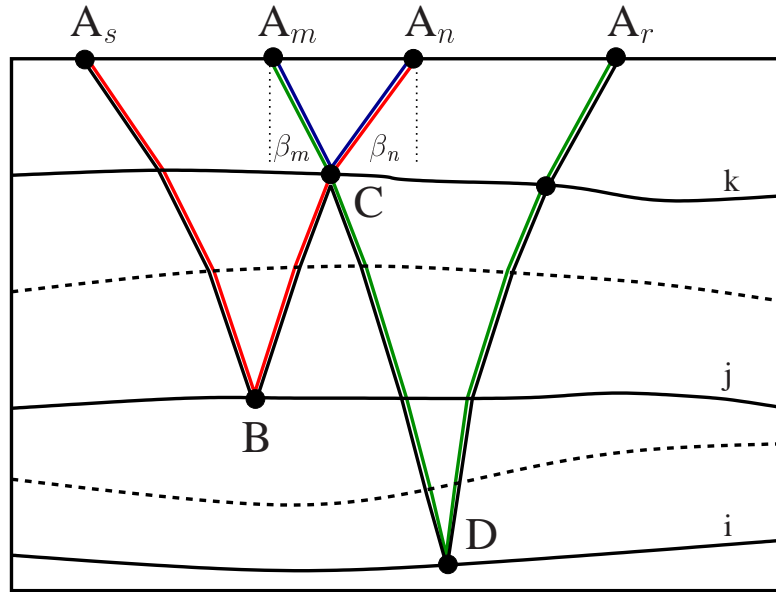


Figure 4.2: Decomposition of the raypath of an interbed multiple $A_s B C D A_r$ (black) into the three primary raypaths $A_s B A_n$ (red), $A_m D A_r$ (green), and $A_m C A_n$ (blue).

Interbed multiples In case of the pure interbed multiple $A_s B A_r$ in Figure 4.1f the situation is different because the downward reflection point B is now located at the interbed generating interface k and not at the surface anymore. In order to describe this first-order interbed multiple by two primaries, the involved primary wavefields have to be continued downward from the surface to the interbed generating interface k . This requires to have explicit knowledge of the subsurface model between the recording surface and the interbed generating interface [e.g. Berkhout and Verschuur, 1997]. For this reason many prediction methods have been limited to surface multiples [e.g. Dragoset and Jericevic, 1998; Berkhout and Verschuur, 1997; Verschuur, 1992].

This restriction was removed by Keydar et al. [1998] who showed that also interbed multiples can be decomposed into primary segments. In particular, as shown in Figure 4.2, the raypath of an interbed multiple $A_s B C D A_r$ can be considered as the sum of the primary raypaths $A_s B A_n$ and $A_m D A_r$ minus the raypath of the primary $A_m C A_n$ reflected at an interbed generating interface k . In fact this idea leads to the statement that *the raypath of any multiple reflection, no matter how complicated it is, can be decomposed using raypaths of primaries*. The smallest unit of a multiple-generating reflection is therefore a primary.

Multiple conditions: If the multiple-generating reflections, corresponding to the primary raypath-segments shown in different colors in Figure 4.2 would be identified, their travel-times could be simply used to predict the multiple traveltime at the receiver position A_r as will be shown below. They can be identified and selected using so-called *multiple conditions*, which require that the emergence angles of the CSP wavefronts corresponding to the involved multiple-generating primaries at the registration surface are identical. This is

again explained in Figure 4.2: The emergence angle of the wavefront of the primary reflection A_sBA_n from reflector j is identical to the emergence angle of the primary reflection A_mCA_n from reflector k and is labeled β_n . Similarly, the emergence angle of the primary reflection A_rDA_m from reflector i is identical to the emergence angle of the primary reflection A_nCA_m from reflector k and is labeled β_m . In summary, the multiple conditions of this particular interbed multiple are:

$$\begin{aligned}\beta_{sn}^j &= \beta_{mn}^k, \\ \beta_{rm}^i &= \beta_{nm}^k,\end{aligned}\tag{4.1}$$

where β_{sn}^j is the emergence angle of the primary A_sBA_n from reflector j , β_{mn}^k is the emergence angle of the primary A_mCA_n from reflector k , β_{rm}^i is the emergence angle of the primary A_rDA_m from reflector i , and β_{nm}^k is the emergence angle of the primary A_nCA_m from reflector k . The upper index denotes the number of the reflector, the first lower index denotes the location of the shot and the second the number of the receiver.

Knowing the emergence angles of the multiple-generating events at each source-receiver location in all CSP gathers it is possible to select those traces which generate a specified multiple using the appropriate multiple conditions, as explained above on the example of a first-order interbed multiple. In the next sections I will use the selected multiple-generating events and the associated wavefront-parameters in order to predict the corresponding multiple, first kinematically, and second, dynamically.

4.3 Kinematic prediction of multiples

4.3.1 Method and implementation

Figure 4.3a shows a simple first-order surface multiple event which has one downward reflection at the intermediate surface point B. According to the previous section this multiple consists of two multiple-generators A_sB and BA_r which could be either primaries or multiples (see Figure 4.1). The question marks in the two raypaths indicate that the exact behavior of the multiple-generating events in the subsurface is unknown and that no explicit knowledge of the subsurface is required. The multiple event A_sBA_r appears in the CSP gather with shot position at A_s in the trace recorded at receiver position A_r .

The task of the prediction procedure is to use the multiple-generators A_sB and BA_r in some way to predict the multiple event A_sBA_r , in the trace recorded at A_r . One way is to find the intermediate surface point B which defines the two traces that contain the multiple-generating events A_sB and BA_r . Assuming source-receiver reciprocity the event BA_r is identical to the event A_rB which is contained in the Common Receiver Point (CRP) gather for receiver position A_r and the situation can be also seen as shown in Figure 4.3b. Knowing

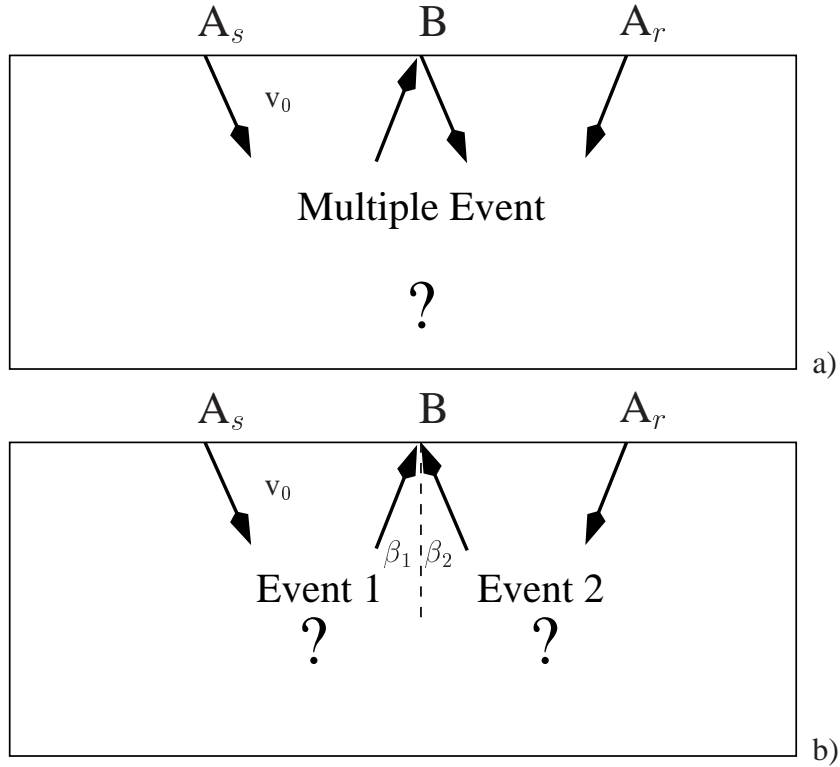


Figure 4.3: a) First-order surface multiple. b) Event 1 is part of the CSP gather with source at A_s while Event 2 is part of the CRP gather of receiver A_r . The multiple condition for this simple case is $\beta_1 = -\beta_2$. The question marks indicate the unknown raypath of the two multiple-generating events.

the emergence angles of these primary events at all source-receiver positions in the CSP and CRP gather, respectively, we can find the two multiple-generating traces by searching for those emergence angles which satisfy the predefined multiple conditions of the specified multiple code, like e.g. a first-order surface multiple. In the example above these conditions would be $\beta_1 = -\beta_2$. Once the subevents $A_s B$ and $B A_r$ are identified, the sum of their traveltimes ($T_1 + T_2$) gives the arrival time (T_{12}) of the multiple $A_s B A_r$. Doing this for all source-receiver distances of the multiple to be predicted leads to a kinematically correct multiple prediction in the CSP gather.

The same idea is valid for instance for the first-order interbed multiple shown in Figure 4.2. Using the multiple conditions in Equation (4.2) associated with this multiple code, i.e. a first-order interbed multiple, allows us to find the location of the two intermediate surface points A_m and A_n . When the multiple-generating primaries are identified the multiple traveltime can be predicted by the following equation:

$$T_{MP} = T_{sn}^j + T_{rm}^i - T_{mn}^k \quad (4.2)$$

$$= T_{s0}^j + \Delta\tau_{sn}^j + T_{r0}^i + \Delta\tau_{rm}^i - T_{m0}^k + \Delta\tau_{mn}^k, \quad (4.3)$$

where T_{sn}^j , T_{rm}^i , and T_{mn}^k are the traveltimes of the multiple-generating primaries. The upper index denotes the number of the reflector, the first lower index denotes the location of the shot-point and the second lower index the location of the receiver; T_{s0}^j , T_{r0}^i , and T_{m0}^k denote the zero-offset traveltimes at the shotpoints A_s , A_r , and A_m ; $\Delta\tau_{sn}^j$ is the moveout correction for a primary reflection from interface j in the CSP gather with shotpoint at A_s and the receiver at A_n . In the same way $\Delta\tau_{rm}^i$, and $\Delta\tau_{mn}^k$ are moveout corrections in different CSP gathers.

Based on these ideas the kinematic multiple prediction of surface as well as interbed multiples was implemented as summarized in the following:

1. Identify multiple-generators in stacked section (e.g. primaries)
2. Estimate emergence angles of the identified multiple-generators at all source-receiver positions in all CSP gathers using one of the methods described in chapter 3.
3. Specify ray-code of a multiple and appropriate multiple conditions as well as accuracy required to satisfy multiple conditions.
4. For each source-receiver offset in the CSP gather find and select the multiple-generating traces using the specified multiple conditions.
5. Use the traveltimes of the multiple-generating events at the selected traces to calculate the multiple traveltimes.
6. Output: Kinematically predicted multiple in CSP gather.

I applied the proposed method on the synthetic as well as on the real marine data set I already used for illustration of the parameter estimation procedure in chapter 3. The results are presented next.

4.3.2 Synthetic example: four layer model

In this section, I use the estimated emergence angles of the synthetic example in section 3.4.2 in order to predict different multiples. Knowing the emergence angles of the multiple-generating primaries for all shot-receiver pairs, I can find those primary traces which generate a specified multiple by using the appropriate multiple conditions. The goal in this example is to predict and attenuate four first-order and one second-order surface related multiple as well as one interbed multiple, see ray-codes in Figure 4.4.

For each shot-receiver position in every CSP gather, the intermediate points satisfying the specified multiple conditions are searched. The traveltimes of the multiple-generating primaries on the traces located at these intermediate points can be used to calculate the multiple arrival times, presuming that the primary traveltimes are known. The predicted traveltimes are shown in three CSP gathers in Figure 4.5 on different locations along the seismic

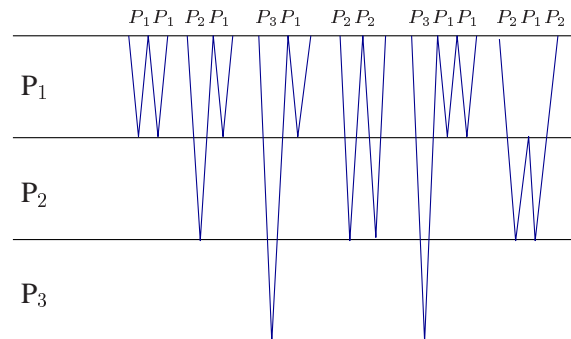


Figure 4.4: Ray-code of six multiple events for which the prediction and attenuation was done. Note that the picture is only schematically.

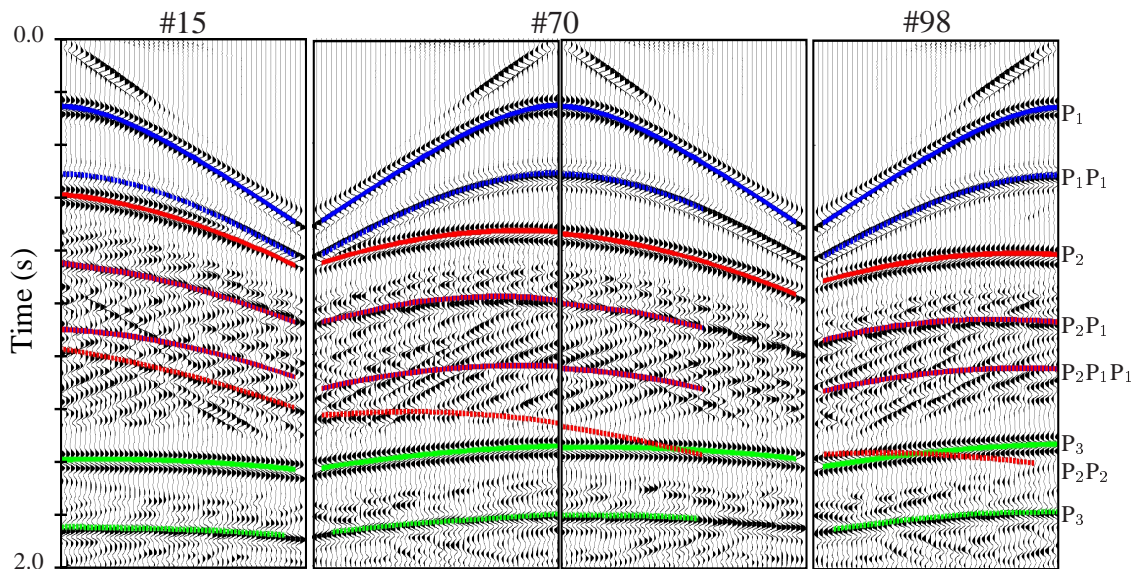


Figure 4.5: Predicted multiple traveltimes in three shot gathers (#15, #70 and #98). Their location on the seismic line is indicated in the model shown in Figure 3.2. The trace increment is 20 m. Automated Gain Control (AGC) has been applied in order to enhance weak multiples. The events are shown in different colors. Labels are according to the multiple ray-codes in Figure 4.4. Note: The moveout of the primaries (P_1 , P_2 and P_3) has been calculated using the estimated emergence angles β_0 and radii of wavefront curvature R_0 in Equation (3.1). Figure from Zaske et al. [1999].

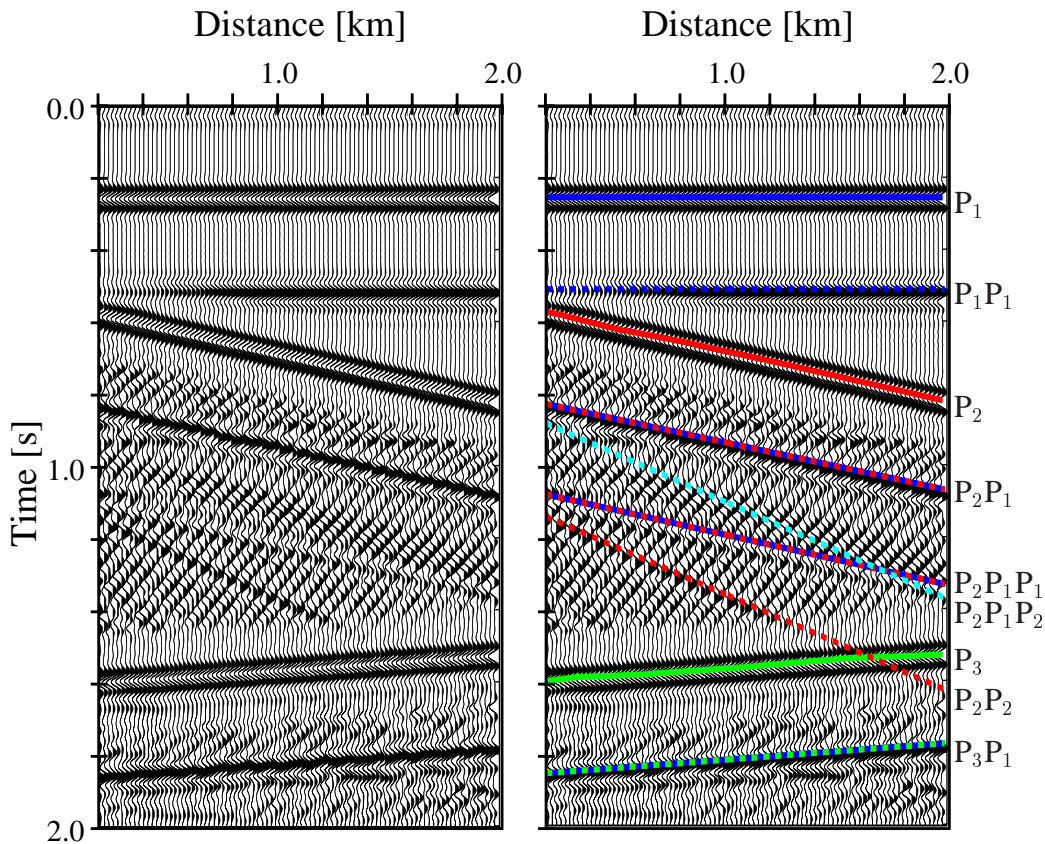


Figure 4.6: *Minimum offset section before multiple attenuation: Left: Minimum offset section Right: Minimum offset section including labeling for picked primaries and predicted multiple events. AGC has been applied in order to enhance multiple energy. The model used for modeling is shown in Figure 3.2. Figure from Zaske et al. [1999].*

line. A very good fit between the predicted traveltimes and that calculated by FD modeling can be observed especially for the first order multiples. The predicted times for the second order surface multiple and the interbed multiple look reasonable but cannot be compared easily with the modeled data because of their weak amplitudes, which are not resolvable in the noisy data set. Note that only the kinematics of the multiples was predicted based on multiple-generating primary reflections, thus, owing to low energy of multiple events amplitudes may be negligible.

The predicted multiple traveltimes are also shown in the minimum offset section in Figure 4.6. I show the minimum offset section after AGC, because here the multiples are not canceled as they might be during stacking. The agreement with the modeled data is again very good. In this case, also the predicted second order surface multiple ($P_2P_1P_1$) can be seen in the modeled data. The interbed multiple prediction ($P_2P_1P_2$) is kinematically correct but still, it cannot be compared with the modeled data set, because of its weak amplitude.

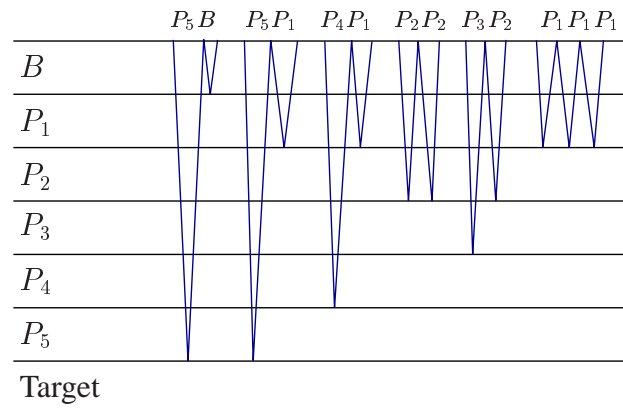


Figure 4.7: Ray-code of six multiple events for which the prediction and attenuation was done. Note that the picture is only schematically.

4.3.3 Real data example: marine data set

Similarly to the previous section I predicted different multiples for the real marine data set introduced in section 3.4.3. In section 3.4.3 different multiple-generators have been picked along the seismic line and the corresponding emergence angles have been estimated at each source-receiver position in every CSP gather along the seismic line using the *global angle analysis* method (section 3.4).

Now, I use these angles for the kinematic prediction of six multiple events, which are shown schematically in Figure 4.7. Figure 4.11 shows one CSP gather with primaries and predicted multiples. A stacked section with the identified multiple-generating primaries and without predicted multiples is shown in Figure 4.8. The same stacked section with the predicted zero-offset times for multiple events is shown in Figure 4.9, and enlarged in Figure 4.10. The predicted multiple traveltimes follow existing events in the stacked sections, as well as in the CSP gather. This is especially obvious in the zoomed section in Figure 4.10.

Note that only the arrival time of the six multiples was predicted based on multiple-generating primary reflections, thus, owing to the stacking process and low energy of multiple events, multiples are not necessarily visible on the stacked section.

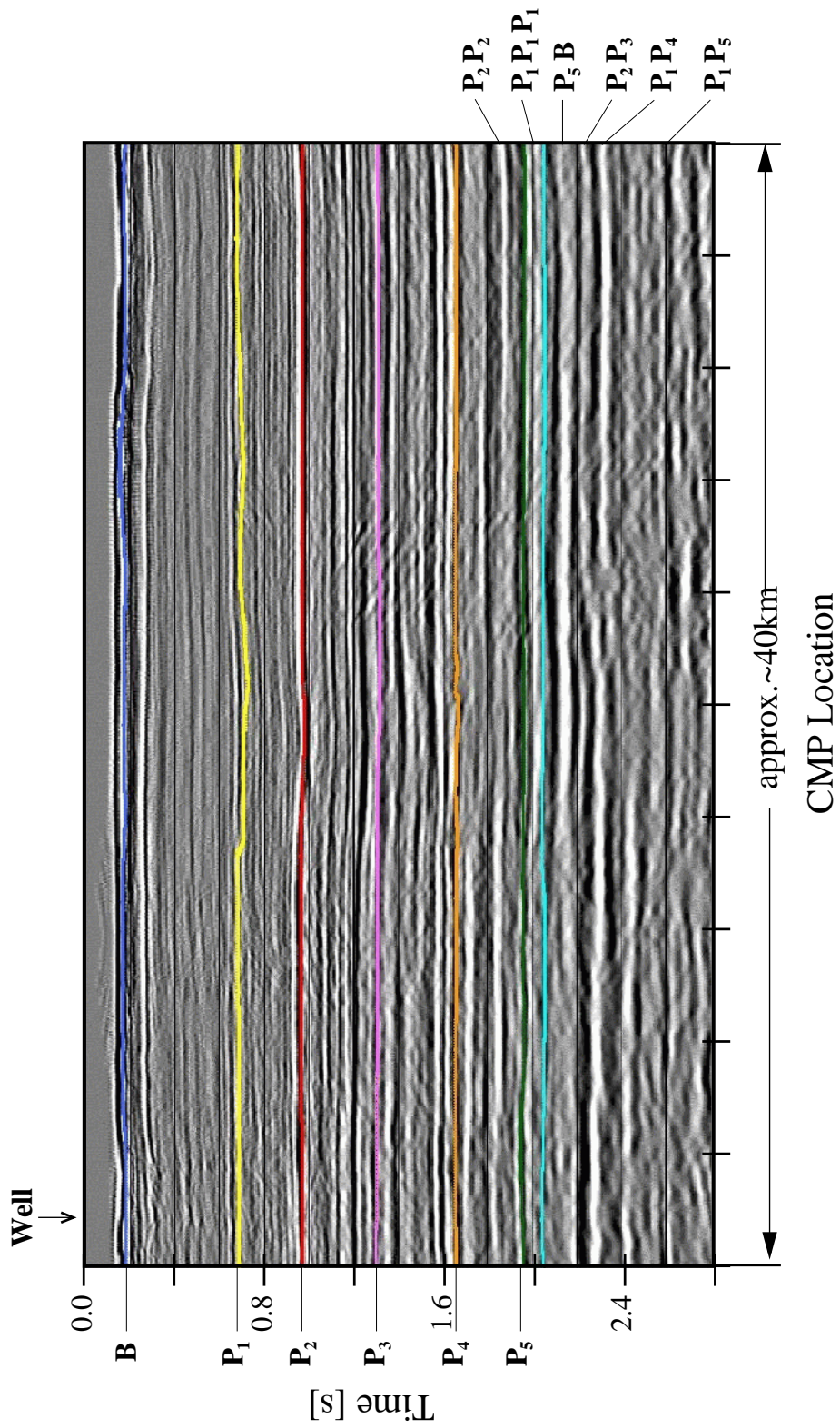


Figure 4.8: Stacked section of marine real data set including six identified multiple-generators.

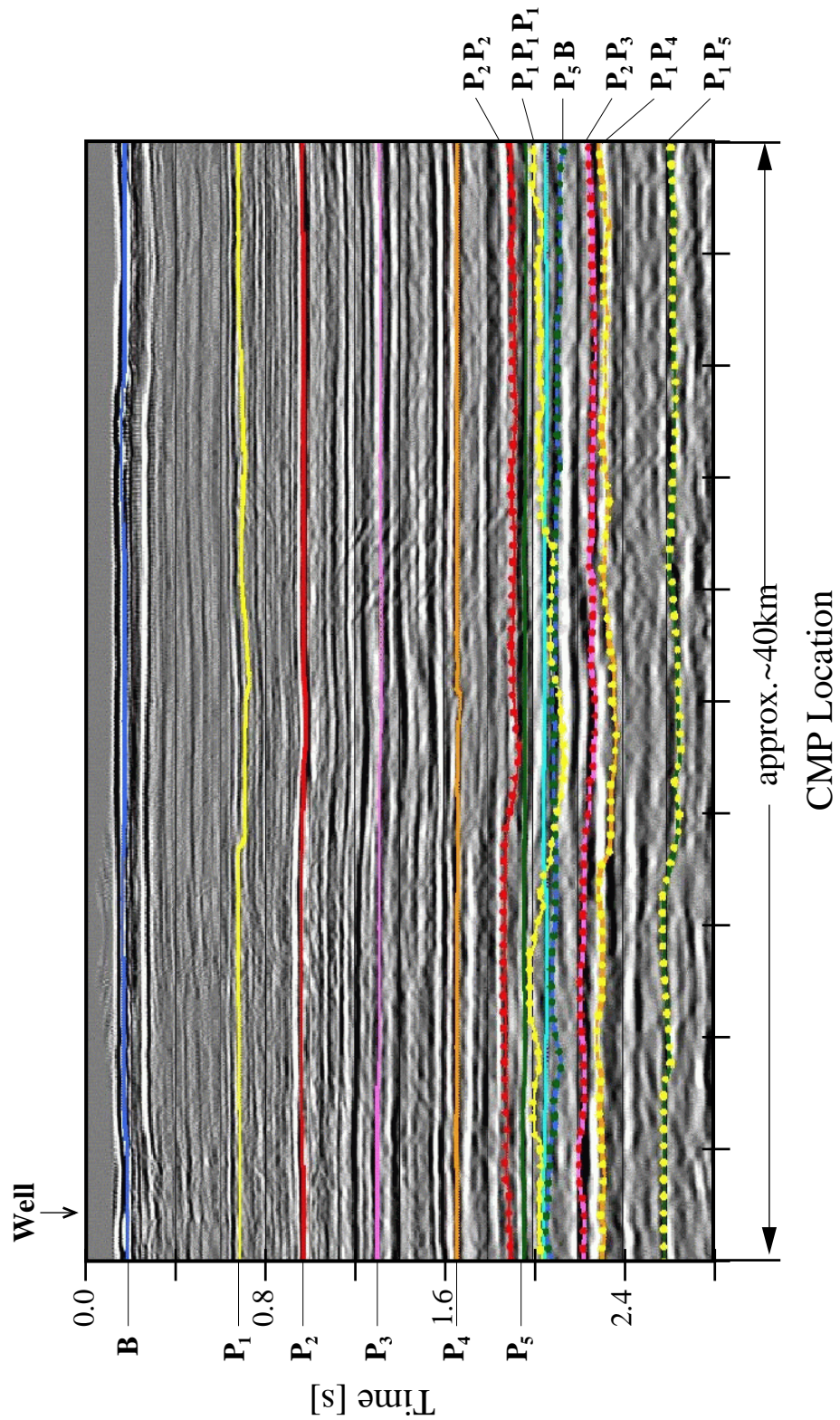


Figure 4.9: Stacked section of marine data set including six identified multiple-generators ($B, P_1, P_2, P_3, P_4, P_5$) and six predicted multiples ($P_2P_2, P_1P_1P_1, P_5B, P_3P_2, P_4P_1, P_5P_1$) in the target region (light blue). The ray-codes of the multiples are shown in Figure 4.7.

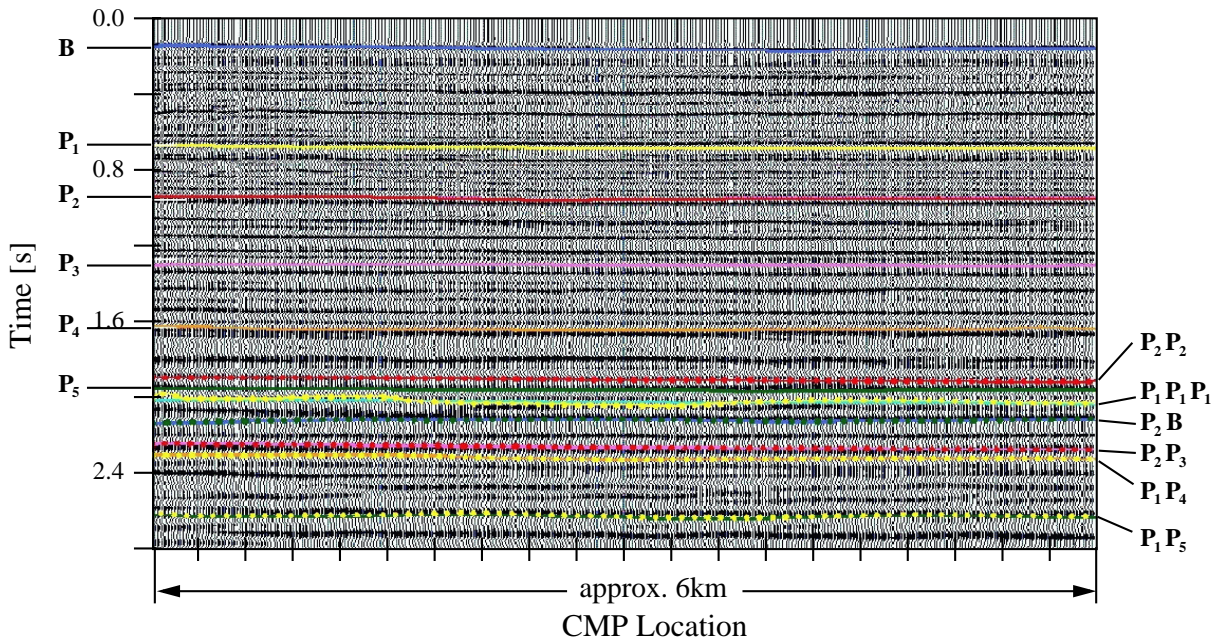


Figure 4.10: Part of the stacked section in Figure 4.9 of the marine data set including six identified multiple-generators and the predicted multiple traveltimes.

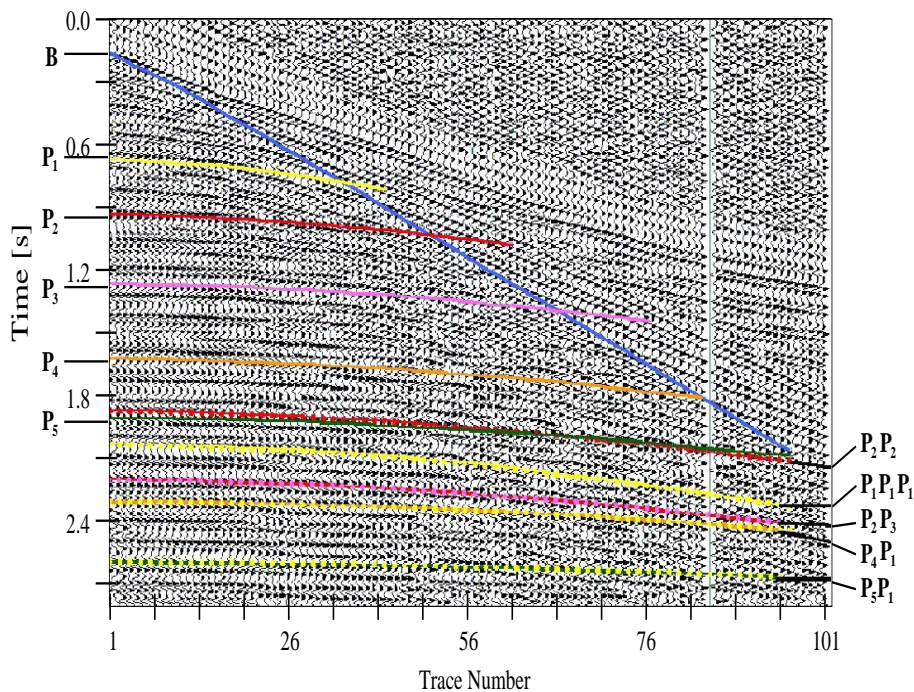


Figure 4.11: CSP gather including the six identified multiple-generating events and the predicted multiples. The moveout of the primaries is calculated using the zero-offset wavefront parameters in Equation (3.1).

4.3.4 Results

I presented a 2D method and implementation for the prestack traveltimes prediction of surface and interbed multiples and showed its target-oriented application. No subsurface information (only the near surface velocity), near offset traces or source waveform information is needed. This method requires only the identification of multiple-generating reflections (e.g. primaries) in a stacked section, and the formulation of so-called multiple conditions for a specified multiple (ray-code) to be predicted. The most important parameter in the prediction process is the emergence angle at each source-receiver position of the multiple-generating reflections. If the emergence angles would be wrong also the prediction of the multiples would be inaccurate or even fail.

In general also multiples can be seen as multiple-generating reflections and in the extreme case two multiples can be used to predict another multiple event. However, the emergence angles and traveltimes of the multiple generating reflections at each source-receiver location must be correctly known. If the moveout of an event would be non-hyperbolic the *local angle analysis* method (see section 3.5) must be applied, and the corresponding non-hyperbolic traveltimes must be used in the prediction procedure. Here, the implementation is only valid for multiple-generating reflections with hyperbolic moveout character.

I applied the prediction method to the synthetic and the real data set I already used in chapter 4.3. In the synthetic example the predicted traveltimes of the surface and interbed multiples follow very well the corresponding modeled multiples, in the CSP gather as well as in the zero-offset section.

Also in the real marine data set the prediction method worked very well and the predicted multiples followed nicely seismic events visible in the CSP gather and the stacked zero-offset section. However, in the real data example it is not easy to decide if the recorded seismic reflections at the predicted traveltimes are really multiples or for instance primaries. For identification purposes amplitude information would be helpful. This topic is addressed in the next section.

4.4 Dynamic prediction of multiples

The kinematic prediction of a multiple defines only the arrival time but gives no information about its amplitude and its impact on the observed wavefield. This fact may lead to problems during multiple attenuation, especially in cases when predicted multiple traveltimes strongly interfere with primaries and both of them cannot be separated according to move-out differences. Also the identification of a multiple would be much easier if amplitude information were included in the prediction. These are the reasons why I tried to extend the kinematic prediction method of the previous section straightforwardly to a method which also includes amplitudes in the multiple prediction.

A concept for the prediction of multiple dynamics is presented in this section. First, I will consider a 1D model with an impulsive plane source and develop a multiple prediction algorithm. Next, I will consider a 1D model with a finite source wavelet. The 1D models make the problem easily understandable and provide a reference point for the more complicated 2.5D model with a point source, considered later. In the 2.5D model I also have to take into account the involved geometrical spreading effects. I consider the geometrical spreading factors of the involved multiple-generating primaries and use their *true amplitudes* in order to predict the multiples. As I will show the geometrical spreading factors of the involved multiple-generating primaries can be calculated using kinematic wavefront characteristics. Finally, a viability study using a numerical example illustrates the proposed concept.

4.4.1 Primaries and their true amplitudes

Assume a laterally inhomogeneous acoustic medium with a planar earth surface. All source-receiver pairs involved in the seismic experiment are located at the earth surface. The two locations of a source-receiver pair can be described by one single coordinate ξ as explained in Schleicher et al. [1993] and the particle displacement vector $U_G(\xi, t)$ of a compressional primary reflection can be expressed as follows using the zero-order ray approximation [Červený and Ravindra, 1971; Hubral, 1983]:

$$U_G(\xi, t) \approx \text{Re}\left\{\frac{Q}{L}F(t - \tau_G(\xi))\right\}\hat{e}, \quad (4.4)$$

where $F(t) = s(t) + ig(t)$ is the analytic point source wavelet. It consists of the real source wavelet $s(t)$ and its Hilbert transform $g(t)$. $F(t)$ is not a function of ξ , i.e. it is the same for all rays under consideration, because it is assumed that the compressional point source is reproducible. t is the time, and $\tau_G(\xi)$ is the traveltime of the primary that propagated along the ray from source S to the receiver point G , \hat{e} is the unit vector approximately tangent to the emerging ray at G .

Q is the total loss in amplitude due to transmission and reflection across all interfaces along

the ray and can be written as [Hubral, 1983]

$$Q = \prod_{j=1}^{2n-1} c_j, \quad (4.5)$$

where c_j for $j \neq n$ is the plane wave transmission coefficient at the intersection point O_j of interface j for a wave which is either incident from above ($j < n$) or from below ($j > n$). c_n is the plane wave reflection coefficient of interface n at the reflection point O_n .

L in Equation (4.4) denotes the normalized geometrical spreading factor and it can be written as

$$L = [-\mathbf{J}]^{1/2} \prod_{j=1}^{2n-1} \sqrt{\frac{\cos(\delta_j)}{\cos(\delta'_j)}}, \quad (4.6)$$

where the Jacobian matrix \mathbf{J} can be computed with respect to a ray centered coordinate system as described below. δ_j and δ'_j label the angle between the ray and the interface normal at the incidence and refraction/reflection side of interface j . The factor L can be computed using dynamic ray tracing from the source to the receiver point if the model is known. It can also be expressed by second order derivatives of the traveltime function and therefore computed directly from traveltimes [Tygel et al., 1992].

Multiplying the original primary P-wave reflection in Equation (4.4) by the appropriate geometrical spreading factor compensates for its geometrical spreading loss and leads to its *true amplitude* signal. The true amplitude of an event recorded at a specified receiver location has the same dynamics as a primary reflection resulting from a plane wave emerging at this receiver location and includes the amplitude change of this plane wave due to the influence of the angle-dependent transmission and reflection coefficients along its raypath. For this reason true amplitudes can be used for deriving properties from primary reflections that are based on plane wave theory [Newman, 1973]. For many realistic models the two-way transmission losses for a primary reflection are small and $Q \approx c_n$ in Equation (4.5). In this situation the true amplitude provides direct information on the angle-dependent reflection coefficient c_n .

For a zero-offset reflection each quantity in $\cos \delta$ occurs twice (once in the nominator and once in the denominator) and Equation (4.6) reduces to

$$L(0) = \sqrt{-\mathbf{J}}. \quad (4.7)$$

Hubral [1983] showed that \mathbf{J} for a primary point source reflection in a 3D medium can be expressed using the 2×2 wavefront curvature matrices \mathbf{K}_{NIP} and \mathbf{K}_N of the emerging *normal incidence point wave* (NIP-wave) and *normal wave* (N-wave), respectively:

$$L^2(0) = \sqrt{-\mathbf{J}} = \frac{4}{\det(\mathbf{K}_{NIP} - \mathbf{K}_N)}. \quad (4.8)$$

Considering the kinematic properties of the NIP-wave and N-wave as needed in this work, the NIP wave is a wave that originates at a point source located at the NIP at a specific interface. The N-wave is identical to the wave generated by the exploding reflector scenario.

The wavefront curvature matrix \mathbf{K}_{CSH} of a reflected primary (here called common shot wavefront), which originated from a point source, can be written at the zero-offset location as [Hubral, 1983]

$$\mathbf{K}_{CSH} = \frac{\mathbf{K}_{NIP} + \mathbf{K}_N}{2}. \quad (4.9)$$

Using Equation (4.9) and Equation (4.8) it follows

$$L^2(0) = \sqrt{-\mathbf{J}} = \frac{1}{\det(\mathbf{K}_{CSH} - \mathbf{K}_N)}. \quad (4.10)$$

Assuming that the wavefront of the reflected common shot wave and the wavefront of the N-wave are spherical in the local vicinity of the zero-offset location, Equation (4.10) can be written as

$$L^2(0) = \frac{1}{(K_{CSH} - K_N)^2} = \frac{1}{\left(\frac{1}{R_{CSH}} - \frac{1}{R_N}\right)^2}. \quad (4.11)$$

Equation (4.11) will be used in order to calculate the geometrical spreading factors of the multiple-generating primary reflections at the zero-offset locations, and to calculate their true amplitudes. This requires only the kinematic wavefront-parameters K_{CSH} and K_N to be known.

4.4.2 Method and Implementation

4.4.2.1 1D problem: impulsive plane source

Consider the very simple 1D model in Figure 4.12 (source and receiver are assumed to be coincident) consisting of flat layers with two interfaces and an impulsive source that causes an explosion at $t = 0$ and generates a vertically downward propagating, spike-like plane wave with an amplitude of 1. It is assumed that in such a medium the earth behaves as a 1D linear filter. In such a situation only one single trace is recorded at the zero-offset location. This trace includes primary and multiple reflections and represents the impulse response of the system [see, e.g. Yilmaz, 1989].

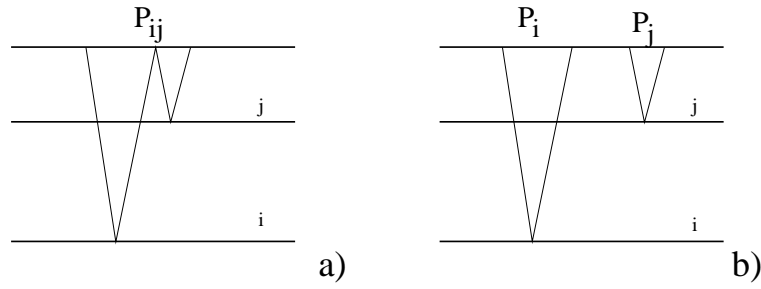


Figure 4.12: Ray scheme of a surface multiple in a 1D model with an ideal impulsive plane source. Sources and receivers are assumed to be coincident. Only one trace is recorded at the zero-offset location. a) First-order surface multiple. b) Decomposition of the raypath of the first-order surface multiple into the raypaths of two primaries.

Let us assume we identified the two primary events P_i and P_j (see Figure 4.12b) corresponding to the primary raypaths which generate the first-order surface multiple in Figure 4.12a. We produce copies of the zero-offset trace where we mute all but the particular primary event P_i and P_j . The resulting *primary traces* are called $P_i(t)$ and $P_j(t)$. Convoluting these two primary traces $P_i(t)$ and $P_j(t)$, and taking into account the downward reflection at the sea surface (reflection coefficient $r_0 \approx -1$) predicts the arrival time and amplitude of the surface multiple event P_{ij} on the *multiple trace* $P_{ij}(t)$ because the traveltime of the multiple is the sum of the two primary traveltimes, and the amplitude of the multiple is the product of the primary amplitudes. Note, in this simple example the amplitudes of the primaries and multiples are of course not influenced by geometrical spreading effects. They only include the reflection and transmission coefficients.

$$P_{ij}(t) = P_i(t) * [-P_j(t)] \quad (4.12)$$

where the operator $*$ indicates convolution between the time series.

Also the interbed multiple event P_{ikj} in Figure 4.13a can be predicted easily in a dynamic way for such a simple 1D model using the identified multiple-generating primary events P_i , P_j and P_k corresponding to the primary raypaths in Figure 4.13b. Similarly to the previous situation imagine, we produce three multiple-generating primary traces $P_i(t)$, $P_j(t)$ and $P_k(t)$ which are used in the prediction process.

First, the two primary traces $P_i(t)$ and $P_j(t)$ are convolved and, second, we correlate the third primary trace $P_k(t)$ including the primary event, reflected from the interbed generating interface, with the result. The convolution amounts to summing up the traveltimes of the primaries P_i and P_j , and by means of correlation the traveltime of the third primary P_k is subtracted. In fact, although it neglects transmission effects across shallower interfaces (between the surface and interface k), this correlation procedure provides information on the reflection coefficient of the upper side of the interbed generating interface k , because the primary P_k is exactly reflected from the multiple-generating interface k (see Figure 4.13b). However, the ray-path of the multiple we want to predict involves the reflection coefficient

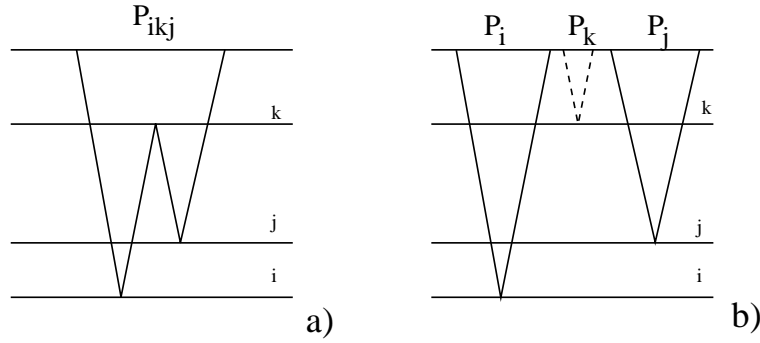


Figure 4.13: Ray-scheme of an interbed multiple in a 1D model with ideal impulsive plane source. Sources and receivers are assumed to be coincident. Only one trace is recorded at the zero-offset location. a) First-order interbed multiple. b) Decomposition of the ray-path of the first-order interbed multiple into the ray-paths of three primaries.

of the lower side of the interbed generating interface k . Therefore, the correct reflection amplitude is given by the minus sign. This leads to the following formulation for the prediction of the multiple trace $P_{ikj}(t)$ containing the predicted interbed multiple event P_{ikj} :

$$P_{ikj}(t) = -P_k(t) \otimes [P_i(t) * P_j(t)], \quad (4.13)$$

where $*$ denotes convolution, and \otimes denotes correlation. $P_i(t)$, $P_j(t)$ and $P_k(t)$ are the traces containing the multiple-generating primary events.

While the convolution process is commutative and involves reversing of the moving array in the calculation, the correlation is not commutative and requires no reversing of the moving array. Both, convolution and correlation correspond to multiplications in the frequency domain [Bracewell, 1965]. A summary about the frequency domain descriptions of convolution and correlation is given in Figure 4.14. In case of convolution the phases are additive whereas for the correlation they are subtractive. The amplitude spectra are multiplied in both mathematical operations. This is exactly the mathematical description of the physical problem. The reflection and transmission coefficients are multiplied while the traveltimes are added and subtracted.

4.4.2.2 1D problem: finite source wavelet

Let us again start with the surface multiple in Figure 4.12. Now we consider a causal source wavelet of finite time duration in the 1D data modeling. If we would apply the same prediction procedure as before in case of the spike-like acquisition wavelet, the predicted surface multiple would be kinematically correct but the shape would be wrong. This is due to the fact that the effects of the acquisition wavelet would be included twice in the predicted multiple because it is included already in both multiple-generating primary traces $P_i(t)$ and $P_j(t)$. Therefore it is necessary to correct for this problem in order to get a correct

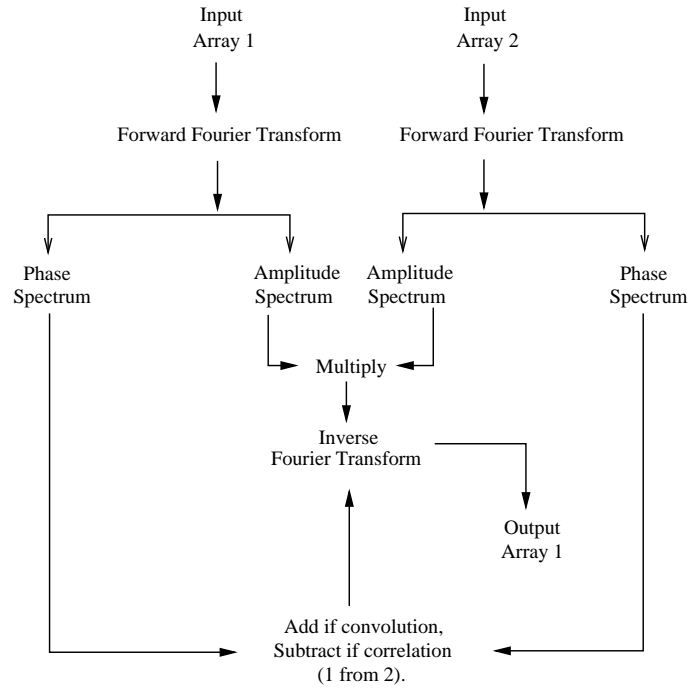


Figure 4.14: *Frequency domain description of the convolution and correlation process. After Yilmaz [1987].*

multiple prediction. This can be done by convolving one multiple-generating primary trace with the inverse source wavelet (deconvolution by inverse filtering) before the convolution with the other multiple-generating primary trace. Now, the source wavelet is included only once in the predicted multiple trace and the prediction is correct. With the same notation as above this can be expressed as

$$P_{ij}(t) = P_i(t) * [P_j(t) * (-S(t)^{-1})]. \quad (4.14)$$

Here, $S(t)^{-1}$ is to denote the inverse source wavelet, i.e. $S(t) * S(t)^{-1} = \delta(t)$.

Similarly, for the first-order interbed multiple example in Figure 4.13 corrections for the source wavelet have to be applied on two of the three multiple generating primaries in order to get the correct multiple prediction results. It follows with the same notation as above:

$$P_{ikj}(t) = [-P_k(t) * S(t)^{-1}] \otimes [P_i(t) * P_j(t) * (S(t)^{-1})]. \quad (4.15)$$

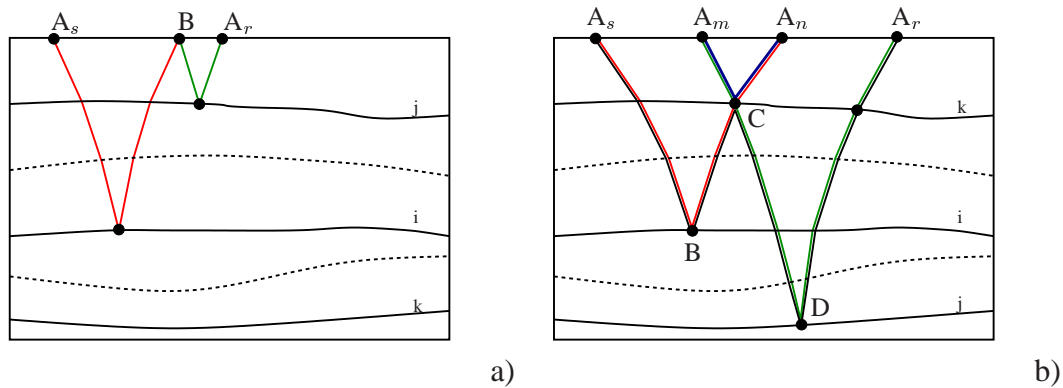


Figure 4.15: 2D laterally inhomogeneous layered subsurface model. a) First-order surface multiple. The raypath of the multiple $A_s B A_r$ can be decomposed into the primary segments $A_s B$ (red) and $B A_r$ (green). b) First-order interbed multiple. The raypath of the multiple $A_s B C D A_r$ (black) can be decomposed into the primary segments $A_s B A_n$ (red), $A_m D A_r$ (green), and $A_m C A_n$ (blue).

4.4.2.3 2.5D problem: point source

Here, I consider a more realistic situation. I assume a dense 2D multicoverage data acquisition and consider 2D multiple and primary reflections (see Figure 4.15a,b). The 2.5D earth-model assumption implies that the model does not change in cross-line direction. A reproducible compressional point source produces 3D seismic waves which include also 3D geometrical spreading. The geometrical spreading has to be considered in the multiple prediction procedure.

Assume we would predict a 2D first-order surface multiple trace at a receiver location A_r in Figure 4.15 by a 1D convolution (as we did in the 1D models) between the two multiple-generating primary traces. This would lead to the correct traveltime but the amplitude would be proportional to the product of the primary geometrical spreading factors, and would be incorrect. The 1D convolution does not consider the 3D geometrical effect in the correct way.

Jakubowicz [1998] proposes a method for the prediction of multiples where he considers the complete primary wavefields for the multiple prediction in multichannel convolutions and correlations, which implicitly include the geometrical spreading correction (pers. communication). The 2D or 3D multichannel convolutions (for 2D or 3D media), involve that each trace of the predicted multiple is the result of convolving and summing several primary traces. However, even if the multichannel convolutions are performed in the frequency domain they are much more time consuming than 1D convolutions.

Despite the increased complexity of 2D or 3D media I am still able to benefit from the simplicity of 1D convolutions and correlations. This is possible because I can identify and select the primary events which generate a certain multiple event recorded at a specified

trace using the appropriate multiple conditions. This means that I know trace and time of the primary events which build up a certain multiple event at a specified trace, and exactly these primary events I want to use in the 1D convolutions and correlations in order to predict the arrival time and amplitude of this multiple. Because of the fact that the 1D convolutions do not imply the 3D geometrical spreading correction, contrary to the method of Jakubowicz [1998], I explicitly have to take into account the geometrical spreading effects in the multiple prediction procedure.

This is done by calculating the *true amplitudes* of the selected multiple-generating primaries prior the convolution and correlations with each other. These true amplitudes include the offset-dependent reflectivity and transmissivity effects which indeed have to be considered in the offset-dependent multiple prediction. As a matter of fact, the convolutions and correlations of the true amplitude primaries predict *true amplitude multiples*. These true amplitude multiples have to be finally corrected for their geometrical spreading loss in order to match the multiples obtained from direct modeling or recorded as field data.

In case of the first-order surface multiple the following equation is used for the dynamic multiple prediction

$$P_{ij}(t) = \frac{P_i(t)L_i * [P_j(t)L_j * (-S(t)^{-1})]}{L_{ij}}, \quad (4.16)$$

where L_i and L_j are the geometrical spreading factors of the two primary events P_i and P_j , respectively. L_{ij} denotes the geometrical spreading factor of the surface multiple event P_{ij} . The rest of the notation is the same as above. For the sake of simplicity I drop here, and in the following, the dependence upon offset x .

Similarly, the interbed multiple can be predicted using

$$P_{ikj}(t) = \frac{[-P_k(t)L_k * S(t)^{-1}] \otimes [P_j(t)L_j * P_i(t)L_i * S(t)^{-1}]}{L_{ikj}}. \quad (4.17)$$

4.4.2.4 Implementation

In order to apply Equation (4.16) or Equation (4.17) we must first calculate the geometrical spreading factors of the involved primaries (L_i, L_j, L_k), and the multiple (L_{ikj}, L_{ij}). We also have to correct for the source wavelet by deconvolution.

If the source waveform were known, then the solution to the deconvolution problem is deterministic, and inverse filtering can be applied. If the source waveform is not known the solution to the deconvolution problem is statistical, and e.g. the Wiener prediction theory can be used [e.g. Robinson and Treitel, 1980; Yilmaz, 1989].

In order to calculate the geometrical spreading factors $L_M(x)$ of the involved primaries at

a certain source-receiver distance x , I calculate at first the geometrical spreading $L_M(0)$ at the zero-offset location of a primary point source reflection from interface M using Equation (4.11), as derived above:

$$\frac{1}{L_M(0)} = \frac{1}{R_{CSH}^M} - \frac{1}{R_N^M}, \quad (4.18)$$

where R_{CSH}^M and R_N^M are the wavefront radii of the reflected CSP wave and the N-wave (created by exploding the reflector) at the zero-offset location, respectively. The radii R_{CSH}^M in Equation (4.18) and the emergence angle are estimated in the CSP gather using the CSP HI method. R_N^M can be estimated in the zero-offset or minimum offset gather [Keydar et al., 1990, 1996]. So far no explicit knowledge of the subsurface is required. Only the near surface velocity v_0 is assumed to be known. However, in Equation (4.16) and Equation (4.17) we need to know the geometrical spreading of the involved primaries and the multiple for non-zero-offset traces which requires approximations, and a horizontally layered earth-model assumption.

The geometrical spreading of a primary P wave reflection for a point source in a horizontally layered medium at an offset x can be approximated using the geometrical spreading at the zero-offset location $L_M(0)$ in the following equation [modified from Ursin, 1990]:

$$L_M(x) = \{L_M(0^2) + [\frac{2R_{CSH}^M}{v_0 t_0} - 1]x^2 + \frac{1}{t_0^2}[\frac{1}{v_0^2} - \frac{t_0}{R_{CSH}^M v_0}]x^4\}^{1/2}, \quad (4.19)$$

where v_0 is the near surface velocity and t_0 the two-way normal-incidence traveltimes.

Finally, the geometrical spreading factor (L_{ikj} or L_{ij}) of the multiple (P_{ikj} or P_{ij}) can be calculated in a horizontally layered medium by algebraic summation of the geometrical spreading factors of the primaries generating the multiple. In case of an interbed multiple, Equation (4.20) can be applied.

$$L_{ikj} = L_i + L_j - L_k \quad (4.20)$$

Using these results in Equations (4.16) and (4.17) makes it possible to predict traveltimes and amplitudes of surface related as well as interbed multiples. The proposed method was applied to synthetic data, as described next.

4.4.3 Synthetic example

A horizontally layered earth-model was used to test the 2D dynamic multiple prediction method, see Figure 4.16a. A shot gather calculated by zero-order dynamic ray-tracing is shown in Figure 4.16b. Full geometrical spreading was used in the data modeling. Only

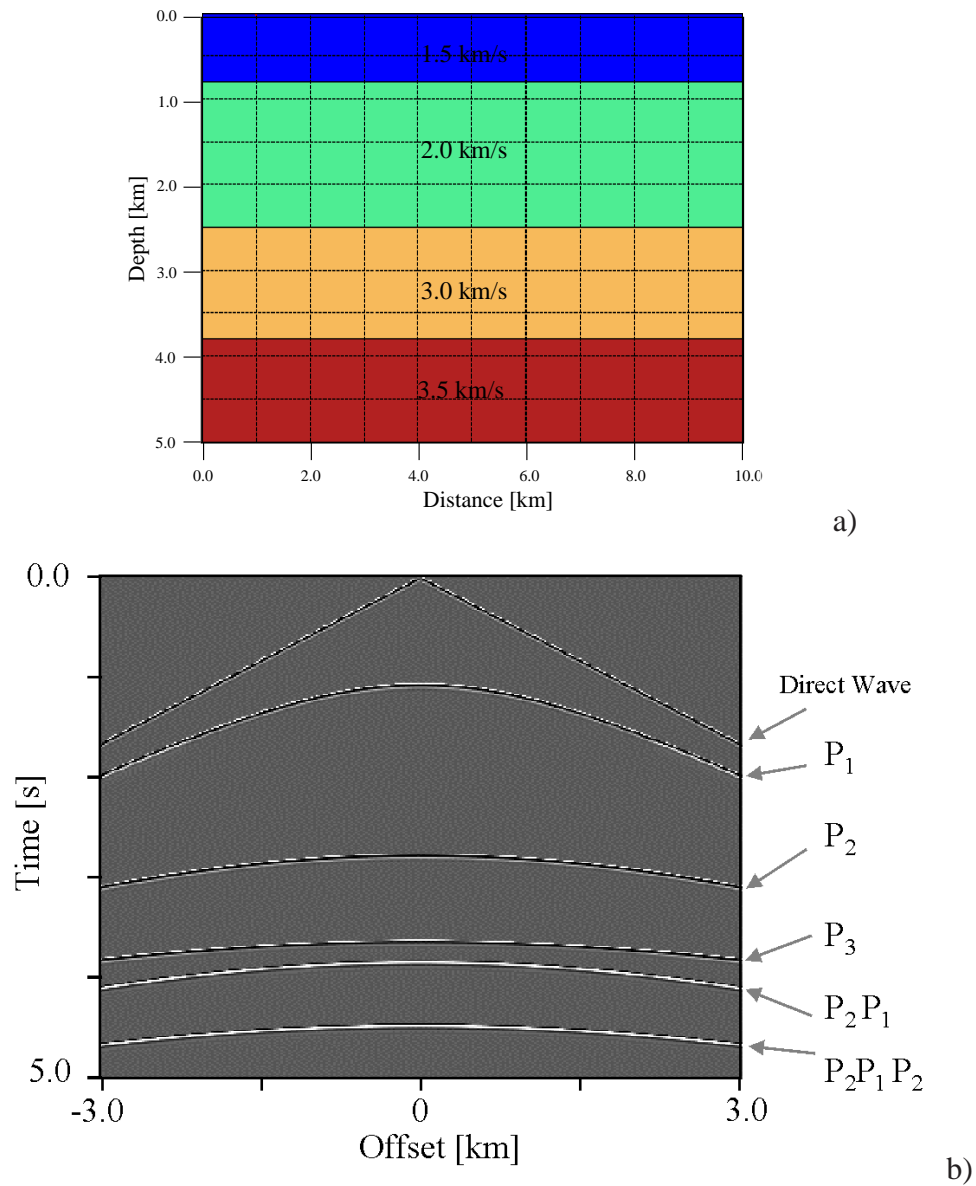


Figure 4.16: a) Horizontally layered earth model. b) Shot gather calculated by ray-tracing using the model in a). The primaries and multiples are indicated.

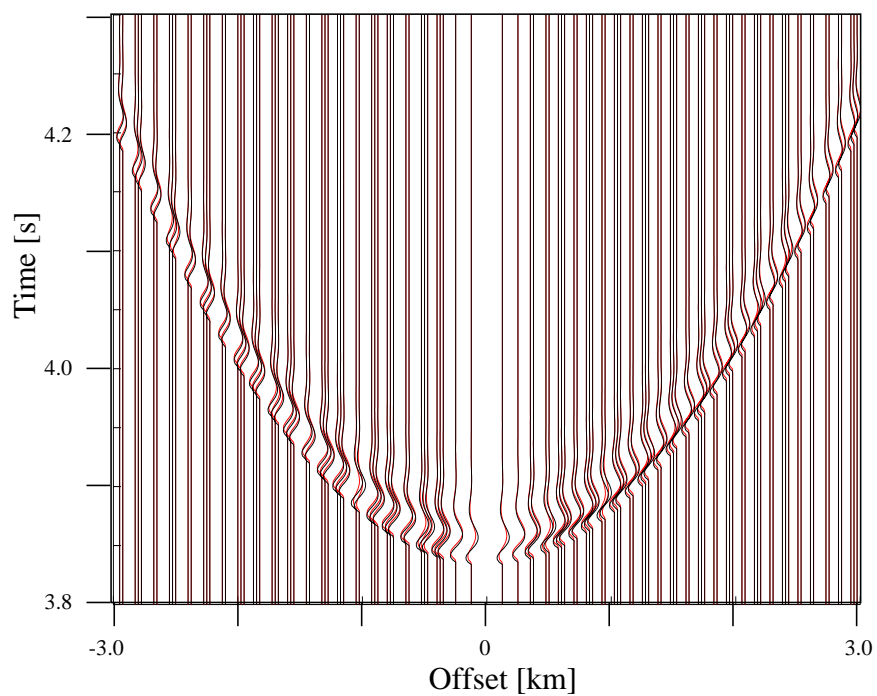
three primaries and two multiples, one surface (P_2P_1) and one interbed multiple ($P_2P_1P_2$), have been considered in the ray-tracing procedure.

The emergence angle β_0 and the radius R_{CSH} at the zero-offset location, as well as the emergence angles at all source-receiver positions have been calculated using the *global angle analysis* procedure (section 3.4). The radius R_N is equal to infinity in case of flat interfaces. Using these radii I calculated the geometrical spreading factor of the primaries, first at zero-offset using Equation (4.18), and second at each source-receiver pair using Equation (4.19).

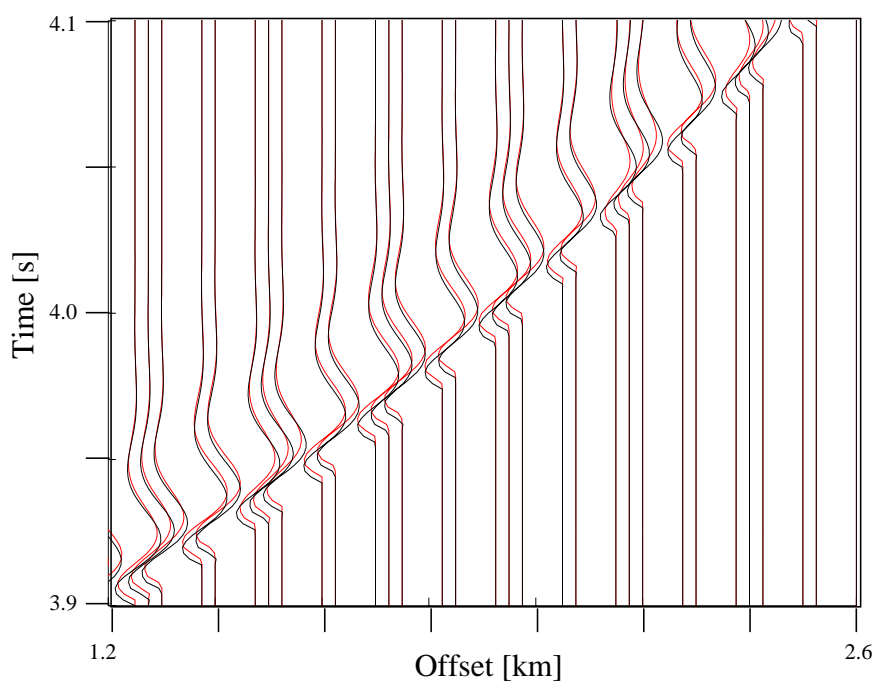
In the next step the primaries, generating the specified multiple, have been selected using the appropriate multiple conditions and the two multiples have been predicted using Equation (4.16) and Equation (4.17). The source signature was extracted from the direct wave, and used for deterministic deconvolution (here, least-squares inverse filtering).

The predicted surface multiple (P_2P_1) and interbed multiple ($P_2P_1P_2$) vs. the directly modeled multiples are shown in Figure 4.17 and Figure 4.18, respectively. For the sake of clarity not all predicted multiple traces are shown. The irregular trace spacing is due to the fact that not at each offset multiple-generating primaries could be selected. The amplitude prediction of the surface multiple in Figure 4.17a shows a very good agreement with the modeled data. Only in the zoomed section in Figure 4.17b small amplitude differences and a small time shift becomes visible. Also, the predicted interbed multiple traces shown in Figure 4.18a match well with the modeled data. The amplitude differences in the zoomed section in Figure 4.18b are larger than in the surface multiple case.

Possible sources for the amplitude deviations between predicted and modeled multiples are the signal deconvolution, and the mentioned approximations in the calculation of the geometrical spreading factors of the primaries as well as small errors in the search of the multiple-generating primary traces. The interbed multiple prediction also includes a scaling error due to the neglect of transmission effects between the surface and the interbed generating interface, which are usually negligible and which are not relevant for the interbed multiple considered in this example.

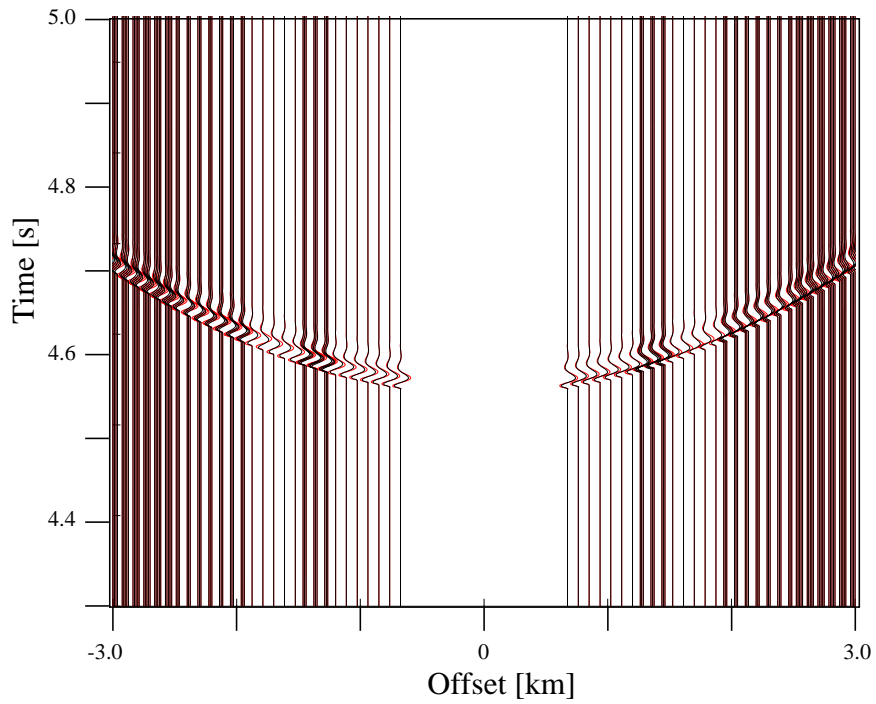


a)

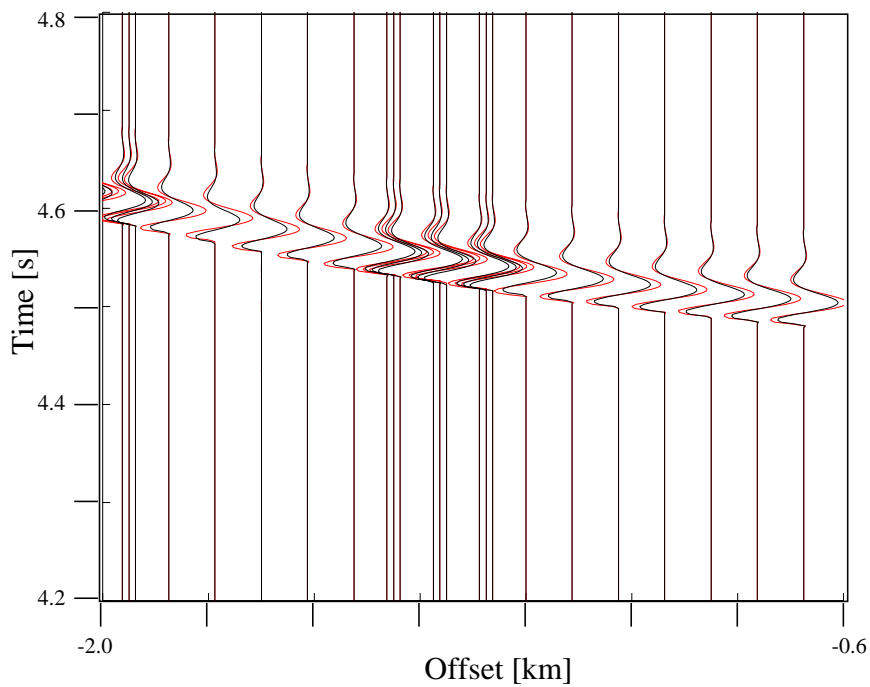


b)

Figure 4.17: a) Predicted surface multiple (P_2P_1) shown in red color vs. modeled surface multiple shown in black color. b) Zoomed section of a).



a)



b)

Figure 4.18: a) Predicted interbed multiple ($P_2P_1P_2$) shown in red color vs. modeled interbed multiple shown in black color. b) Zoomed section of a).

4.4.4 Results

I extended the target-oriented 2D kinematic multiple prediction method straightforwardly to a target-oriented 2D dynamic multiple prediction method taking into account full geometrical spreading.

The user interaction is still limited to an identification of multiple generating primary reflections in a simulated zero-offset section. Contrary to the kinematic prediction method, corrections for the source wavelet have to be applied and the geometrical spreading effects must be taken into account. Also an additional wavefront curvature, namely K_N of the N-wave must be estimated in the zero-offset section in case that curved interfaces are considered.

In the present implementation corrections for the source wavelet are done by deterministic deconvolution and require the knowledge of the source waveform. The consideration of the full geometrical spreading effects in the 2D multiple prediction method requires additional approximations and assumptions on the subsurface. The fact that I know the traces and times of the primary events which build up a certain multiple at a specified trace allows simple 1D convolutions and correlations in the prediction procedure.

The geometrical spreading of the primaries and multiples at the zero-offset location can be calculated using the kinematic wavefront-parameters (R_{CSH}, R_N) without any subsurface information other than the near surface velocity. The extrapolation of the geometrical spreading factor from zero-offset to non-zero finite offset is an approximation and implies horizontally layered interfaces. Also the calculation of the geometrical spreading factor of the multiple using the geometrical spreading factors of the multiple-generating primaries, requires horizontal layering. In case of the dynamic prediction of interbed multiples the transmission loss between the surface and the interbed generating interface is neglected which could lead to scaling problems. Also Jakubowicz [1998] mentions this scaling problems for interbed multiples.

I applied the procedure to a 2D data set for a model with horizontal interfaces. One surface and one interbed multiple have been predicted. In case of the surface multiple the amplitude prediction results matched the directly modeled data very well. Also in case of the interbed multiple a good match was obtained. However, the amplitude difference to the modeled data was larger.

4.5 Summary

In this chapter I presented two 2D multiple prediction methods. The first can be used for the traveltimes prediction of surface and interbed multiples. This method requires no subsurface information other than the near surface velocity. Based on the identification of multiple-generating reflections in a stacked section and the specification of a desired multiple (ray-code), the kinematics of this multiple can be predicted in CSP gathers. After the source-

receiver pairs of the multiple-generating events have been selected, a simple summing and subtracting of traveltimes leads to the desired arrival time of the corresponding multiple.

The second introduced method is for the 2D dynamic prediction of surface and interbed multiples in consideration of full geometrical spreading. While this method is still based on the same methodology, it requires additional informations on the data acquisition as well as assumptions and approximations on the subsurface model. Instead of simple summing and subtracting of primary traveltimes, selected multiple generating primary events are now simply 1D convolved and correlated with each other. Corrections for the source wavelet and the geometrical spreading effects have to be applied, While the method might be a good approximation for moderately dipping interfaces it is strictly speaking only exact for 3D horizontally layered laterally homogeneous media. Nevertheless, instead of 2D or even 3D convolutions as used in other methods, only 1D convolutions and correlations are performed. The amplitude information can be an advantage especially in situations where the primaries and multiples show no moveout differences. Also for the multiple identification a rough amplitude estimation of the predicted multiple can be very helpful for an interpreter.

Both 2D multiple prediction methods require physical consistency between primary and multiple events. This means that for a certain multiple which is part of the recorded wavefield also the multiple generating primaries must be part of the recorded wavefield and vice versa. For a 2D survey this requires a 2.5D underlying model. However these assumptions might be violated in real measurements by a cross-line dip, variations in the source wavelet, too coarse sampling in source and receiver positions, and other effects.

Chapter 5

Attenuation of predicted multiples using the parabolic Radon transform

5.1 Introduction

After the multiples have been predicted they have to be eliminated or at least attenuated. I prefer the terms 'attenuation' or 'suppression' because a complete elimination of multiples without affecting primaries is possible only in exceptionally simple cases. Especially in real data a complete separation of primaries and multiples is hardly ever achievable. Problems arise especially in situations where an undesired multiple traveltime curve closely follows a desired primary. That means that their zero-offset time and moveout are approximately equal to each other. In such cases it is very difficult to attenuate the multiple without damaging the primary even when the multiple is correctly predicted. However, in the simpler and much more common case that primaries and multiples are only crossing each other different techniques might be applied which allow the effective multiple attenuation without damaging primaries.

In this chapter, I use the kinematically predicted multiples, which have been determined using wavefront characteristics of primaries (section 4.3) in the multiple attenuation process. The successful attenuation of predicted multiples without damaging primaries using a moveout-based filtering method requires a certain differential moveout between primaries and multiples. Such moveout differences can be better exploited in other data spaces, as in the f - k , linear τ - p , hyperbolic τ - p , or parabolic τ - p space rather than in the x - t domain, because here the event separation is better (see chapter 1.2). Multiple filtering based on the separability between primaries and multiples in the f - k or linear τ - p domain works effectively for long-period multiples at far-offset traces where the moveout differences are usually larger but they might fail at short offsets where moveout differences are rather small and slowness values similar. The standard linear τ - p transform, which is also known as slant stack or linear Radon transform, uses a straight line stacking operator and maps hyperbolic reflection events into ellipses and linear refraction events or direct waves into

points in the linear τ - p domain [see Schultz and Claerbout, 1978; Diebold and Stoffa, 1981; Zhou and Greenhalgh, 1994; Treitel et al., 1982]. In this case the parameter τ labels the intercept time and p the slowness. Primary and multiple reflections have rather hyperbolic trajectories and are much better approximated by hyperbolic stacking operators instead of straight line stacking operators [see Hampson, 1986; Kostov and Biondi, 1987; Jou et al., 1996]. This is the reason why the focusing of energy in the transform domain is much better using a hyperbolic Radon transform instead of a linear Radon transform. In particular the multiples can be better isolated from the desired signal than in the x - t , f - k , or linear τ - p domain at both, near and far offset traces [Zhou and Greenhalgh, 1994, 1996].

Thorson and Claerbout [1985] proposed an algorithm for velocity stack along a hyperbolic trajectories instead of a straight line, which can be seen as one form of the generalized Radon transform. The computational realization of this method is quite expensive due to the time variable transform. Hampson [1986] introduced the parabolic Radon (τ - p) transform, which is a more practical and cheaper approach because it allows an explicit solution to be derived. The parabolic Radon transform has the important advantage that it is time invariant for a specific value of velocity [Yilmaz, 1989]. Before the parabolic Radon transform is carried out the hyperbolic events should be transformed into parabolic events. This can be realized by NMO correcting or by t^2 -stretching of the CMP gathers. Hampson [1986] proved that the NMO correction transforms hyperbolic events into approximately parabolic events and used this parabolic modeling scheme before the parabolic Radon (τ - p) transform is carried out. However, the deviation of the NMO corrected events in a CMP gather from the ideal parabolic form leads to amplitude smearing in the parabolic τ - p domain and reduces event separation, which is essential for noise filtering. Another problem is the loss of far-offset data due to the NMO stretch-muting, which is usually applied after NMO correction. In order to circumvent these problems Yilmaz [1989] introduced a t^2 -stretching of the time axis before the parabolic Radon (τ - p) transform is carried out in order to correctly transform hyperbolic into parabolic events. This reduces the amplitude smearing caused by wrongly chosen NMO velocities and allows a better separation of primaries and multiples in the parabolic τ - p space. The separated multiples can be suppressed by muting the multiple energy in the parabolic τ - p domain and inverse mapping of the primaries only [Zhou and Greenhalgh, 1996; Landa et al., 1999a,c; Zaskie et al., 1999].

Of particular interest for multiple attenuation is the definition of the multiple reject zone. Normally multiple suppression in the τ - p domain is done manually by muting the area where the multiple energy is assumed to be concentrated. The decision whether a particular event is a primary or a multiple is often a difficult task and is usually based on velocity discrimination. An important advantage of the predict and subtract method in this work is that the multiple reject area of the filter can be found automatically by using the already in chapter 4 predicted multiple traveltimes. There exist different approaches which incorporate a predicted multiple model for the automatic definition of multiple reject zones. Zhou and Greenhalgh [1996] developed a gain function which defines the multiple muting area based on the energy ratio between a wave equation based predicted multiple model and the original parabolic Radon transformed gather including primaries and multiples. Landa et al. [1999a] suggest different possibilities for the multiple attenuation using a kinemat-

ically predicted multiple model and the parabolic Radon transform. They also propose a semblance weighted parabolic Radon transform, which enhances the event separation further more. The drawback of this method is that an exact reconstruction of the data in the x - t domain is not guaranteed.

In this chapter I present three different multiple attenuation techniques. They all work fully automatic with no user interaction and make use of the parabolic Radon transform in order to get 'maximum' separation between the predicted multiples and interfering primaries. The first technique was introduced by Landa et al. [1999a], the second by Zhou and Greenhalgh [1996] and in the third one I propose a method which is using aspects of both of them. There are two principal differences between the latter and the former methods. First, the final multiple filtering is done in the x - t domain instead of the parabolic τ - p domain. Second, I use another wavefield representation in the final multiple filtering process, whereby the original seismogram is separated into normalized seismogram and envelope; the filtering is performed using the latter one. The different techniques are illustrated using synthetic and real data examples.

5.2 Multiple attenuation in the parabolic τ - p domain

5.2.1 Elliptical multiple rejection filter

5.2.1.1 The method

Landa et al. [1999a] use predicted multiple traveltimes in order to define a multiple model in the x - t domain and propose two different methods for their automatic attenuation using the parabolic τ - p transform. Both techniques are based on the automatic definition of the multiple reject zone in the parabolic τ - p domain: In the first technique they use a gain function originally introduced by Zhou and Greenhalgh (1996), in the second they automatically define ellipse-shaped τ - p multiple reject zones corresponding to the main multiple energy which can be defined using the predicted multiple traveltimes. In this section I will review the latter method, the former will be discussed in the next section.

In Figure 5.1 the determination of the multiple reject zone is explained in the x - q domain after the nonlinear t^2 -stretching of the time axis in a CSP or CMP gather in the x - t domain was performed. The variable q equals the squared zero-offset time t_0^2 , p denotes the squared slowness, x labels the source-receiver distance in a CSP or CMP gather, x_{min} and x_{max} denote the source-receiver distance to the minimum and maximum offset trace, and T is the dominant period of the signal in the x - q space. The t^2 -stretching of the time axis in a CSP or CMP gather was applied in order to make the hyperbolic events parabolic [Yilmaz, 1989]. The maximum energy of an event located at zero-offset time q_0 is gathered in the parabolic τ - p domain in an area limited in the p -direction by $1/v_{min}^2$ and $1/v_{max}^2$. The variable p labels the squared horizontal slowness and τ the squared zero-offset time. This area corresponds

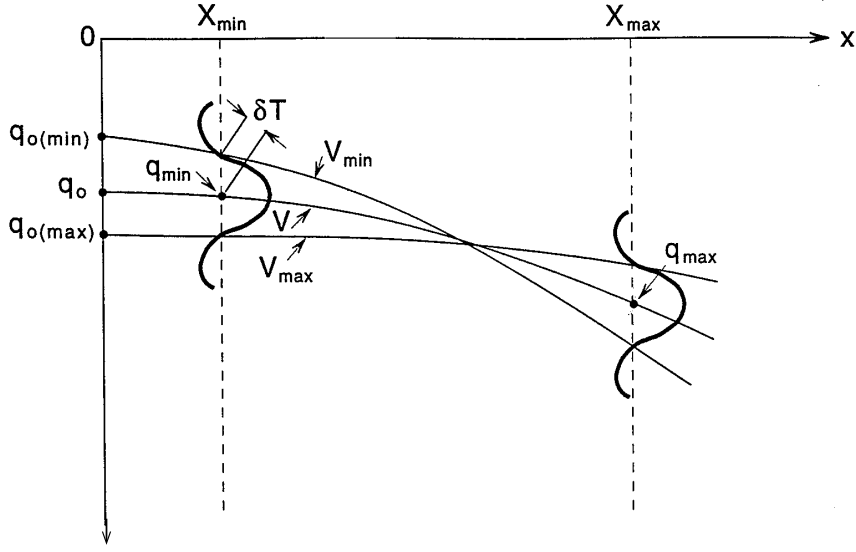


Figure 5.1: *Determination of the multiple reject zone after Landa et al. [1999a]. The maximum energy of an event located at zero offset time q_0 is gathered in the parabolic τ - p domain in an area limited in the p -direction by $1/v_{min}^2$ and $1/v_{max}^2$. This corresponds to the maximum time shift (1/2 period) between minimum and maximum offset considering a coherent summation along the parabolic stacking operators.*

to the maximum time shift at the largest offset x_{max} which differs no more than 1/4 signal period from the correct time shift at the largest offset (Figure 5.1). Only in this window a coherent summation can be performed. Now, the question is how to estimate the size and direction of the muting area corresponding to the maximum energy of a multiple event in the transform domain. The center of the signal in (Figure 5.1) at minimum and maximum source-receiver distance can be expressed using the following parabolic expressions:

$$\begin{aligned} q_{min} = \Delta\tau_k^{min} &= q_0 + \frac{X_{min}^2}{v^2}, \\ q_{max} = \Delta\tau_k^{max} &= q_0 + \frac{X_{max}^2}{v^2}. \end{aligned} \quad (5.1)$$

Also the limits of the coherent summation can be defined:

$$\begin{aligned} q_{min} - \frac{T}{4} &= q_{0(min)} + \frac{X_{min}^2}{v_{min}^2}, \\ q_{max} + \frac{T}{4} &= q_{0(max)} + \frac{X_{max}^2}{v_{min}^2}, \\ q_{min} + \frac{T}{4} &= q_{0(max)} + \frac{X_{min}^2}{v_{max}^2}, \end{aligned} \quad (5.2)$$

$$q_{max} - \frac{T}{4} = q_{0(max)} + \frac{X_{max}^2}{v_{max}^2}.$$

Using Equations (5.2) it follows for v_{min} and v_{max} :

$$v_{min} = \sqrt{\frac{x_{max}^2 - x_{min}^2}{q_{max} - q_{min} + \frac{T}{2}}}, \quad (5.3)$$

$$v_{max} = \sqrt{\frac{x_{max}^2 - x_{min}^2}{q_{max} - q_{min} - \frac{T}{2}}},$$

and the size (δp , $\delta \tau$) and orientation (α) of the muting area in parabolic τ - p domain can be defined. δp labels the length of the multiple reject area in p -direction, $\delta \tau$ in τ -direction, and α the dip of the reject area:

$$\delta p = \frac{1}{v_{min}^2} - \frac{1}{v_{max}^2}, \quad (5.4)$$

$$\delta \tau = q_{0max} - q_{0min} = x_{max}^2 \delta p - \frac{T}{2}, \quad (5.5)$$

$$\tan \alpha = \frac{\delta \tau}{\delta p}. \quad (5.6)$$

Using Equation (5.4)–(5.6) a multiple rejection area can be defined. Landa et al (1999) choose an elliptic reject area with the main axes a and b and the dip α (Figure 5.2):

$$a = \frac{\delta \tau}{\sin \alpha}, \quad (5.7)$$

$$b = \sqrt{\frac{\frac{T^2}{4} - a^2 \sin^2 \alpha}{\cos^2 \alpha}}.$$

This muting ellipse corresponds to a half period of the signal. In practice the parameter b is multiplied by a scalar proportional to the wavelet length. In case of good separation the ellipse can be chosen larger, in case of bad separation the ellipse should be smaller of course with the drawback of stronger residual multiple energy. In case of bad separation there is always a tradeoff between maximum attenuation and preservation of the primaries.

The resolution of the parabolic Radon operator can be improved by multiplication of each sample in the τ - p domain with a non-linear semblance function calculated on the input data along the same parabolic stacking trajectories which are used in order to obtain the

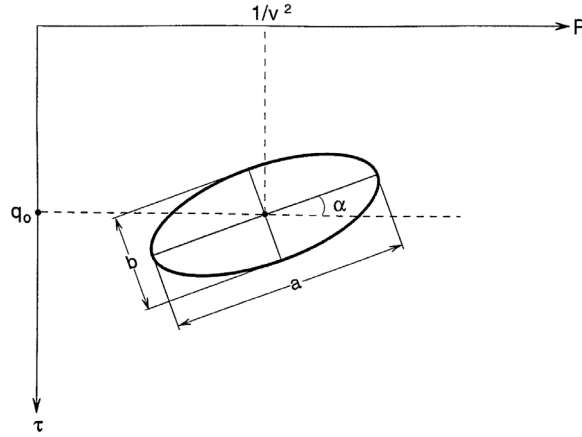


Figure 5.2: Definition of an elliptical multiple muting area after Landa et al. [1999a].

τ - p transformation. Considering this semblance function as a weighting function $w(h)$ it follows:

$$u_w(p, \tau) = \int_0^{\infty} w(h) d(h, t) dh. \quad (5.8)$$

$u_w(p, \tau)$ denotes the semblance weighted output data, $d(h, t)$ the input data, $w(h)$ the weighting function, and h the offset. This semblance weighted parabolic stacking improves the event separation in the parabolic τ - p domain. However, the drawback is that an exact reconstruction of the original x - t data is not guaranteed.

In the following the complete processing flow of the explained multiple attenuation technique is given:

1. Input: CMP gather including multiples and primaries. Predicted multiple traveltimes in CMP gather.
2. Perform t^2 -stretching of seismic input data in order to transform hyperbolic events into parabolic events.
3. Perform t^2 -stretching of predicted multiple traveltimes and approximate the results by a parabolic traveltime function $t(q_0, v)$.
4. Transform the data obtained in step 2, which include multiples and primaries in the parabolic τ - p domain. Also semblance weighting can be applied in order to increase resolution, see text.
5. Transform the predicted multiple traveltimes obtained in step 3 in the parabolic τ - p domain. This defines the central point $(q_0, 1/v^2)$ of the multiple muting area in the parabolic τ - p domain.

6. Define elliptic multiple rejection area around the central point, specified in step 5, by using the predicted zero-offset multiple traveltimes, minimum and maximum source-receiver offset as well as an estimated dominant period of the source wavelet in Equations (5.3)-(5.7).
7. Mute predicted multiple reject area, defined in step 6, in the parabolic τ - p domain.
8. Inverse parabolic τ - p transform the filtered data obtained in step 7.
9. Perform inverse t^2 -stretching of data obtained in step 8.
10. Output: CMP gather after multiple attenuation.

Note, the attenuation method is based on a kinematic multiple model, which can be obtained by applying the presented multiple prediction method using wavefront characteristics of primaries in chapter 4. The method is illustrated in the following synthetic example.

5.2.1.2 Synthetic example: flat layer model

Using a five layer model with horizontal interfaces a CSP gather was calculated by acoustic modeling. The trace spacing was 20 m, the time sample rate 4 ms and a 25 Hz Ricker source wavelet was used. Several multiples have been predicted using wave front characteristics of primaries. In Figure 5.3 the CSP gather is shown together with the predicted multiple traveltimes, which follow nicely the modeled multiple events.

An explanation of the event labeling is given in the Figure caption. The goal is to attenuate the very well predicted multiples without damaging the primaries. This might be especially difficult in situations where primaries and multiples interfere with each other (e.g. R_1 and $BM1$). After t^2 -stretching of the CSP gather a semblance weighted parabolic τ - p transform was calculated, see Figure 5.4a. It is obvious that interfering events in the x - t domain are much better separated. According to Equations (5.6)-(5.7) elliptical multiple muting areas are defined which are shown as solid lines in Figure 5.4a. The results of the multiple filtering after inverse t^2 -stretching are shown in Figure 5.4b. The multiples are well suppressed and only the primaries are left. However, an exact reconstruction of the original x - t data is not guaranteed in this case due to the mentioned semblance weighting. Therefore, I will not use semblance weighting in the rest of this work.

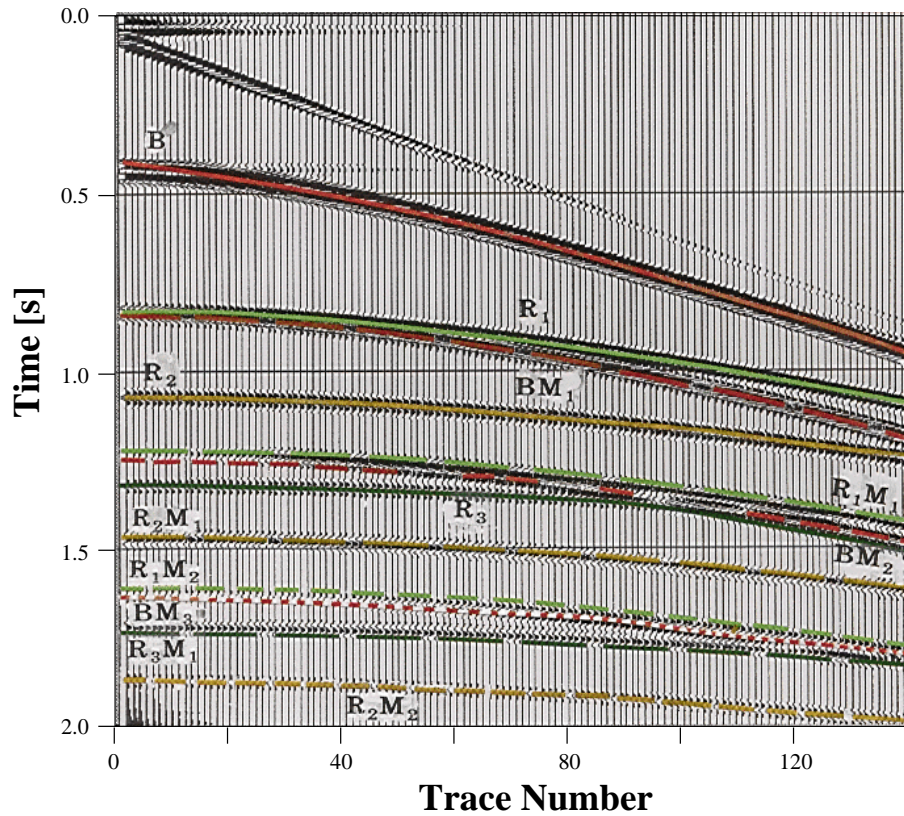


Figure 5.3: Synthetic CSP gather calculated by acoustic modeling (from Keydar et al. [1998]). The primary reflections B , R_1 , R_2 and R_3 are labeled on the gather. The water bottom multiples of the first, second, third and fourth order are labeled BM_1 , BM_2 , BM_3 and BM_4 . The same notation is used for the multiples from the reflector B , R_1 , R_2 and R_3 .

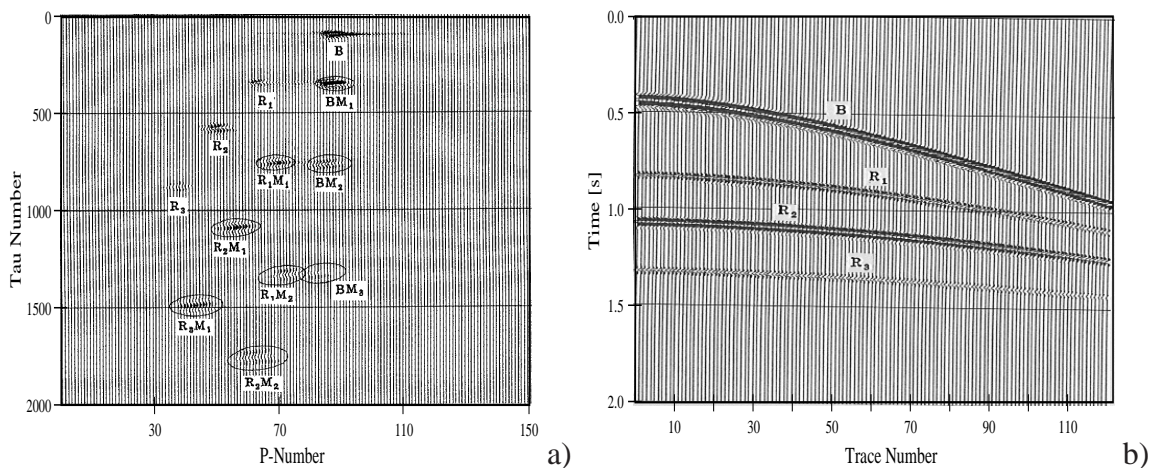


Figure 5.4: a) Semblance weighted parabolic τ - p transform of the data in Figure 5.3. The ellipses shown in solid lines indicate the multiple muting areas. b) CSP gather after multiple filtering and inverse parabolic τ - p transform followed by inverse t^2 -stretching (From Landa et al. [1999a]).

5.2.2 Data adaptive 2D demultiple filter

5.2.2.1 The method

Another elegant approach to define a multiple suppression filter in the parabolic τ - p domain based on the prediction of multiple model traces was proposed by Zhou and Greenhalgh [1996]. In their approach the multiple reject areas are determined automatically by comparing the energy of the multiple model and the original input data in the τ - p space. For the prediction of the multiple model they used wavefield extrapolation. Landa et al. [1999a] and Zasko et al. [1999] used this approach also for the attenuation of kinematically predicted multiples. They constructed a dynamic multiple model by removing the wavefield in time windows around the predicted multiple traveltimes from the original data. Alternatively, the dynamically predicted multiples of section 4.4 could be used as a multiple model. The multiple model defines where the multiple energy in the original data should be attenuated. By comparing the energy of the predicted multiple model with the input data including primaries and multiples at each τ - p point a non-linear multiple rejection filter is designed. Similarly to Zhou and Greenhalgh [1996] and Landa et al. [1999a] I use a Butterworth-type gain function for the adaptive weighting (filter function), which has to be applied at each pixel in the parabolic τ - p domain. The gain function can be written as

$$g(\tau, p) = \frac{1}{\sqrt{1 + \frac{B(\tau, p)}{(\epsilon A(\tau, p))^n}}}, \quad (5.9)$$

where $B(\tau, p)$ is the windowed sum of the absolute amplitude of the pixel centered at τ - p on the τ - p -transformed predicted multiple model traces; $A(\tau, p)$ is that on the τ - p -transformed input data, including primaries and multiples; n controls the smoothness of the filter, and ϵ is the multiple rejection parameter. If ϵ is large relatively, strong residual multiples will be left in the filtered data, while a small ϵ may lead also to attenuation of primary information. An initial estimate can be set at the ratio between the average trace amplitude for the multiple model and the original input data [see Zhou and Greenhalgh, 1996]. The final choice depends on the separation of multiples and primaries. A relatively small ϵ can be used for good separated data, a small ϵ may give better results if the data are poorly separated. The demultiple filter will automatically define the multiple rejection areas and taper the rejection boundary in the parabolic τ - p space. If the pixel energy ratio B/A is less than the multiple rejection parameter ϵ (where no multiples are present), g produces a flat (approximately one) response; If B/A is larger than ϵ the filter's gain function is close to zero. The complexity of the filter depends totally on the complexity of the predicted multiple model in the parabolic τ - p space.

In the following I give the complete processing flow of this multiple attenuation method.

1. Input: CMP gather including multiples and primaries.

2. Predict multiple traveltimes using wavefront characteristics of primaries.
3. Construct a multiple model by extracting the wavefield from the input data in time windows around the predicted multiple traveltimes obtained in step 2.
4. Perform t^2 -stretching of seismic input data and predicted multiple model traces of step 3 in order to transform hyperbolic events into parabolic events.
5. Transform the data obtained in step 4 in the parabolic τ - p domain.
6. Use results obtained in step 5 in Equation (5.9) to construct a multiple attenuation filter in the parabolic τ - p domain.
7. Apply the demultiple filter defined in step 6 to the parabolic τ - p transformed input data in step 5.
8. Inverse parabolic τ - p transform the filtered data calculated in step 7.
9. Perform inverse t^2 -stretching of data obtained in step 8.
10. Output: CMP gather after multiple attenuation.

The power of this method is shown in the following synthetic example.

5.2.2.2 Synthetic example: flat layer model

In this section I use the same flat layer example as in section 5.2.1. A CSP gather, which is described in detail in Figure 5.3, is shown in Figure 5.5a. This time the wavefield in time windows around the predicted multiple traveltimes is used as the multiple model in the attenuation process (Figure 5.5c). The multiple filtering is done in the parabolic τ - p domain by applying the demultiple filter calculated using Equation (5.9). In order to transform the hyperbolic events into parabolic events t^2 -stretching was applied to the original data (Figure 5.5a) and the predicted multiple model (Figures 5.5c). Time resampling was performed to reduce aliasing problems below 1 s. Figure 5.5b,d shows the results of the parabolic Radon transform on the t^2 -stretched CSP gathers in Figures 5.5a and c are shown. The events which interfered with each other in the x - t domain are much better separated in the parabolic τ - p domain (e.g. R_1 and BM_1 , see arrows). In the next step a multiple filter was defined using the τ - p transformed data (Figures 5.5b,d) in Equation (5.9). The chosen smoothness parameter n was 8 and the rejection parameter ϵ was 0.3. The results of the filtering in the parabolic τ - p domain are shown in Figure 5.5f. After inverse parabolic Radon transform and inverse t^2 -stretching the demultiplied CSP gather in Figure 5.5e is obtained. All multiples are very well suppressed at near and far offsets and only the primaries are left.

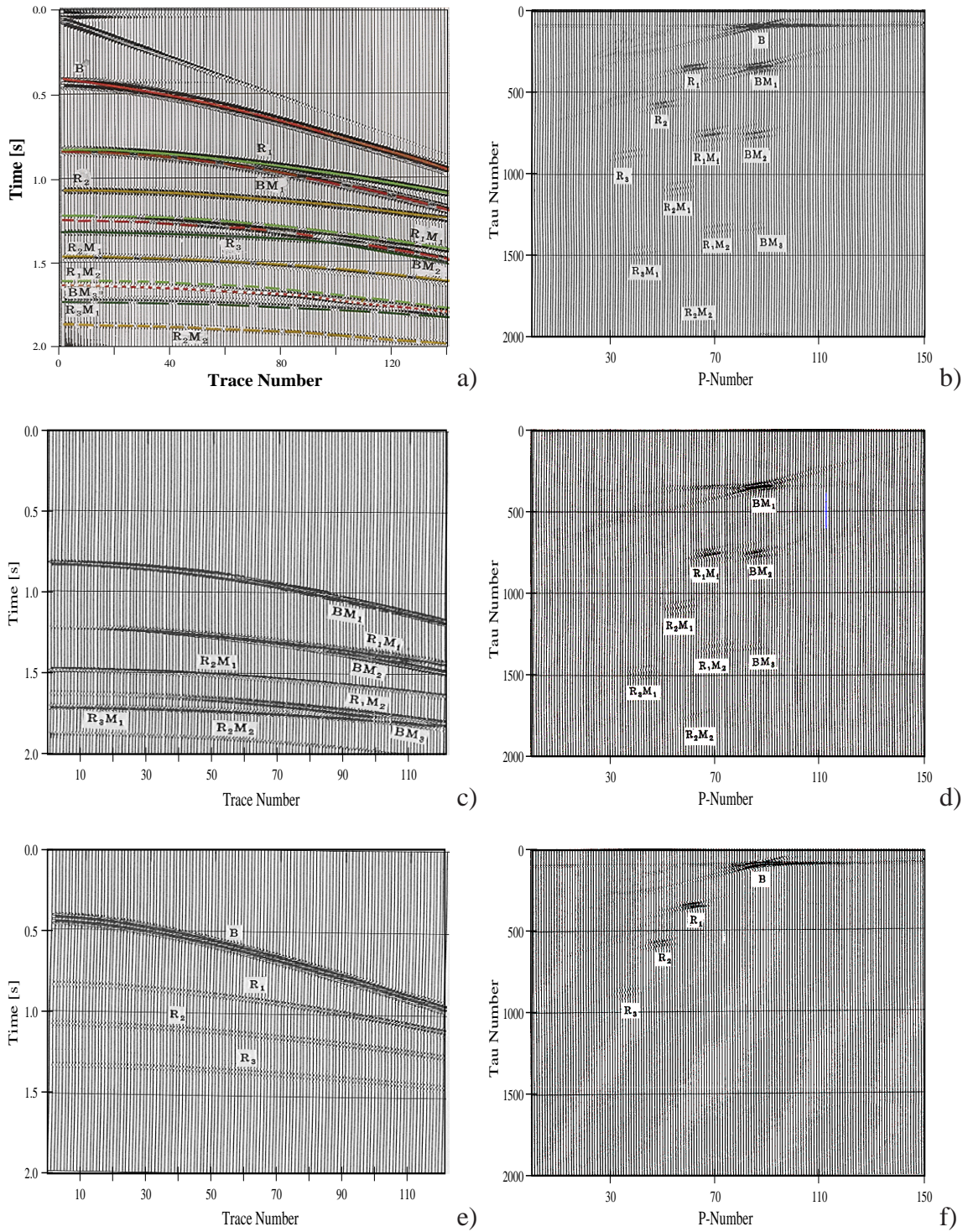


Figure 5.5: Multiple attenuation after Landa et al. [1999a]. a) Shot gather including predicted multiples and primaries. b) Parabolic τ - p transform of t^2 -stretched shot gather in a). c) x - t Multiple model extracted from shot gather in a) in time windows around predicted multiple traveltimes. d) Parabolic τ - p transform of x - t multiple model in c). e) Results of multiple filtering in the parabolic τ - p domain using gain function in Equation (5.9). Only the primaries are left. f) Results of multiple filtering in the x - t domain obtained after inverse τ - p transform and inverse t^2 -stretching of the filtering results shown in f).

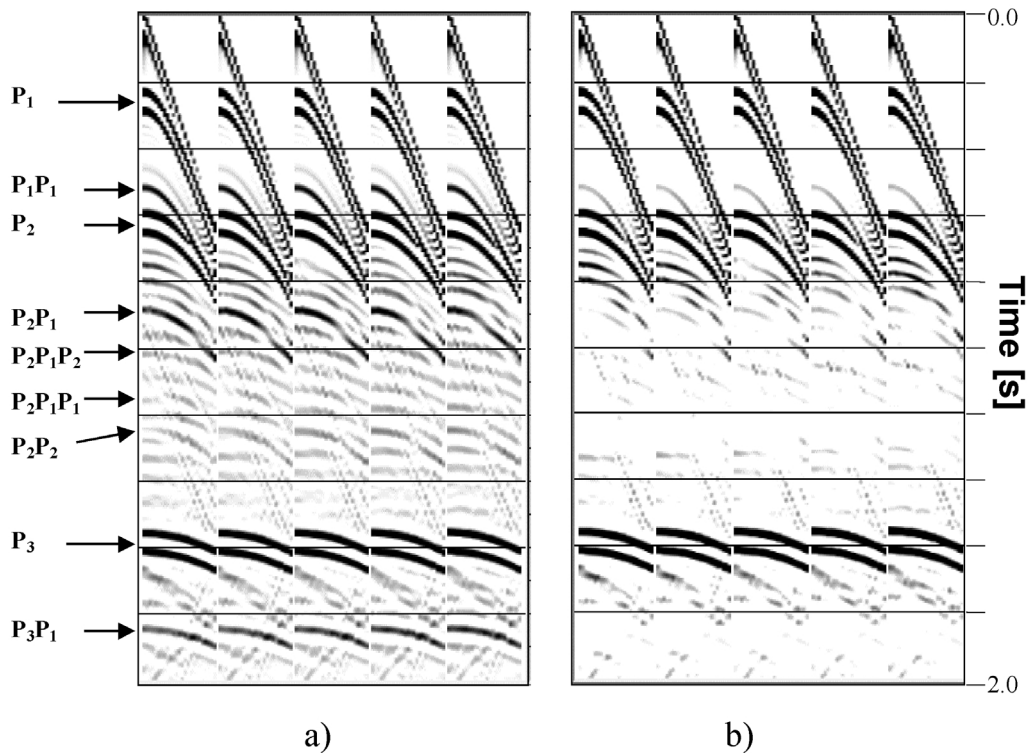


Figure 5.6: Multiple attenuation results in a collection of five CMP gathers, which are located at about $x=250$ m in Figure 3.2: a) before multiple attenuation b) after multiple attenuation. All multiples are strongly attenuated. Because of noise and very weak amplitudes, the higher order and interbed multiple can hardly be seen in the seismic data. Figure from Zaske et al. [1999].

5.2.2.3 Synthetic example: four layer model

In this section I continue with the 'four layer model' example. I use the kinematically predicted multiples (section 4.3.2, Figure 4.5) in the multiple attenuation process. The wavefield cut from the original data within time windows around the predicted multiple traveltimes serves as multiple model in the multiple attenuation process described in the previous section. As input gathers for the multiple attenuation procedure CMP gathers are used. After t^2 -stretching of the original data and the multiple model data, the multiple attenuation (filtering) was done automatically in the parabolic τ - p domain using the presented demultiple filter in Equation (5.9). After the inverse τ - p transform, followed by inverse t^2 -stretching, we obtain the results of the multiple filtering in the x - t domain, which are shown for five CMP gathers in Figure 5.6. All predicted multiples are strongly attenuated. In Figure 5.7 a stacked section before and after multiple attenuation is shown. The only difference in the processing scheme between the two sections is the multiple attenuation. Although differential moveout between primaries and multiples already reduced multiple energy during stacking, the significant improvement due to the multiple attenuation is obvi-

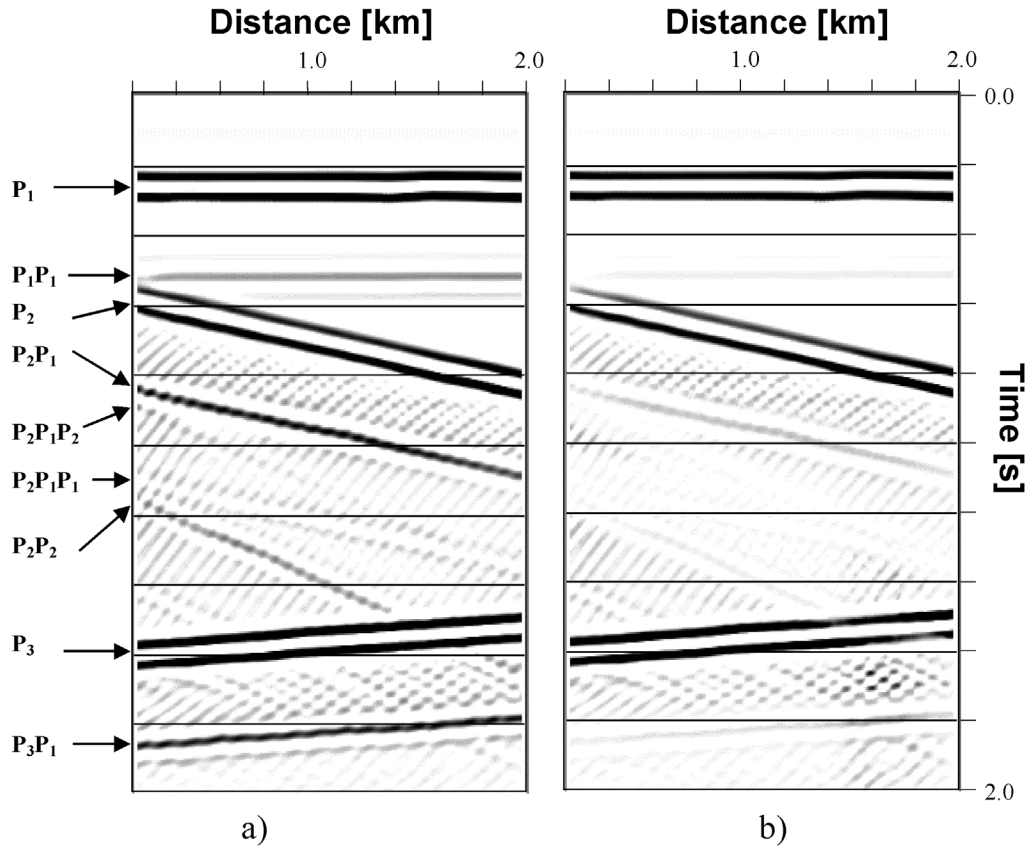


Figure 5.7: Stacked section after optimal velocity analysis: a) before multiple attenuation. The labels denote the primaries and predicted multiple events. b) after multiple attenuation. All multiples are well attenuated. Because of noise and very weak amplitudes, the higher order and interbed multiple can hardly be recognized in the seismic data. The residual wavefield is very well preserved, whereas the predicted multiples are strongly attenuated. Figure from Zaske et al. [1999].

ous: all predicted multiples are attenuated and only the primaries and the residual wavefield are left.

5.2.3 Remarks and limitations

I presented two different methods and implementations, which can be used in order to attenuate multiples based on predicted multiple traveltimes, and demonstrated their effectiveness using synthetic data examples. The successful multiple attenuation using these methods without damaging primaries demands a certain differential moveout between primaries and multiples. If the differential moveout is too small to get a sufficient separation between primaries and multiples in the parabolic τ - p domain, the multiple suppression acts at the expense of interfering primaries or strong residual multiples are left in the data, de-

pending on the chosen filter parameters. However, multiple filtering in the parabolic τ - p space has also certain limitations due to the two-way parabolic τ - p transform, which are explained in the following.

Hyperbolic events in the original CMP gather (x - t domain) are transformed to parabolic events in the t^2 -stretched CMP gather (x - t^2 domain). Due to the fact that the parabolic Radon transform is principally a stacking procedure, which is stacking along parabolic trajectories, it emphasizes energy associated with events that follow parabolic traveltimes in the x - t^2 domain, i.e. hyperbolic events in the x - t domain. For the same reasons events with non-hyperbolic moveouts in the x - t domain, which may be associated with more complex geological structures, and noise, uncorrelated from trace to trace can be significantly excluded from mapping in the parabolic τ - p space properly. Hence after multiple filtering, inverse parabolic τ - p transform, and inverse t^2 -stretching the non-hyperbolic energy and random noise in the modeled CMP gather (x - t domain) can be dramatically reduced. On the one hand the reduction of random noise and non-hyperbolic coherent noise might be a positive aspect, on the other hand the loss of non-hyperbolic primary energy is certainly considered as a negative byproduct because this information might be important for further processing, as e.g. Amplitude Versus Offset (AVO) analysis.

Even hyperbolic events (e.g. primaries) which are exposed to a two-way parabolic τ - p transform might be damaged due to the fact that the discrete summation over a finite range of source-receiver offsets causes amplitude smearing in the parabolic τ - p domain and inaccuracies in the inverse-transformed gather [Zhou and Greenhalgh, 1996]. This effect can be reduced by performing a p -direction deconvolution in the forward parabolic τ - p transform.

Also the t^2 -stretching which is necessary to apply in order to transform hyperbolic into parabolic events prior the forward parabolic Radon transform may affect the modeled wavefield. The t^2 -stretching causes compression below 1 s and stretching after 1 s traveltimes. This is a potential problem of aliasing at small times causing frequency distortion of shallow events [see Yilmaz, 1989]. In order to reduce these aliasing problems I perform time resampling for traveltimes below 1 s.

Finally, filtering using the gain function in Equation (5.9) smoothes out random noise because it is a form of a 2D moving average filter [see Zhou and Greenhalgh, 1996]. The problem is that in this context noise is everything which is not properly modeled by the parabolic τ - p transform and may also include useful wavefield components like desired primaries.

The mentioned problems can be reduced if the multiple attenuation is done in the x - t domain and the parabolic τ - p transform is used for multiple modeling instead of multiple filtering. Such an approach will be presented in the next section.

5.3 Multiple attenuation in the x - t domain

In the previous sections I explained two different methods for the attenuation of multiples in the parabolic τ - p space based on the predicted multiple traveltimes. By applying this strategy for the attenuation of certain predicted multiples also the residual wavefield (i.e. all except of these undesired predicted multiples) might be damaged due to the limitations of a two-way parabolic Radon transform, as described in section 5.2.3.

The multiple prediction method presented in this work is especially useful as a target-oriented approach. This implies that there might be only a few particular predicted multiples to be attenuated in the attenuation process. This means that the residual wavefield which is unnecessarily exposed to be damaged might be the major part of the total wavefield. The risk of affecting the residual wavefield can be reduced by performing the multiple attenuation in the original CMP gather (x - t domain).

Yilmaz [1989], Zhou and Greenhalgh [1996] and Landa et al. [1999a] mention the possibility to redefine their demultiple filters into τ - p multiple-pass filters in order to model multiples instead of attenuating them. I follow this idea of multiple modeling and propose a new method for multiple attenuation in the x - t domain, which includes another wavefield representation, in order to reduce instabilities due to phase and amplitude variations of both the original and predicted multiples. In this method the residual wavefield is not exposed to a parabolic Radon transform at all and the original texture of the data can be preserved. In particular, shallow events and non-hyperbolic events which are not interfering with predicted multiples, such as e.g. diffractions or primary reflections, are not damaged during the multiple attenuation procedure. In this chapter, I present the new method and its implementation. I illustrate its effectiveness on a real data example.

5.3.1 The method

In order to perform the multiple filtering in the original CMP gather (x - t domain) I could directly use the *initial* multiple model in the x - t domain, which is essentially the extracted wavefield in time windows around the predicted multiple traveltimes. However, this is not a very effective way, because the problem of interfering primaries and multiples in the initial multiple model still might exist. For this reason I try to separate the primaries and multiples using a data space where they are optimally separated. The parabolic τ - p domain is such a data space. After transforming the t^2 -stretched CMP gather into the parabolic τ - p domain, I filter the residual wavefield (i.e. all but the predicted multiples) in order to get a τ - p multiple model. After the inverse parabolic τ - p transform and an inverse t^2 -stretching I get an *improved* multiple model in the x - t domain, which in the ideal case includes the predicted multiples only. The envelope of this improved multiple model serves later as the *final* multiple model in the multiple attenuation process. It is used in the introduced gain function in Equation (5.9) but this time in the x - t domain instead of the parabolic τ - p domain.

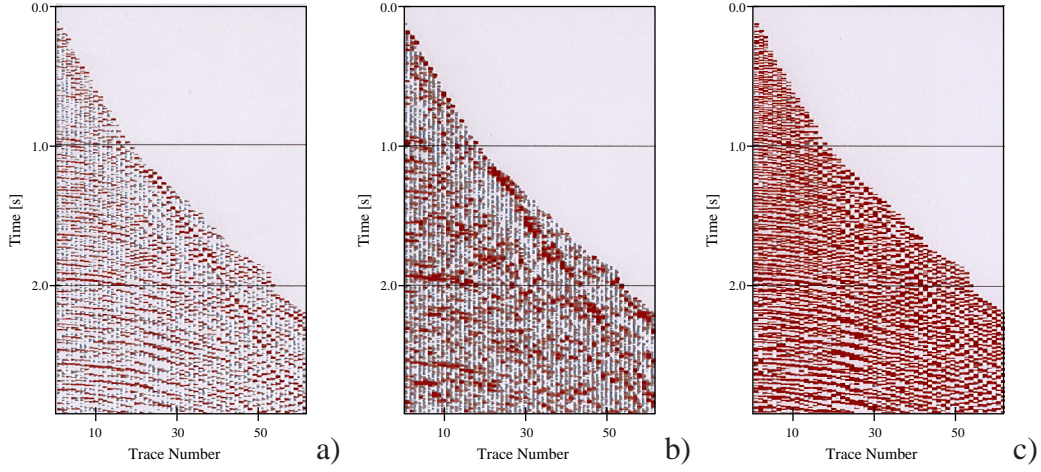


Figure 5.8: a) A CMP gather, b) its envelope, and c) its normalized seismogram.

For the multiple modeling in the parabolic τ - p domain I can redefine one of the two presented multiple suppression filters in Equation (5.9) or Equations (5.6)-(5.7) as multiple pass filters. The multiple attenuation depends to a large extent on amplitude and phase variations of both the predicted multiple model and the original seismogram. In order to reduce instabilities I use another wavefield representation for the multiple filtering, namely I separate the original CMP gathers into envelope and normalized seismogram.

The seismic wavefield $u(x, t)$ with the source-receiver distance x and the travelttime t can be represented as a product of envelope $A(x, t)$ and normalized seismogram $\cos(\phi(x, t))$ using the following Equations:

$$u(x, t) = A(x, t) \cos(\phi(x, t)) \quad (5.10)$$

with

$$A(x, t) = \sqrt{u(x, t)^2 + u^*(x, t)^2}, \quad (5.11)$$

$$\cos(\phi(x, t)) = \frac{u(x, t)}{A(x, t)}. \quad (5.12)$$

In Figure 5.8a a real data CMP gather, b) its envelope and c) its 'normalized seismogram' are shown for illustration. Each trace at an offset x in the envelope $A(x, t)$ of the CMP gather is calculated using the corresponding Hilbert transformed original trace $u^*(x, t)$, and the original trace $u(x, t)$ in Equation (5.3.1). Each trace in the normalized seismogram

$\cos(\phi(x, t))$ is calculated by division of the corresponding initial trace $u(x, t)$ by its envelope $A(x, t)$. The normalized seismogram keeps the frequency of the original seismogram while the envelope has a much lower frequency characteristic. The simple product reproduces the original data record without losing any information.

The new idea is to attenuate multiple energy included in the original CMP gather by using the *final* multiple model (i.e. the envelope of the *improved* multiple model, see above) and the envelope of the original data including multiples and primaries. Because of the fact that the envelope has a much lower frequency characteristic than the original seismogram the sensitivity of the filtering to phase and amplitude variations (instabilities) is reduced. In order to restore the original high frequency character of the resulting filtered data, I multiply the (envelope) attenuation results with the original normalized seismogram. The explained procedure was implemented as follows:

1. Input: Original CMP gather including multiples and primaries.
2. Predict multiple traveltimes using wavefront characteristics of primaries.
3. Use predicted traveltimes obtained in step 2 in order to define a multiple model in the τ - p domain. This is done similar to the procedure in section 5.2.1. This time, all but the predicted multiples in the elliptic τ - p areas is muted and a multiple model is obtained in the τ - p domain (see Figure 5.10).
4. Perform inverse parabolic τ - p transform of the τ - p multiple model in step 3, followed by an inverse t^2 -stretching in order to get an *improved* multiple model in the x - t domain (see Figure 5.11a).
5. Calculate envelope of *improved* multiple model obtained in step 4. The result gives the *final* multiple model (Figure 5.11b).
6. Calculate envelope and normalized seismogram of original input data in step 1 including primaries and multiples (see Figure 5.8).
7. Define a nonlinear filter using Equation (5.9) in the x - t instead of the parabolic τ - p domain using the *final* multiple model obtained in step 5 and the envelope of the original input data obtained in step 6; Now A denotes the *final* multiple model and B the envelope of the original input data in the x - t domain (Figure 5.11c).
8. Apply multiple-rejection filter defined in step 7 on envelope of original input data calculated in step 6.
9. Multiply filtered data obtained in step 8 by the normalized seismogram of the input data calculated in step 6 in order to restore the original high frequency character.
10. Output: Filtered CMP gather (see Figure 5.11d).

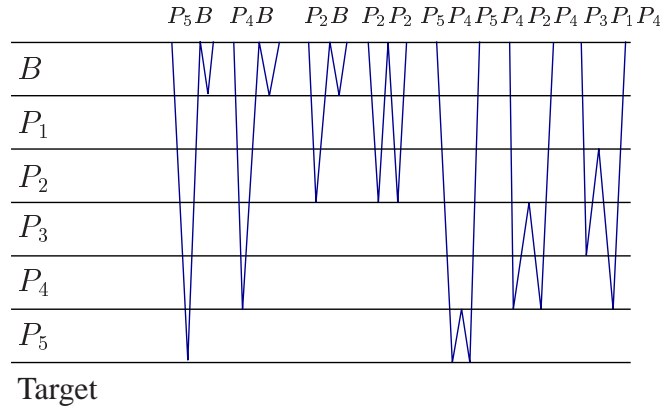


Figure 5.9: Ray code of seven multiple events for which the prediction and attenuation was done. Note that the rays are shown only schematically, there is no requirement for flat horizontal layers or any other subsurface information.

By applying this procedure the residual wavefield is not exposed to a double parabolic τ - p transform and can be preserved (e.g. hyperbolic and non-hyperbolic primaries which are sufficiently separated from multiples). The following real marine data example illustrates the proposed method.

5.3.2 Real data example: marine data set

The multiple attenuation procedure described in the previous section was applied to the marine real data example I already used for the kinematic prediction of multiple traveltimes in section 4.3.3. The aim was to attenuate seven multiple events shown in Figure 5.9: four surface related (P_5B , P_4B , P_2B , P_2P_2) and three interbed multiples ($P_5P_4P_5$, $P_4P_2P_4$, $P_3P_1P_4$).

In the first step a multiple model in the parabolic τ - p domain is calculated using the predicted multiple traveltimes. After t^2 -stretching of the input CMP gather it is transformed into the parabolic τ - p domain. Using a redefinition of the elliptical demultiple filter in Equation (5.9) as an elliptical multiple-pass filter the τ - p multiple model is obtained. This is illustrated in Figure 5.10 for the four predicted surface multiples. Figure 5.10a shows the parabolic τ - p transformed data of one CMP gather and Figure 5.10b the corresponding multiple model for the four predicted surface multiples. After performing the inverse parabolic τ - p transform of the τ - p multiple model followed by an inverse t^2 -stretching the improved multiple model in the x - t domain is obtained (Figure 5.11a). In the next step the final multiple model, which is the envelope of the improved multiple model, is calculated using Equation (5.3.1) (Figure 5.11b). The non-linear x - t multiple filter is defined by Equation (5.9): In this case A denotes the envelope of the improved multiple model and B the envelope of the original data (Figure 5.8b). As the smoothing parameters I chose $\epsilon = 0.3$ and $n = 8$. Instead of applying this filter in the τ - p domain, I apply it in the x - t space

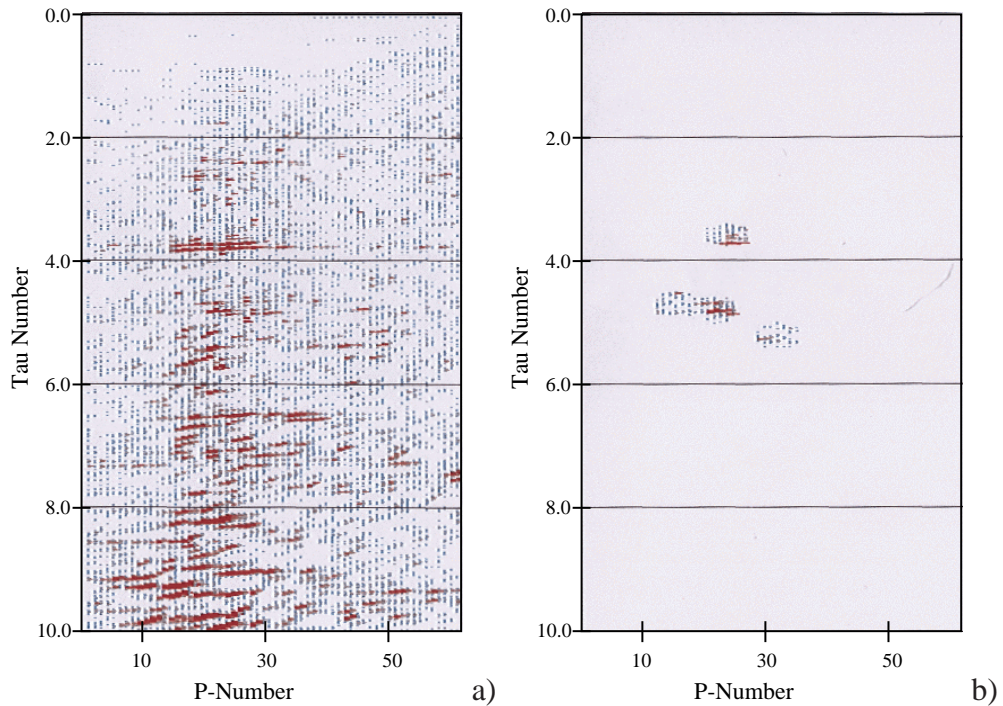


Figure 5.10: a) The τ - p transformed CMP gather. b) The extracted τ - p multiple model for four surface multiples.

to the envelope of the original CMP gather (Figure 5.8b) and multiply the results with the normalized original seismogram (Figure 5.11b) to restore the high frequency information. The result is shown in Figure 5.11d. Figures 5.12a and b) illustrate the attenuation results on three CMP gathers. The arrows indicate regions where multiple attenuation is evident.

This attenuation procedure was applied to about 2000 CMP gathers of the marine data set with the purpose to attenuate all predicted surface and internal multiples, see ray codes in Figure 5.9. The zero-offset stacked section calculated using the CMP gathers before multiple attenuation is shown in Figure 5.13, while the zero-offset stacked section calculated using the CMP gathers after multiple attenuation is shown in Figure 5.14. The only difference in the processing scheme is the application of the multiple attenuation procedure. In order to analyze where and to which extent multiple energy has been removed the difference section between the original (Figure 5.13) and demultiplied (Figure 5.14) stacked section has been calculated, see Figure 5.15. It can be clearly seen that coherent seismic energy was subtracted. Several arrows indicate sections where this is especially evident. However, in case of real data it is difficult to be sure that this energy really corresponds to multiples.

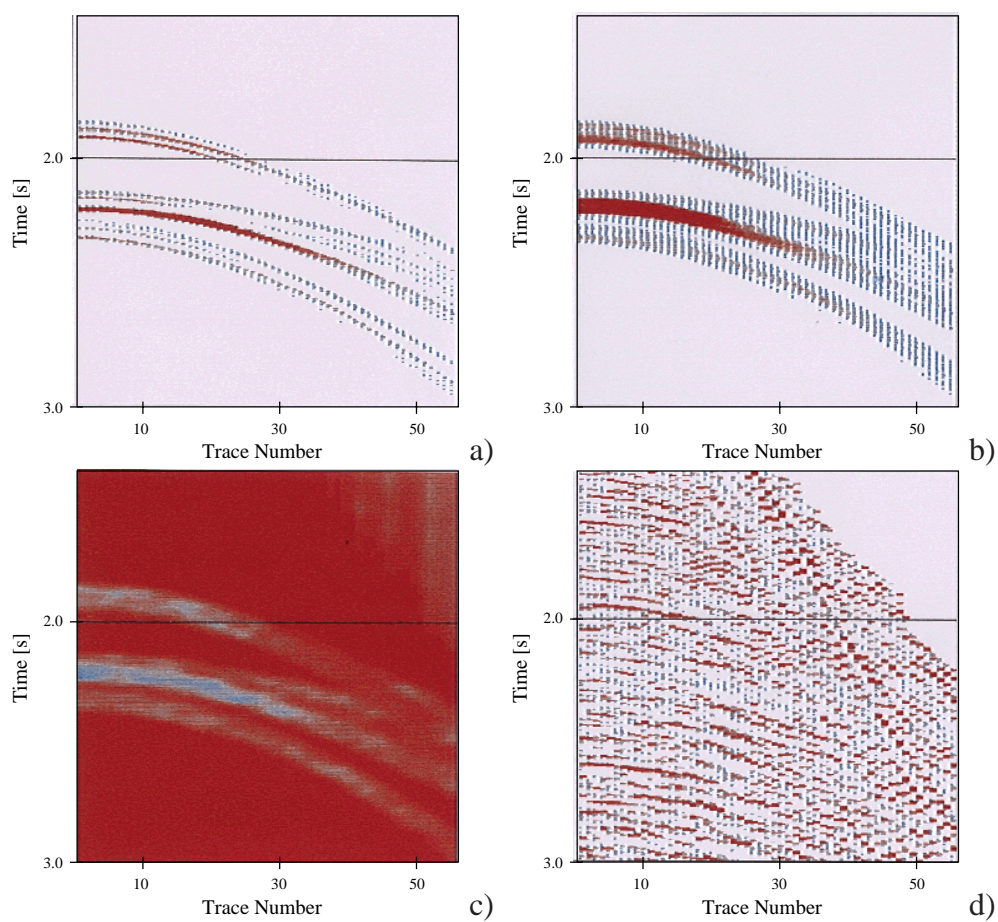


Figure 5.11: a) Multiple model; b) Envelope of multiple model; c) Gain function of nonlinear filter (red ≈ 1 , blue ≈ 0); d) Result of multiple subtraction in CMP gather.

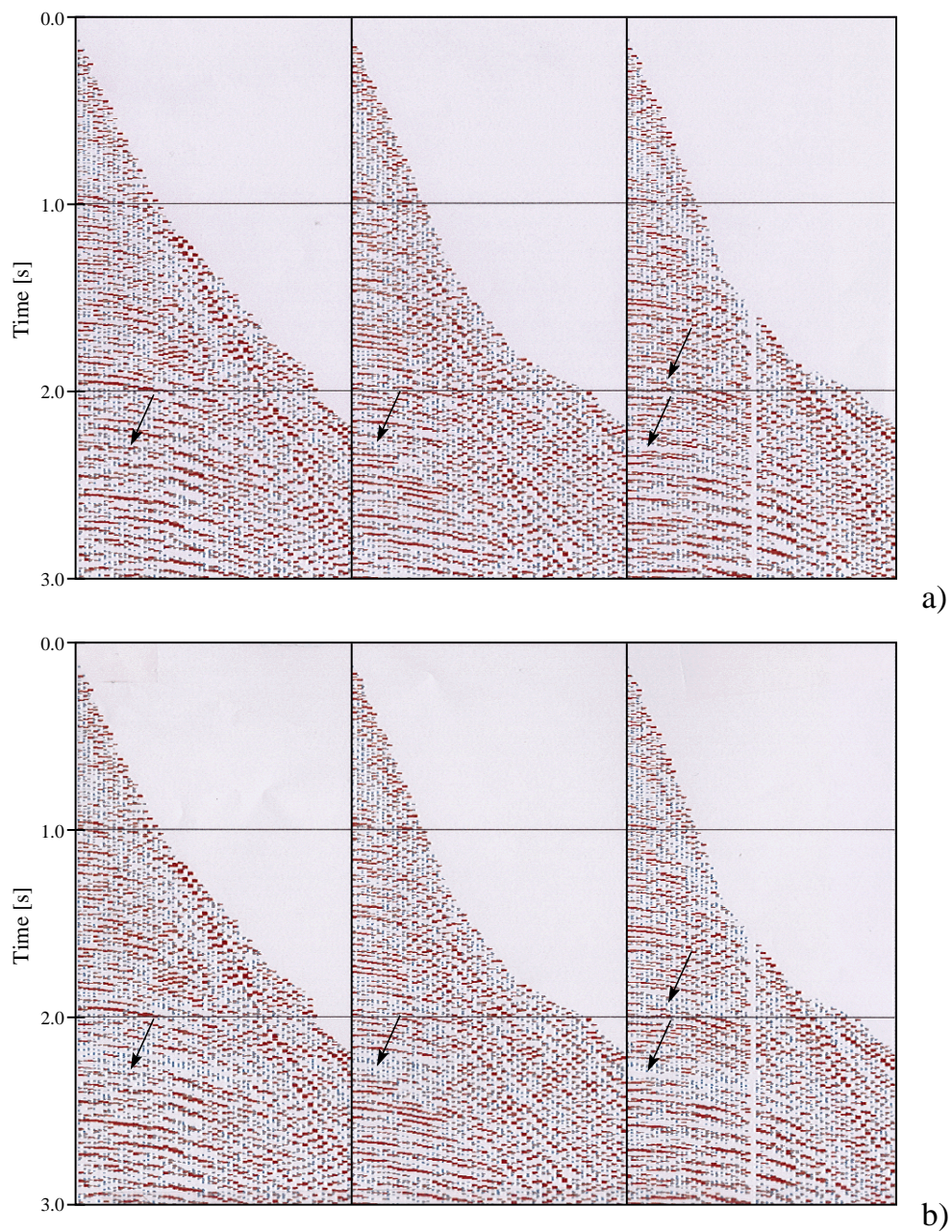


Figure 5.12: a) Three CMP gathers before multiple attenuation and b) after multiple attenuation. The arrows indicate regions of major multiple attenuation.

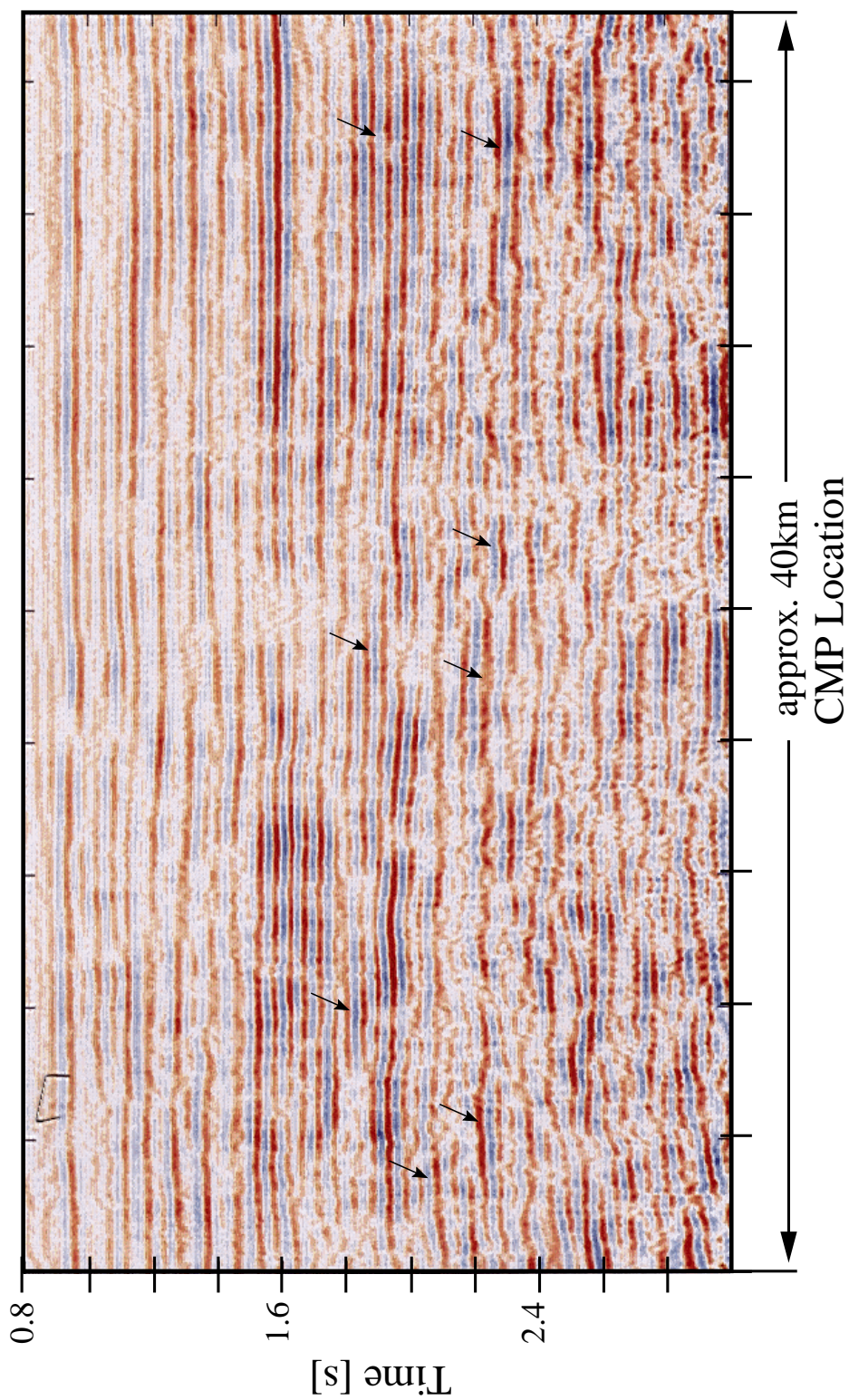


Figure 5.13: Stacked section calculated using the data before multiple attenuation. The arrows indicate regions of major identified multiple energy.

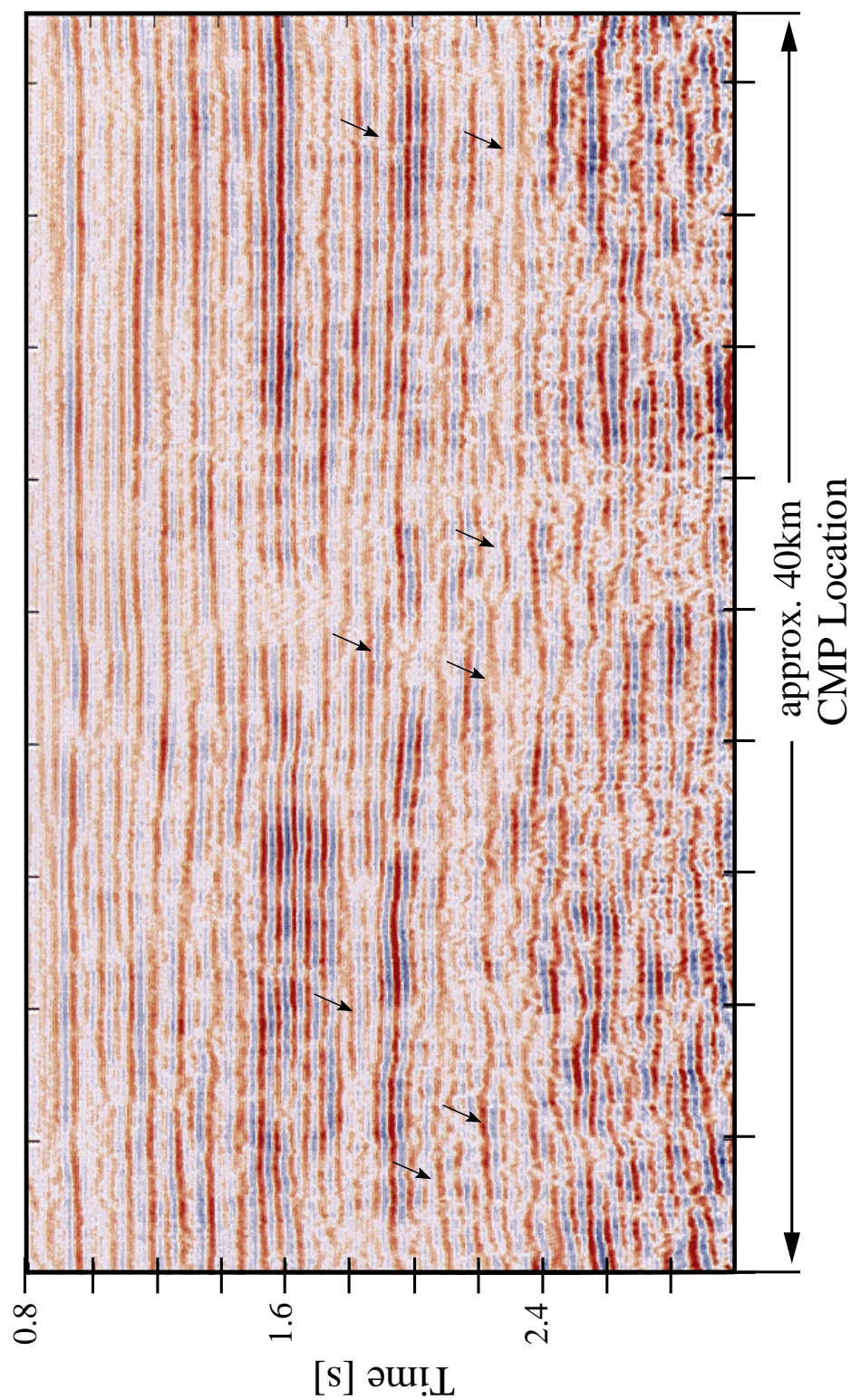


Figure 5.14: Stacked section calculated using the data after multiple attenuation. The target zone around 2.0 s is much better emphasized than before multiple attenuation in Figure 5.13. The arrows indicate regions of major multiple attenuation.

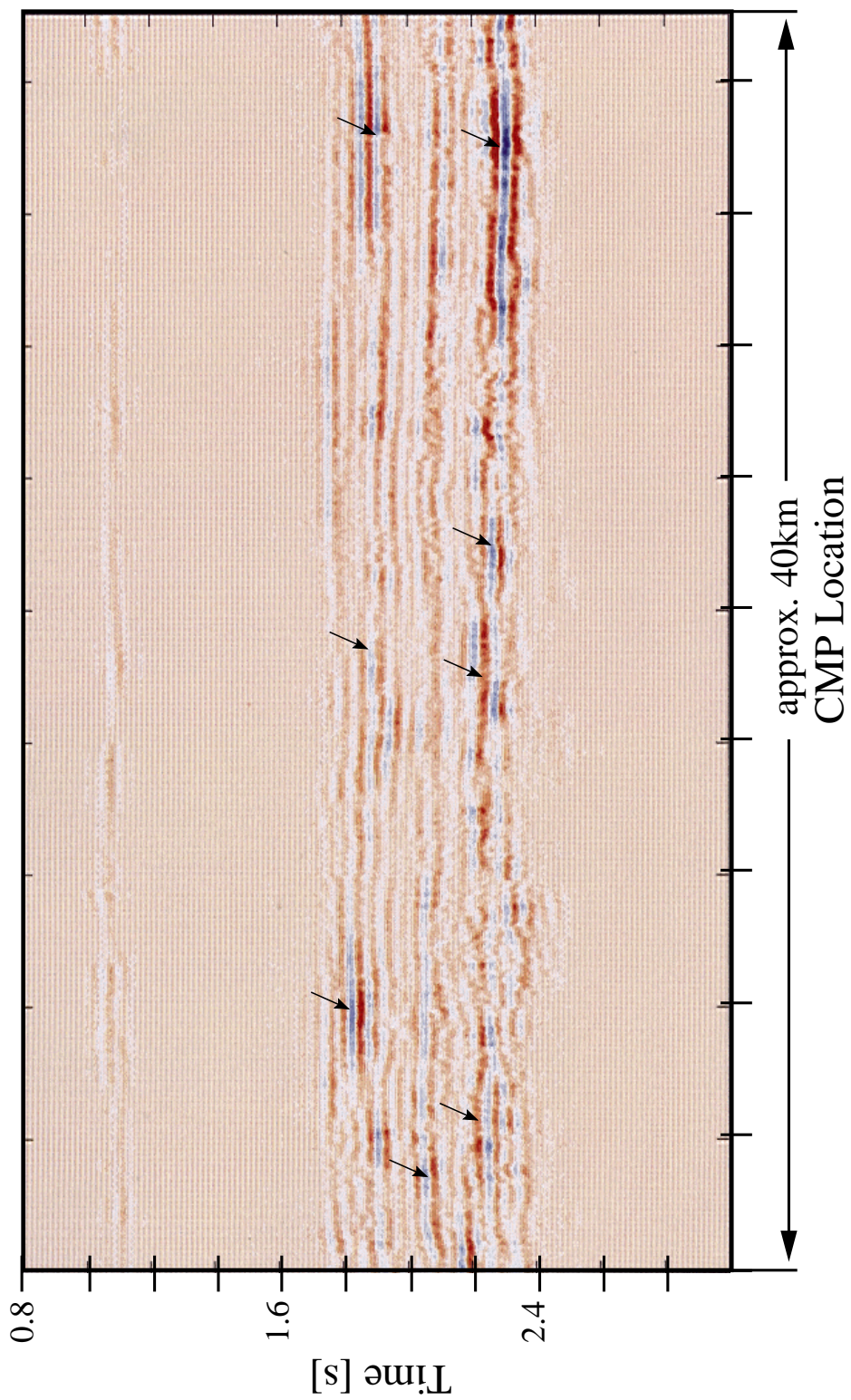


Figure 5.15: Difference section between the two stacked sections before and after multiple attenuation in Figures 5.13 and 5.14. The arrows indicate regions of major multiple attenuation.

5.4 Results

All presented multiple filters are based on the assumption that primaries and multiples can be separated in the parabolic τ - p domain and therefore at least a small differential moveout in the x - t domain is necessary. However, this does not mean that multiples and primaries cannot interfere in the x - t domain.

An advantage of the final multiple filtering in the x - t domain instead of the parabolic τ - p domain is that the residual wavefield (i.e. all but the predicted multiples) can be preserved because it is not exposed to numerical damaging due to a two-way parabolic τ - p transform. In this case it is guaranteed that the primaries which are sufficiently separated from multiples are not affected at all.

Doing a wavefield separation into envelope and normalized seismogram, and performing the attenuation on the envelope reduces instabilities during the data adaptive filtering in the x - t domain due to amplitude and phase variations of both the modeled as well as the original multiples.

Usually the multiple filtering in the parabolic τ - p domain is done manually and therefore the multiples have to be identified in the parabolic τ - p domain. This is very difficult in complex geological situations. The presented attenuation methods in this dissertation may be considered as a surgical multiple filtering technique, where a major advantage lies in the fact that the multiple positions in the parabolic τ - p domain are determined automatically without any assumption about the macro-velocity-model.

While the successful attenuation of the kinematically predicted multiples needs at least some small differential moveout between primaries and predicted multiples, it is important to recognize that multiple identification does not depend on this assumption.

Chapter 6

Conclusions

The 2D multiple prediction and attenuation methods as proposed in this thesis have been applied successfully to synthetic and real 2D data sets. The main advantages of these methods are that apart from the near surface velocity no further explicit information on the subsurface model is required and that surface multiples as well as interbed multiples can be predicted and attenuated. All required information can be obtained directly from the measured data. The prediction and attenuation is done on prestack data, so that other prestack processing methods, like e.g. AVO might follow up in the processing sequence. The identification of multiple generating events (e.g. primaries) in a simulated zero-offset section requires user-interaction and allows an effective target-oriented application.

Multiple attenuation using wavefront characteristics implies a three-step procedure: The first step involves the estimation of the kinematic wavefront-parameters, in particular the emergence angles of the identified multiple generating events at each source-receiver pair in all CSP gathers. In the second step the multiple is predicted using the estimated wavefront-parameters, and in the third step the predicted multiples are attenuated. For all of these three processing steps different methods with particular advantages and disadvantages have been developed in this dissertation.

The estimation of the kinematic wavefront-parameters is the crucial part in this procedure, because the prediction of multiples can only be successful if these parameters are known sufficiently close to reality. I developed two horizon-based methods for the estimation of kinematic wavefront-parameters of a multiple-generating event, identified in a simulated zero-offset section. The output of these methods are the kinematic wavefront-parameters of the identified event at each source-receiver pair in all CSP gathers along the seismic line.

The first approach can be used in case of multiple-generating events with approximately hyperbolic traveltime curves and is called *global angle analysis*. In the first step of this method the wavefront-parameters corresponding to the normal ray are estimated at all zero-offset locations along the seismic line. This can be done in a fully automatic or interactive manner, depending on the complexity of the data. The interactive application allows to resolve problems due to multi-modal correlation functionals, e.g. in conflicting dip situations.

Leading criteria in the interactive procedure are a priori information, e.g. from boreholes, and the smoothness of the wavefront-parameters along the seismic line. After the zero-offset wavefront-parameters are estimated they are extrapolated to finite source-receiver distances in the CSP gathers. The *global angle analysis* has been successfully applied to representative synthetic and real data sets. In case of the synthetic data the results agreed very well with the analytically calculated results. An advantage of the global angle analysis is the very fast calculation and that only the zero-offset arrival time of a multiple generating event has to be interpreted.

For traveltime curves of non-hyperbolic character this method leads to inaccurate results in the estimated wavefront-parameters due to the fact that one wavefront-parameter set, i.e. one emergence angle and one radius of wavefront curvature estimated at the zero-offset location, which defines a global hyperbolic traveltime curve in a CSP gather is not sufficient to correctly describe a non-hyperbolic traveltime curve at all source-receiver positions. For such situations, I developed a local parameter estimation procedure, which estimates the emergence angle together with the radius of wavefront curvature locally at each receiver in a CSP gather by performing local coherency measurements. I call this method *local angle analysis*. This method requires the traveltimes of an identified event to be known at all source-receiver pairs in the CSP gathers. In complicated situations primary traveltime curves must be identified in the CSP gather. For simple cases, I introduced a technique which follows the moveout automatically starting from the zero-offset traveltime which can be identified in a simulated zero-offset section. The application of this method to synthetic data sets with non-hyperbolic moveouts demonstrated the successful wavefront parameter estimation also for non-hyperbolic moveouts. This means that also multiple-generating events with complicated moveout curves can be considered in the multiple prediction procedure proposed in this work.

Furthermore, I developed two 2D multiple prediction methods. The first one predicts only the kinematics of a multiple, the second also its dynamics. In both procedures the source-receiver pairs of the multiple-generating primaries are selected using the estimated emergence angles. In the kinematic version the traveltimes of the selected primaries are used to predict the arrival time of the multiple. This kinematic prediction method does not require any explicit knowledge of the subsurface, the source signature or near offset traces. Only the near surface velocity is presumed to be known. Synthetic and real data examples demonstrated the successful multiple prediction.

The second introduced method is for the 2D dynamic prediction of surface and interbed multiples in consideration of full geometrical spreading. This method is a straightforward extension of the kinematic multiple prediction method and is still valid for surface as well as for interbed multiples. While it is based on the same methodology as the kinematic version, it requires additional informations on the data acquisition as well as assumptions and approximations on the subsurface model. Instead of simply summing and subtracting primary traveltimes, the selected multiple generating primary events are now convolved and correlated with each other. Instead of 2D or even 3D convolutions as used in other methods for the dynamic multiple prediction, only 1D convolutions and correlations can be performed.

This is possible because it is exactly known which primary signals generate a certain multiple signal at a certain source-receiver location. Corrections for the seismic signal and the geometrical spreading effects have to be applied separately. While the method might be a good approximation for moderately dipping interfaces it is strictly speaking only exact for horizontally layered media. The amplitude information can be an advantage especially in situations where the primaries and multiples show no moveout differences. Also for the multiple identification a rough amplitude estimation of the predicted multiple can be very helpful for an interpreter.

Different methods for the attenuation of kinematically predicted multiples have been developed. All of these methods work fully automatic and make use of a better separation of primaries and multiples in the parabolic τ - p domain instead of the original seismogram (x - t). The main difference between these methods is that final multiple filtering is done either in the parabolic τ - p or in the x - t domain. The multiple reject areas in both cases are determined automatically using the predicted multiple traveltimes. A 2D data adaptive non-linear filter for amplitude attenuation is automatically defined by comparing the energy on the traces of the multiple model and the original input data in the parabolic τ - p or x - t domain. The latter technique uses the parabolic τ - p transform only for multiple modeling and guarantees that the residual wavefield, i.e. all but the predicted multiples, is not affected by any numerical damping due to a two-way parabolic τ - p transform. In this case the primaries which are sufficiently separated from predicted multiples are surely preserved. From my experience it turned out that the use of envelopes and normalized seismograms instead of the original seismograms reduces the sensitivity of the filter process to phase changes and instabilities of the seismic data. The successful multiple attenuation without affecting the primaries was demonstrated on synthetic and real data sets. The main advantage of the multiple filtering methods using the parabolic τ - p transform based on the multiple prediction using wavefront characteristics, is the automatic and macro-velocity-model independent definition of the multiple rejection filter.

The 2D multiple prediction and attenuation method using wavefront characteristics could be extended straightforwardly to a 3D method. The parameter search would be performed in the prestack multi-coverage data set using a moveout formula, which depends on five parameters instead of only two in 2D, namely two emergence angles and a matrix of curvatures with three independent parameters. Of course the effort to estimate five wavefront-parameters would be much higher than for two in the 2D situation. In order to be able to predict also 3D multiples the cross-line recording aperture would have to be large enough so that the 3D primary legs are also part of the recorded wavefield. However, in practice the typical 3D marine data acquisition with only a narrow cross-line recording aperture usually cannot provide this situation.

References

- Aki, K. and Richards, P. G. (1980). *Quantitative Seismology, Theory and Methods*. Freeman, New York.
- Berkhout, A. J. and Verschuur, D. J. (1997). Estimation of multiple scattering by iterative inversion, part I: Theoretical considerations. *Geophysics*, 62(5):1586–1595.
- Berkovitch, A. and Gelchinsky, B. (1989). Inversion of common reflecting element (CRE) data (migration combined with interval velocity determination). 59th Annual Internat. Mtg., Soc. Expl. Geophys., Expanded Abstracts, page 1250.
- Berkovitch, A., Gelchinsky, B., and Keydar, S. (1994). Basic formulae for multifocusing stack. 56th Mtg. Eur. Assoc. Expl Geophys., Extended Abstracts, Session:P140.
- Berryhill, J. R. and Kim, Y. C. (1986). Deep-water peglegs and multiples: Emulation and suppression. *Geophysics*, 51(12):2177–2184.
- Biondi, B. (1992). Velocity estimation by beam stack. *Geophysics*, 57(08):1034–1047.
- Bracewell, R. (1965). *The Fourier transform and its applications*. McGraw-Hill.
- Bronstein, I. N. and Semendjajew, K. A. (1989). *Taschenbuch der Mathematik - Teil 2*. Harri Deutsch, Frankfurt.
- Calderón-Macias, C., Sen, M. K., and Stoffa, P. L. (1997). Hopfield neural networks, and mean field annealing for seismic deconvolution and multiple attenuation. *Geophysics*, 62(3):992–1002.
- Carrion, P. M. (1986). A layer-stripping technique for suppression of water-bottom multiple reflections. *Geophysical Prospecting*, 34:330–342.
- Červený, V. (1985). *Seismic Shear Waves, Part A: Theory*, volume 15A. Geophysical Press, section 1. seismic exploration edition.
- Červený, V. and Ravindra, R. (1971). *Theory of seismic head waves*. Toronto, University of Toronto Press.
- de Bazelaire, E. (1988). Normal moveout revisited - inhomogeneous media and curved interfaces. *Geophysics*, 53(2):143–157.

- de Bazelaire, E. and Viallix, J. R. (1994). Normal moveout in focus. *Geophysical Prospecting*, 42(5):477–499.
- Diebold, J. B. and Stoffa, P. L. (1981). The travelttime equation, tau-p mapping and inversion of common midpoint data. *Geophysics*, 46(3):238–254.
- Dix, C. H. (1955). Seismic velocities from surface measurements. *Geophysics*, 20(1):68–86.
- Dragoset, W. and Jericevic, Z. (1998). Some remarks on surface multiple attenuation. *Geophysics*, 63(02):772–789.
- Essenreiter, R. (1999). *Identification and Attenuation of Multiple Reflections with Neural Networks*. PhD thesis, University of Karlsruhe.
- Gelchinsky, B. (1989). Homeomorphic imaging in processing and interpretation of seismic data- fundamentals and schemes. 59th Annual Internat. Mtg., Soc. Expl. Geophys., Expanded Abstracts, pages 983–988.
- Gelchinsky, B., Berkovitch, A., and Keydar, S. (1999a). Multifocusing homeomorphic imaging. Part 1. Basic concepts and formulas. *Journal of Applied Geophysics*, 42(3-4):229–242.
- Gelchinsky, B., Berkovitch, A., and Keydar, S. (1999b). Multifocusing homeomorphic imaging. Part 2. Multifold data set and multifocusing. *Journal of Applied Geophysics*, 42(3-4):243–260.
- Gelchinsky, B. and Keydar, S. (1993). Basic HI formulae of general theory of local time correction. 63rd Annual Internat. Mtg., Soc. Expl. Geophys., Expanded Abstracts, pages 1145–1148.
- Gelchinsky, B., Landa, E., and Shtivelman, V. (1985). Algorithms of phase and group correlation. *Geophysics*, 50(04):596–608.
- Hampson, D. (1986). Inverse velocity stacking for multiple elimination. *Journal of Canadian Society of Exploration Geophysics*, 22(01):44–55.
- Helbig, K. and Brouwer, J. H. (1993). Surface multiples as a tool of calibration in shallow AVO studies. 55th Mtg. Eur. Assoc. Expl Geophys., Extended Abstracts, Session:A040.
- Hubral, P. (1983). Computing true amplitude reflections in a laterally inhomogeneous earth. *Geophysics*, 48(8):1051–1062.
- Hubral, P., Höcht, G., and Jäger, R. (1998). An Introduction to the Common Reflection Surface Stack. 60th Mtg. Eur. Assoc. Expl Geophys., Extended Abstracts, Session: 01-19.
- Hubral, P. and Krey, T. (1980). *Interval velocities from seismic reflection travelttime measurements*. Soc. Expl. Geophys.

- Jakubowicz, H. (1998). Wave equation prediction and removal of interbed multiples. 61th Mtg. Eur. Assoc. Expl Geophys., Extended Abstracts, Session: 01-28.
- Jou, H.-T., Kim, H.-J., Suh, J.-H., and Youn, O.-K. (1996). A new slant-stack technique based on hyperbolic statistics. *Journal of Seismic Exploration*, 5:203–212.
- Keydar, S., Gelchinsky, B., and Berkovitch, A. (1996). Common shot point stacking and imaging method. *Geophysical Prospecting*, 5:261–274.
- Keydar, S., Gelchinsky, G., Shtivelman, V., and Berkovitch, A. (1990). Common evolute element (cee) stack and imaging (zero-offset stack). 60th Annual Internat. Mtg., Soc. Expl. Geophys., Expanded Abstracts, pages 1719–1722.
- Keydar, S., Landa, E., Gelchinsky, B., and Belfer, I. (1998). Multiple prediction using the homeomorphic-imaging technique. *Geophysical Prospecting*, 46:423–440.
- Kostov, C. and Biondi, B. (1987). Improved resolution of slant stacks using beam stacks. 57th Annual Internat. Mtg., Soc. Expl. Geophys., Expanded Abstracts, pages 792–794.
- Landa, E., Belfer, I., and Keydar, S. (1999a). Multiple attenuation in the parabolic τ - p domain using wave front characteristics of multiple generating primaries. *Geophysics*, 64(6):1806–1815.
- Landa, E., Gurevich, B., Keydar, S., and Trachtman, P. (1999b). Application of multifocusing method for subsurface imaging. *Journal of Applied Geophysics*, 42(3-4):283–300.
- Landa, E., Keydar, S., and Belfer, I. (1999c). Multiple prediction and attenuation using wavefront characteristics of multiple-generating primaries. *The Leading Edge*, 18:60–64.
- Mann, J., Jäger, R., Müller, T., Höcht, G., and Hubral, P. (1999). Common-reflection-surface stack – a real data example. *Journal of Applied Geophysics*, 42(3-4):301–318.
- Müller, T. (1998). Common Reflection Surface Stack versus NMO/Stack and NMO/DMO/Stack. 60th Mtg. Eur. Assoc. Expl Geophys., Extended Abstracts, Session:1-20.
- Müller, T. (1999). *The Common Reflection Surface Stacking Method, Seismic Imaging without explicit knowledge of the velocity model*. PhD thesis, University of Karlsruhe.
- Neidell, N. S. and Taner, M. T. (1971). Semblance and other coherency measures for multichannel data. *Geophysics*, 36:482–497.
- Newman, P. (1973). Divergence effects in a layered earth. *Geophysics*, 38(03):481–488.
- O’Doherty, R. F. and Anstey, N. A. (1971). Reflections on amplitudes. *Geophysical Prospecting*, 19(03):430–458.
- Peacock, K. L. and Treitel, S. (1969). Predictive deconvolution: Theory and practice. *Geophysics*, 34:155–169.

- Robinson, E. A. and Treitel, S. (1980). *Geophysical Signal Analysis*. Prentice-Hall.
- Schleicher, J., Tygel, M., and Hubral, P. (1993). 3-D true-amplitude finite-offset migration. *Geophysics*, 58(8):1112–1126.
- Schneider, W. A., Prince, E. R. J., and Giles, B. F. (1965). A new data-processing technique for multiple attenuation exploiting differential normal moveout. *Geophysics*, 30(03):348–362.
- Schultz, P. S. and Claerbout, J. F. (1978). Velocity estimation and downward-continuation by wavefront synthesis. *Geophysics*, 43(04):691–714.
- Shapiro, S. A. and Hubral, P. (1999). *Elastic Waves in Random Media - Fundamentals of Seismic Stratigraphic Filtering*. Springer Lecture Notes in Earth Sciences.
- Sheriff, R. E. (1991). *Encyclopedic Dictionary of Exploration Geophysics*. Society of Exploration Geophysicists.
- Shultz, P. S. and Claerbout, J. F. (1978). Velocity estimation and downward continuation by wavefront synthesis. *Geophysics*, 43(02):691–714.
- Sword, C. H. (1987). *Tomographic determination of interval velocities from reflection seismic data: The method of controlled directional reception*. PhD thesis, Stanford University.
- Taner, M. T. (1980). Long-period sea-floor multiples and their suppression. *Geophysical Prospecting*, 28(01):30–48.
- Thorson, J. R. and Claerbout, J. F. (1985). Velocity stack and slant stochastic inversion. *Geophysics*, 50(12):2727–2741.
- Treitel, S., Gutowski, P., and Wagner, D. (1982). Plane-wave decomposition of seismograms. *Geophysics*, 47(10):1357–1401.
- Tygel, M., Santos, L., and Schleicher, J. (1999). Multifocus moveout revisited: Derivations and alternative expressions. *Journal of Applied Geophysics*, 42(3-4):319–332.
- Tygel, M., Schleicher, J., and Hubral, P. (1992). Geometrical spreading corrections of offset reflections in a laterally inhomogeneous earth. *Geophysics*, 57(08):1054–1063.
- Ursin, B. (1990). Offset-dependent geometrical spreading in a layered medium. *Geophysics*, 55(04):492–496.
- Verschuur, D. J. (1992). Surface-related multiple elimination in terms of Huygens' sources. *Journal of Seismic Exploration*, 1:49–59.
- Weglein, A. B. (1999). Multiple attenuation: an overview of recent advances and the road ahead (1999). *The Leading Edge*, 18(1):40–44.

- Weglein, A. B., Gasparotto, F., Carvalho, P., and Stolt, R. (1997). An inverse scattering series method for attenuating multiples in seismic reflection data. *Geophysics*, 62:1975–1989.
- Wiggins, J. W. (1988). Attenuation of complex water-bottom multiples by wave-equation-based prediction and subtraction. *Geophysics*, 53(12):1527–1539.
- Yilmaz, O. (1987). *Seismic data processing*. Investigations in Geophysics. Soc. Expl. Geophys. (Doherty, S. M., Ed.).
- Yilmaz, O. (1989). Velocity-stack processing. *Geophysical Prospecting*, 37(04):357–382.
- Zaske, J., Keydar, S., and Landa, E. (1999). Estimation of kinematic wavefront parameters and their use for multiple attenuation. *Journal of Applied Geophysics*, 42(3-4):333–346.
- Zhou, B. and Greenhalgh, S. A. (1994). Linear and parabolic τ - p transforms revisited. *Geophysics*, 59(7):1133–1149.
- Zhou, B. and Greenhalgh, S. A. (1996). Multiple suppression by 2D filtering in the parabolic τ - p domain: a wave-equation-based method. *Geophysical Prospecting*, 44:375–401.

Appendix A

Derivation of the CSP HI moveout formula

Assuming the same conditions on the subsurface and the seismic experiment as described in section 2 and section 3, I derive the local CSP HI moveout formula with respect to an arbitrary chosen central ray in a CSP gather. This moveout formula is based on a local circular wavefront approximation. Furthermore, I will show that the kinematic wavefront parameters (time, emergence angle and radius of the wavefront curvature) corresponding to an arbitrary chosen central ray in a CSP gather can be used in order to calculate the kinematic wavefront parameters of a paraxial ray, which is a ray in its local vicinity.

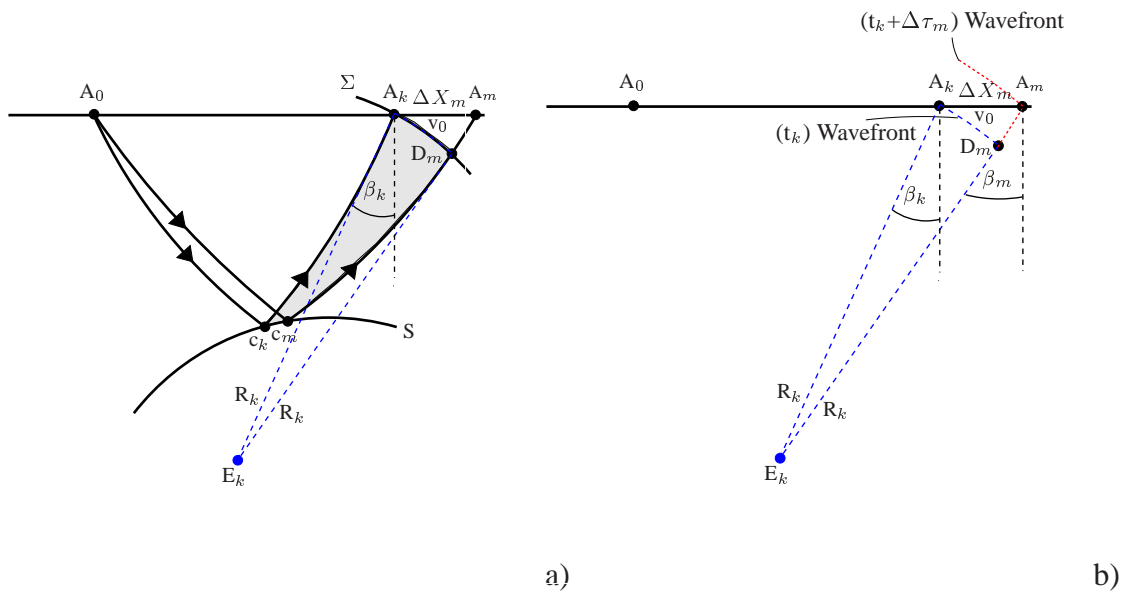


Figure A.1: a) Geometrical construction of the CSP moveout $\Delta\tau_m$. b) Simplified geometrical situation in the effective medium with constant velocity v_0 .

Figure A.1a shows a CSP seismic experiment in a 2D laterally inhomogeneous, isotropic, layered earth model. A reflector is labeled S . The source is fixed at the position A_0 , and connected via two reflected rays to the surface points A_k and A_m , which are located at the flat recording surface. The wavefront Σ emerges at the surface point A_k at the time t_k with an incidence angle β_k . The near surface velocity in the vicinity of A_k is considered to be known and to be constant. It is assumed that the true wavefront Σ can be approximated locally by an effective circular wavefront (shown in blue) with the same emergence angle β_k and radius R_k . This effective wavefront relates to the propagation in an effective medium with its front caustic located at E_k . The simplified situation in the effective medium is shown in Figure A.1b. The local moveout $\Delta\tau_m$ with respect to the central point A_k is given by the time it takes for the wavefront Σ to travel the distance $\overline{D_m A_m}$ from point D_m to point A_m

$$\Delta\tau_m = \frac{\overline{D_m A_m}}{v_0}. \quad (\text{A.1})$$

From the law of cosine within the triangle $A_k \widehat{E_k} A_m$ it follows:

$$\overline{A_m E_k}^2 = \overline{A_k A_m}^2 + \overline{A_k E_k}^2 - 2\overline{A_k E_k} \overline{A_k A_m} \cos\left(\frac{\pi}{2} + \beta_k\right) \quad (\text{A.2})$$

Identifying $\overline{A_k A_m} = \Delta x_m$, $\overline{A_k E_k} = \overline{D_m E_k} = R_k = 1/K_k$, and $\overline{A_m E_k} = R_k + \overline{D_m A_m}$, substituting into Equation (A.2), solving for $\overline{D_m A_m}$, and using Equation (A.1) leads to the searched time moveout correction formula:

$$\Delta\tau_m = \frac{\sqrt{R_k^2 + 2R_k \Delta x_m \sin \beta_k + \Delta x_m^2} - R_k}{v_0}. \quad (\text{A.3})$$

The sign of the square root is chosen according to the physical condition that $\Delta\tau_m$ has to be positive for a positive wavefront curvature K_k .

Performing a Taylor expansion up to the second order of the time correction formula in Equation (A.3) around the central point ($\Delta x_m \rightarrow 0$), and neglecting the higher order terms in Δx_m leads to the well known equation, see e.g. Equation 4.41. in Hubral and Krey [1980]:

$$\Delta\tau_m = \frac{\sin \beta_k}{v_0} \Delta x_m - \frac{\cos^2 \beta_k}{2R_k v_0} \Delta x_m^2 + \sigma(\Delta x_m^3), \quad (\Delta x_m \rightarrow 0). \quad (\text{A.4})$$

From Equation (A.4) it can be easily seen that for plane waves, i.e. $R_k = \infty$, the formula reduces to the local slant stack moveout formula:

$$\Delta\tau_m = \frac{\sin \beta_k}{v_0} \Delta x_m \quad (\text{A.5})$$

From Figure A.1b it follows furthermore from simple geometrical considerations that the kinematic wavefront parameters β_m and radius R_m of the wavefront Σ' (red) in the vicinity of the central ray (i.e. as long as the spherical wavefront assumption holds and the near surface velocity is constant in Figure A.1a can be calculated using the wavefront parameters β_k and R_k of the central ray. It follows for the emergence angle β_m and radius R_m of the wavefront Σ' at the surface location A_m at a time $(t_k + \Delta\tau_m)$:

$$\sin \beta_m = \frac{\Delta x_m + R_k \sin \beta_k}{\sqrt{R_k^2 + 2R_k \Delta x_m \sin \beta_k + \Delta x_m^2}}, \quad (\text{A.6})$$

$$R_m = \sqrt{R_k^2 + 2R_k \Delta x_m \sin \beta_k + \Delta x_m^2}. \quad (\text{A.7})$$

Note: The presented local moveout correction formula as well as the other formulas can be used with respect to any arbitrary receiver location, as done in section 3.5. In case of $k = 0$ the central point is identical to the source location and the corresponding stacking operator can be used in order to obtain a simulated zero-offset section using the CSP data, as done by Keydar et al. [1996] (see chapter 2).

Appendix B

Search of wavefront radius (\mathbf{R}_{CSH})

In appendix B.1 I will describe the non-linear one dimensional optimization method used for the determination of the radius of wavefront curvature in the wavefront parameter search procedure in chapter 3.3, namely the golden section search. The radius search must be limited to a certain range because technically it cannot be performed from $-\infty$ to $+\infty$. In appendix B.2 I show how the radius search can be limited to a reasonable range.

B.1 Golden section search

If $f(x)$ is uni-modal¹ in $[a,b]$ it is possible to reduce the interval of uncertainty in the search for the minimum by comparing the values of $f(x)$ at two interior points, step by step using the golden section algorithm, as explained in the following [see Bronstein and Semendjajew, 1989].

Golden section algorithm: $f(x)$ is assumed to be uni-modal in the interval (a^0, b^0) . Now, we search in this interval (a^0, b^0) for the minimum of the function $f(x)$. Therefore we calculate first $\tau = \sqrt{5} - 1 \approx 0.618$, and the starting points x_1^0, x_2^0 , as well as the values of the function $f(x)$ at these points, $f(x_1^0)$, and $f(x_2^0)$:

$$x_1^0 = a^0 + (1 - \tau)(b^0 - a^0), \quad (\text{B.1})$$

$$x_2^0 = a^0 + \tau(b^0 - a^0), \quad (\text{B.2})$$

$$f(x_1^0) \quad , \quad f(x_2^0). \quad (\text{B.3})$$

Based on Table B.1 we calculate the sequence (a^i, b^i) . This gives us an interval nesting to find the minimum. The length of the search interval reduces at each step by the factor of τ

¹uni-modal functions are functions with one extremum only.

compared to the length of the previous interval (because each interval is the larger part of the golden section of the previous interval).

	$f(x_2^i) > f(x_1^i)$	$f(x_2^i) \leq f(x_1^i)$
a^{i+1}	a^i	x_1^i
b^{i+1}	x_2^i	b^i
x_1^{i+1}	$a^i + (1 - \tau)(x_2^i - a^i)$	x_2^i
x_2^{i+1}	x_1^i	$b^i - (1 - \tau)(b^i - x_1^i)$
Calculate	$f(x_1^{i+1})$	$f(x_2^{i+1})$

Table B.1: The golden section algorithm to find a minimum of a function $f(x)$.

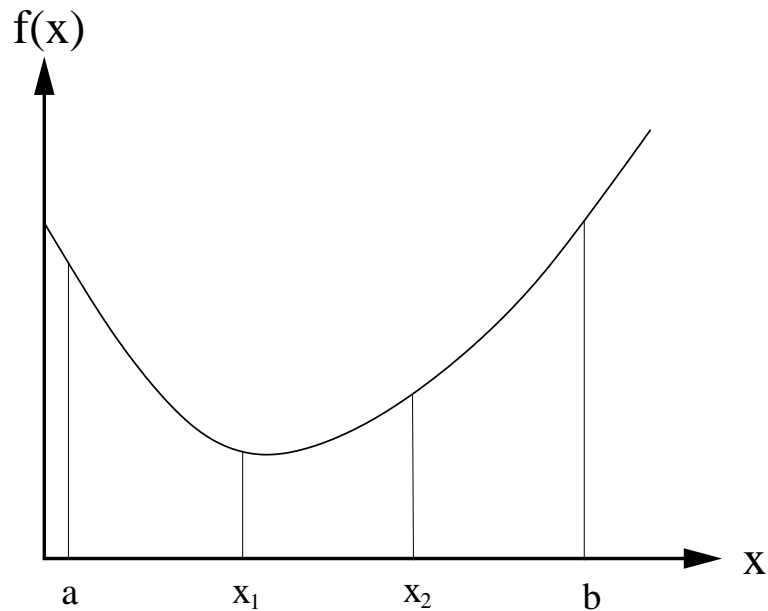


Figure B.1: Position of the search points x_1 and x_2 in an interval $[a,b]$ using the golden section algorithm.

B.2 Limits of radius search

In section 3.3 I present a method for the estimation of the optimal wavefront parameters corresponding to a specified time sample and central point location in a CSP gather.

For a specified emergence angle β_k , aperture Δx_{max} , near surface velocity v_0 in Equation (A.3) I limit the search range of the radius R_k in the optimization procedure in section 3.3 by $[R_k^{min}, R_k^{max}]$, as explained in the following.

Lets assume that we can distinguish between a plane wave ($R_k = \infty$) and a wave with a circular wavefront with radius of wavefront curvature $R_k = R_k^{max}$ if the two wavefronts are at least separated by a time difference $\epsilon \Delta t$ at the maximum considered aperture Δx_{max} .

This time difference $\epsilon \Delta t$ can be expressed by the subtraction of the traveltimes associated with a circular wavefront in Equation (A.4) from the linear plane-wave time correction formula in Equation (A.5). This leads to the maximum R_k^{max} and minimum R_k^{min} radius of wavefront curvature which can be distinguished from a plane wave ($R_k = \infty$).

$$R_{min}, R_{max} \leq \pm \frac{\cos^2 \beta_k \Delta x_{max}^2}{2v_0 \epsilon \Delta t}, \quad (\text{B.4})$$

where β_k the currently specified emergence angle, Δx_{max} is the used aperture, Δt the time sampling rate, and ϵ an adjustment parameter.

Depending on the chosen emergence angle β_k , the aperture Δx_{max} , and ϵ , the limits for the radius search R_k^{min} and R_k^{max} are specified using Equation (B.4). In the next step the golden section algorithm (Appendix B.1) is applied in order to find the corresponding optimum of wavefront curvature within the search interval $[R_k^{min}, R_k^{max}]$.

This procedure is repeated for each specified emergence angle β_k in the optimization procedure, as explained in section 3.3).

Appendix C

Forward calculation of kinematic wavefront parameters

If the subsurface structure of a synthetic model is known the kinematic wavefront parameters used in this work, namely the travelttime, emergence angle and radius of wavefront curvature associated with any arbitrary ray can be determined exactly by forward calculation. First of all, the raypath of a particular ray has to be known. It can be computed by ray-tracing [Červený and Ravindra, 1971] which is based on the ray method. Starting ray-tracing from a specified source point and a given incidence angle of the ray, the complete raypath can be determined including the emergence angle at the receiver point.

Hubral and Krey [1980] showed how the radius of wavefront curvature of any wavefront can be calculated along an arbitrarily chosen ray based on the law of *transmission, refraction* and *reflection*. These formulas are used in the following way:

Starting from the source point the radius of wavefront curvature is calculated in downward direction successively along a specified raypath connecting source and receiver. Knowing also the local radius of curvature of the interfaces for each point along an interface, the radius of wavefront curvature of the wavefront originating at the source point can be determined at any position of the ray. In order to calculate the wavefront curvature at the receiver point it is necessary to calculate the wavefront curvature along each ray segment connecting two interfaces and to consider the change in wavefront curvature due to the transmission of the wavefront from on side of the interface to the other, as well as due to the reflection at the reflector.

Using the *transmission law* the radius of curvature R_{end} at the end of a straight ray segment of distance $v\Delta t$ within a layer of velocity v can be computed from an initial radius of curvature R_{start} by

$$R_{end} = R_{start} + v\Delta t, \quad (\text{C.1})$$

with v being the layer velocity and Δt being the traveltime required by the wave to travel along the specified straight ray segment.

The change of wavefront curvature for transmitted waves from one side of an interface to the other can be calculated using the *refraction Law*:

$$\frac{1}{R_T} = \frac{v_T \cos^2 \epsilon_I}{v_I \cos^2 \epsilon_T} \frac{1}{R_I} + \frac{1}{\cos^2 \epsilon_T} \left[\frac{v_T}{v_I} \cos \epsilon_I - \cos \epsilon_T \right] \frac{1}{R_F}, \quad (\text{C.2})$$

R_I and R_T denote the radii of wavefront curvature on the incident side and refracted side of the interface, respectively. Similarly, v_i and v_T label the layer velocity on the incident side and the refracted side of the interface. ϵ_I is the angle of incidence and ϵ_T the angle of refraction. R_F denotes the radius of curvature of the interface at the point of intersection of the specified ray with the interface. R_F is positive if the interface is convex to the incoming wave.

The change in wavefront curvature due to the reflection of a wave at an interface is given by the *reflection law*:

$$\frac{1}{R_R} = \frac{v_R \cos^2 \epsilon_I}{v_I \cos^2 \epsilon_R} \frac{1}{R_I} + \frac{1}{\cos^2 \epsilon_R} \left[\frac{v_R}{v_I} \cos \epsilon_I + \cos \epsilon_R \right] \frac{1}{R_F}, \quad (\text{C.3})$$

with R_I and R_R denoting the radii of wavefront curvature on the incident wavefront and reflected wavefront on the same side of the interface. The velocities v_I and v_R are the corresponding velocities.

In the calculation procedure we start at the source location S and calculate the radii of curvature of the common-shot-wavefront along a specified ray until we reach the receiver location G . The initial radius of wavefront curvature at the source point is per definition equal to zero ($R_{start} = 0$).

Danksagung

Herrn Prof. Dr. Peter Hubral danke ich für die Übernahme des Hauptreferats. Weiter möchte ich ihm dafür danken, daß er mir die Teilnahme an internationalen Konferenzen ermöglichte, was mir die Gelegenheit gab Erfahrungen zu sammeln und Kontakte zu knüpfen. Frau Payne danke ich für ihre Hilfsbereitschaft und Unterstützung in administrativen Fragen.

Herrn Prof. Dr. Friedemann Wenzel danke ich für die Übernahme des Korreferats.

Many thanks to Dr. Evgeny Landa and Dr. Shemer Keydar for the numerous productive, critical and always enthusiastic discussions about multiples, multifocusing, and the real life. I very much appreciate the advice and friendship I received and want to thank you for the hospitality during my stay at the Geophysical Institute of Israel and of course for the corrections of my thesis.

Thanks a lot to Dr. Tijmen Jan Moser for the help in ray-tracing problems, programming, the many fruitful discussions, as well as for the evenings at Panorama. Thank you also to Dr. Boris Gurevich for the helpfulness and the always critical discussions. I also want to thank both of you for reading my thesis.

Furthermore I wish to thank Dr. Igor Belfer for the help concerning the parabolic τ - p transform and Matlab.

Herzlichen Dank an Dr. Martin Karrenbach, der immer für Fragen offen war und mir oft mit guten Tips und Ideen zu Rate stand. Danke auch für das Korrekturlesen meiner Dissertation.

Thanks to Dr. Josef Paffenholz and Dr. Chad Harding for the interest in my work, the many motivating discussions, and the chance to work for three weeks at BHP Petroleum in Houston. It was a pleasure for me to participate in such a great international project.

Danke auch an Dr. Sven Treitel für das Interesse an meiner Arbeit und die vielen kritischen Anmerkungen, Ideen und Korrekturen in diversen Berichten.

I also wish to thank Prof. Enders Robinson and Prof. Lourenildo Leite for the discussions about amplitude-prediction of multiples.

Bei Kai-Uwe Vieth möchte ich mich für die zahlreichen intensiven und motivierenden Diskussionen über CRS stack und Multiple bedanken. Außerdem für das Korrekturlesen

dieser Arbeit.

Dr. Robert Essenreiter danke ich für den ständigen fachlichen Austausch, die gemeinsame Zeit in Karlsruhe, Hawaii und Houston sowie für die langjährige Freundschaft durch Studium und Promotion.

Großer Dank auch an Jürgen Mann für die Hilfe in allerlei Computerfragen sowie für das kritische Korrekturlesen dieser Arbeit. Hierfür möchte ich mich auch bei German Höcht und Erik Sänger bedanken.

Danke auch an Peter Dausch und Petra Knopf für die ständige Unterstützung in Hardware und Softwarefragen. Weiter danke ich Thomas Hertweck für die Hilfe beim Lösen der Linux Probleme.

Desweiteren möchte ich mich herzlich bei Matthias Riede für die vielen fachlichen und auch nicht-fachlichen Diskussionen im letzten Jahrzehnt bedanken und überlasse ihm hiermit die rote Laterne.

Allen Mitarbeitern, Mitarbeiterinnen, Studenten und Studentinnen des Geophysikalischen Instituts, die mich unterstützt haben, aber nicht namentlich erwähnt wurden, möchte ich an dieser Stelle danken.

Bei meiner Freundin Kirsten bedanke ich mich für ihr Verständnis und ihre moralische Unterstützung. Auch meinen Eltern und meinem Bruder möchte ich an dieser Stelle für ihre Unterstützung während des Studiums und der Promotion danken.

Lebenslauf

Persönliche Daten:

Name:	Jörg Helmut Zaske
Geburtsdatum:	14.07.1967
Geburtsort:	Esslingen a. Neckar
Nationalität:	Deutsch

Schulbildung:

1974 – 1978	Grundschule in Magstadt
1978 – 1987	Stiftsgymnasium in Sindelfingen

Studium und Promotion:

1989 – 1997	Studium der Geophysik an der Universität Karlsruhe
1993 – 1994	Studium der Geophysik an der University of Hawaii at Manoa, U.S.A.
10.09.1997	Diplom
seit 1997	Doktorand an der Fakultät für Physik der Universität Karlsruhe

